

Deciphering oncogene dependencies and signaling pathway
alterations in non small cell lung cancer

Inaugural Dissertation

zur
Erlangung des Doktorgrades
Dr. nat. med.
der Medizinischen Fakultät
und
der Mathematisch-Naturwissenschaftlichen Fakultät
der Universität zu Köln



vorgelegt von
Dipl. Biol. Jonathan Weiß
aus Köln

Köln, 2011

Berichtersteller:

Professor Dr. Hinrich Abken
Professor Dr. Matthias Hammerschmidt

Tag der letzten mündlichen Prüfung:

4 April 2011

Contents

1. List of publications from projects within the thesis	1
2. Abstract	2
2. Zusammenfassung.....	3
3. Introduction.....	4
3.1 The origins and general classification of cancer	4
3.2 The development of a tumor	4
3.3 (Cell) Biology of Cancer	6
3.4 The Oncogene dependency model	9
3.5 The pathology of lung cancer	9
3.6 Treatment of lung cancer	10
3. Aims of the thesis	12
4. Publications with own contributions	13
4.1 PTEN Loss Contributes to Erlotinib Resistance in EGFR-Mutant Lung Cancer by Activation of Akt and EGFR	13
4.2 Predicting drug susceptibility of non–small cell lung cancers based on genetic lesions.....	14
4.3 Identifying genotype-dependent efficacy of single and combined PI3K- and MAPK- pathway inhibition in cancer	16
4.4 Chemogenomic Profiling Provides Insights into the Limited Activity of Irreversible EGFR Inhibitors in Tumor Cells Expressing the T790M EGFR Resistance Mutation	17
4.5 Analysis of Compound Synergy in High-Throughput Cellular Screens by Population-Based Lifetime Modeling.....	18
4.6 Frequent and Focal FGFR1 Amplification Associates with Therapeutically Tractable FGFR1 Dependency in Squamous Cell Lung Cancer.....	19
5.0 Discussion	21
6.0 References.....	24
7.0 Appendix.....	27
7.1 Acknowledgments	27
7.2 Academic Curriculum Vitae	28
7.3 Erklärung	31

1. List of publications from projects within the thesis

Frequent and focal FGFR1 amplification associates with therapeutically tractable FGFR1 dependency in squamous cell lung cancer.

Weiss J, Sos ML, Seidel D, Peifer M, Zander T, Heuckmann JM, Ullrich RT, Menon R, Maier S, Soltermann A, Moch H, Wagener P, Fischer F, Heynck S, Koker M, Schöttle J, Leenders F, Gabler F, Dabow I, Querings S, Heukamp LC, Balke-Want H, Ansén S, Rauh D, Baessmann I, Altmüller J, Wainer Z, Conron M, Wright G, Russell P, Solomon B, Brambilla E, Brambilla C, Lorimier P, Sollberg S, Brustugun OT, Engel-Riedel W, Ludwig C, Petersen I, Sängler J, Clement J, Groen H, Timens W, Sietsma H, Thunnissen E, Smit E, Heideman D, Cappuzzo F, Ligorio C, Damiani S, Hallek M, Beroukhim R, Pao W, Klebl B, Baumann M, Buettner R, Ernestus K, Stoelben E, Wolf J, Nürnberg P, Perner S, Thomas RK. *Sci Transl Med*. 2010 Dec 15;2(62):62ra93.

Analysis of compound synergy in high-throughput cellular screens by population-based lifetime modeling.

Peifer M, **Weiss J***, Sos ML, Koker M, Heynck S, Netzer C, Fischer S, Rode H, Rauh D, Rahnenführer J, Thomas RK.

PLoS One. 2010 Jan 27;5(1):e8919.

*Contributed equally

Chemogenomic profiling provides insights into the limited activity of irreversible EGFR Inhibitors in tumor cells expressing the T790M EGFR resistance mutation.

Sos ML, Rode HB, Heynck S, Peifer M, Fischer F, Klüter S, Pawar VG, Reuter C, Heuckmann JM, **Weiss J**, Ruddigkeit L, Rabiller M, Koker M, Simard JR, Getlik M, Yuza Y, Chen TH, Greulich H, Thomas RK, Rauh D.

Cancer Res. 2010 Feb 1;70(3):868-74.

Identifying genotype-dependent efficacy of single and combined PI3K- and MAPK-pathway inhibition in cancer.

Sos ML, Fischer S, Ullrich R, Peifer M, Heuckmann JM, Koker M, Heynck S, Stückrath I, **Weiss J**, Fischer F, Michel K, Goel A, Regales L, Politi KA, Perera S, Getlik M, Heukamp LC, Ansén S, Zander T, Beroukhim R, Kashkar H, Shokat KM, Sellers WR, Rauh D, Orr C, Hoeflich KP, Friedman L, Wong KK, Pao W, Thomas RK.

Proc Natl Acad Sci U S A. 2009 Oct 27;106(43):18351-6.

Predicting drug susceptibility of non-small cell lung cancers based on genetic lesions.

Sos ML, Michel K, Zander T, **Weiss J***, Frommolt P, Peifer M, Li D, Ullrich R, Koker M, Fischer F, Shimamura T, Rauh D, Mermel C, Fischer S, Stückrath I, Heynck S, Beroukhim R, Lin W, Winckler W, Shah K, LaFramboise T, Moriarty WF, Hanna M, Tolosi L, Rahnenführer J, Verhaak R, Chiang D, Getz G, Hellmich M, Wolf J, Girard L, Peyton M, Weir BA, Chen TH, Greulich H, Barretina J, Shapiro GI, Garraway LA, Gazdar AF, Minna JD, Meyerson M, Wong KK, Thomas RK.

J Clin Invest. 2009 Jun;119(6):1727-40. doi: 10.1172/JCI37127.

*Contributed equally

PTEN loss contributes to erlotinib resistance in EGFR-mutant lung cancer by activation of Akt and EGFR.

Sos ML, Koker M, Weir BA, Heynck S, Rabinovsky R, Zander T, Seeger JM, **Weiss J**, Fischer F, Frommolt P, Michel K, Peifer M, Mermel C, Girard L, Peyton M, Gazdar AF, Minna JD, Garraway LA, Kashkar H, Pao W, Meyerson M, Thomas RK.

Cancer Res. 2009 Apr 15;69(8):3256-61.

2. Abstract

Lung cancer is the leading cause of cancer related death worldwide with 1.4 million cases in 2008. Thus, there is an unmet need to identify novel treatment options for lung cancer patients in the clinic and foster the understanding of tumor biology. The Ph.D. thesis presented here focuses on the identification and characterization of novel oncogenes that play a role in the onset of lung tumor development as well as on the characterization of signaling pathway recruitment downstream of oncogenic receptor tyrosine kinases (RTKs).

In this regard, we were able to identify two genes encoding for protein kinases being causative for tumor development and furthermore we were able to functionally validate both genes as being the relevant target of the respective inhibitor *in-vitro*. In detail, we identified:

- amplifications of the human version of *v-src avian sarcoma (Schmidt-Ruppin A-2) viral oncogene (cSRC)* as being causative and predictive for the sensitivity towards the clinical approved Src-Abl inhibitor dasatinib
- amplifications of the *fibroblast growth factor receptor 1 (FGFR1)* as being causative and predictive for the sensitivity towards the FGFR protein family inhibitor PD173074
- frequent amplifications of *FGFR1* in squamous cell but no other type of NSCLC cells. Hence, we strongly suggest to treat patients suffering from *FGFR1* amplified squamous cell lung tumors with *FGFR1* inhibitors.

Furthermore, we utilized *in-vitro* chemical-genomic approaches and genetic engineering to functionally validate both, *cSRC* and *FGFR1*, as the relevant targets of the respective inhibitors in amplified cell lines.

And finally, we extended our already established high-throughput screening platform to be able to screen up to 1500 compounds as well as combinations of various signaling pathway inhibitors. To this end, we have screened 136 inhibitor combinations on 105 genetically defined cell lines to identify novel treatment options as well as specific signaling pathway recruitments within defined genetic conditions.

Thus, amplifications of *cSRC* as well as *FGFR1* lead to responsiveness towards small molecule inhibitors in NSCLC cells harboring amplification of either gene. We show that high throughput cell based screening of inhibitor combinations can be utilized to shed light into the complex recruitment of signaling pathways downstream of RTKs and lead to novel treatment strategies for patients suffering from lung cancer. And finally, we identified *FGFR1* amplifications in up to 20% primary squamous cell lung cancer specimens, strongly suggesting to treat these patients with *FGFR1* inhibitors.

2. Zusammenfassung

Lungenkrebs ist die häufigste Ursache für Krebs bezogene Todesfälle mit 1,4 Millionen Fällen im Jahr 2008. Daraus ergibt sich ein dringender Bedarf sowohl an neuen therapeutischen Ansätzen als auch an einem besseren Verständnis der zugrundeliegenden Tumorbiologie. Die vorliegende Doktorarbeit beschäftigt sich mit der Identifikation und Validierung von Onkogenen die verantwortlich sind für die Lungentumorgenese und darüber hinaus mit der Charakterisierung von Signalwegen die von Onkogen wirkenden Rezeptor Tyrosin Kinasen (RTKs) rekrutiert werden.

Der in dieser Doktorarbeit benutzte experimentelle Ansatz, beruht auf der systematischen Untersuchung einer grossen Menge an NSCLC-Zelllinien. Diese Zelllinien wurden bereits im Zuge von Vorarbeiten genetisch charakterisiert und es konnte gezeigt werden, dass alle charakterisierten Zelllinien zusammen ein akkurates Abbild der genetischen Landschaft von primären Lungentumoren bilden. Zunächst wurde die Zelllinien-Sammlung zunächst mit dem Tyrosinkinase-Inhibitor Dasatinib behandelt um mit den gewonnenen Sensitivitätsinformationen, zusammen mit den genetischen Informationen, einen genetischen Marker zu identifizieren, der die Sensitivität von NSCLC Zellen vorhersagt. Hierzu wurde die Target Enriched Sensitivity Prediction (TESP) Methode entwickelt und angewandt. Dabei wurden *v-SRC Avian Sarcoma (Schmidt-Ruppin A-2) Viral Oncogene (SRC)* Gen-Amplifikationen als mit therapeutisch nutzbarer SRC-Abhängigkeit vergesellschaftet identifiziert. Weitere funktionelle Experimente in einer Zelllinie mit SRC Amplifikation (H322M) bestätigen das von SRC codierte Protein als therapeutisch relevanter Interaktionspartner von Dasatinib *in-vitro*. Diese Abhängigkeit kann bereits heute mit dem klinisch verfügbaren SRC-ABL Hemmer Dasatinib therapeutisch genutzt werden. In einem weiteren Experiment wurde die eingangs erwähnte Zelllinien Sammlung mit PD173074, einem Hemmer der *Fibroblasten Wachstumsfaktor Rezeptor* Familie (*FGFRs*), behandelt. In diesem Falle wurde mit Hilfe des K-Nearest Neighbor (KNN) Algorithmus die Amplifikation des Chromosomenabschnitts 8p12 – in dem das *FGFR1* Gen lokalisiert – als einziger signifikanter Prädiktor für die Sensitivität gegenüber PD173074 gefunden. Weitere funktionelle *in-vitro* Experimente bestätigten, dass das FGFR1 Protein das Ziel von PD173074 in *FGFR1*-amplifizierten NSCLC Zellen ist. Darüber hinaus konnte dieser Befund in *in-vivo* Xenograft Mausmodellen bestätigt werden bei denen implantierte *FGFR1*-amplifizierte Tumore eine Regression zeigten nach der Behandlung der Mäuse mit PD173074. Weitere Untersuchungen von primären Lungentumor Proben ergaben, dass in bis zu 20% der untersuchten Plattenepithel Karzinome jedoch lediglich in 1% der untersuchten Adeno Karzinome fokale und starke *FGFR1* Amplifikationen detektierbar sind. Diese Ergebnisse zeigen zum ersten Mal ein neues therapeutisches Ziel, speziell im Plattenepithel Subtyp von NSCLC Tumoren.

Die zweite Frage die die vorliegende Doktorarbeit zu beantworten sucht, ist welche Signalwege durch RTK - Onkogene aktiviert werden um die Tumorentwicklung voranzutreiben. Da die meisten Onkogene mehr als einen Signalweg aktivieren ist es ein vielversprechender Ansatz verschiedene Signalwege miteinander zu kombinieren. In einer ersten Studie konnten wir zeigen, dass die Kombination eines Phosphatidyl-Inositol 3 Kinase (PI3K) Signalwegs Inhibitor (PI103) mit einem Mitogen-Activated Protein Kinase (MAPK) Signalweg Inhibitor (PD0325901) synergistisch zu einer signifikant höheren Induktion von Apoptose in NSCLC Zelllinien führt. Im weiteren Verlauf der Doktorarbeit wurden darüber hinausgehend systematisch 136 verschiedene Signalwegs-Hemmer Kombinationen auf 105 genetisch annotierten Zelllinien getestet. Signifikant synergistisch wirkende Kombinationen wurden mithilfe, eines ebenfalls im Verlauf der Doktorarbeit erarbeiteten mathematisch/biologischen Modells identifiziert.

Zusammenfassend konnten in dieser Arbeit neue Beispiele für möglicherweise klinisch relevante Onkogenabhängigkeit erarbeitet werden. Darüber hinaus konnten wir die Signaltransduktion im Kontext von aktivierten Onkogenen entschlüsseln und so zur Erhellung der komplexen Biologie genetisch definierter Subtypen des Bronchialkarzinomes beitragen.

3. Introduction

3.1 The origins and general classification of cancer

The term *carcinoma*, the greek word for crayfish, was first introduced by Hippocrates (460 - 370BC) because of "the veins stretched on all sides as the animal the crab has its feet, whence it derives its name" (1). The latin doctor Celsus (ca. 25BC – 50AD) later translated the greek word "*carcinoma*", to today's latin word "*cancer*" (1). Today, the term cancer is commonly used to describe a disease where a group of cells is abnormally proliferating - forming a tumor - and, over time, spread to distant parts of the body and form metastases.

In general, tumors are classified into benign and malignant categories. Benign tumors are separated from surrounding tissue by a basal membrane, can only grow locally restricted and lack the ability to spread into distant parts of the body. Therefore, benign tumors can be retracted by surgery and have a favorable clinical outcome. In stark contrast, due to lack of a basal lamina, malignant tumors grow more aggressively, can spread to distant parts of the body and have a more severe clinical outcome.

Malignant tumors are classified based on the specialized cell type they originate from and the most predominant and clinically most relevant group of malignant tumors are carcinomas. They account for 80% of cancer related deaths in the western world (2); due to the fact that carcinomas can arise from epithelial tissue originating from all three germ layers (ectoderm e.g., lung, mesoderm e.g., ovarian and endoderm e.g., liver).

The remaining cancer related deaths are caused by tumors arising from:

- connective tissues originating from the mesoderm (sarcomas), e.g., osteoblasts;
- blood forming tissues (hematopoietic system), e.g., leukemias and lymphomas; or
- components of the central and peripheral nervous system (neuroectodermal tumors), e.g., gliomas and neuroblastomas.

To fully term a tumor, the aforementioned classification is stated together with the name of the organ where the primary tumor arises from.

Taken together, the disease "cancer" means the abnormal proliferation of cells that subsequently form a tumor. Tumors are classified based on the presence of a basal lamina, the organ and tissue they arise from (2).

3.2 The development of a tumor

During this process, the genome is affected by a multitude of alterations ultimately leading to a fully transformed malignant tumor. Genomic alterations (mutations and chromosomal alterations) accumulate over the years and are accelerated by external mutagenic agents (e.g., tobacco smoke (3,4)). When certain combinations of genomic alterations accumulate in the same cell, transformation takes place and tumorigenic cell behavior occurs (2). This model of tumor development explains three key observations. First, an increasing risk to develop a tumor later in life, simply because of more time to accumulate genomic alterations. Second, patients that already harbor inherited genetic risk-factors (e.g., mutations in tumor suppressor genes), are more likely to develop a tumor early in life (e.g., *BRAC1* or *2* mutations in breast cancer (5)). And third, the observation that exposure to carcinogenic agents (e.g., tobacco smoke) also leads to earlier development of lung cancer due to a higher genomic mutation rate (3,4).

From a cell-biology point of view, the process of tumor development must include several key steps in order to facilitate the malignant phenotype. A commonly accepted idea for a "skill set" that a tumor cell has to acquire, was proposed by Douglas Hanahan and Bob Weinberg in the year 2000, namely evading apoptosis, unlimited cell division, growth factor independency, become prone to anti-growth signals, attract new blood vessels and to metastasize to distant parts of the body (6).

3.2.1 The ability to circumvent programmed cell death (apoptosis).

In healthy cells of the adult body, apoptosis occurs when a cell is irreversibly damaged. Apoptosis can be triggered from outside signals (e.g., by activation of death receptors via the trail ligand) or from signals within a cell (e.g., after extensive DNA damage). A fine balance between pro- and anti-apoptotic signals tightly regulates initiation of apoptosis. For example, in case of irreparable DNA damage, the balance is shifted towards pro-apoptotic signals and irreversible apoptosis is induced.

In tumor cells, the balance is heavily shifted towards the anti-apoptotic signaling side; thus tumor cells are prone to signals triggering apoptosis (2). Genomic alterations fostering this ability are a mandatory prerequisite to initiate tumor formation. For example, tumor cells frequently activate of the PI3K pathway leads to inhibition of pro-apoptotic and amplification of anti-apoptotic signals via the protein kinase Akt (7).

3.2.2 The ability to become independent of growth signals

Proliferation of healthy cells only occur in a tightly controlled manner, for example following stimulation of membrane-bound receptors by growth-signal molecules released from neighboring cells or even from a different parts of the body. Upon binding of these molecules (e.g., Epidermal Growth Factor (EGF)) the corresponding receptor is activated and initiates intrinsic cell signaling pathways. To proliferate independently from external growth factor signals, tumor cells utilize two mechanisms. First, the growth signal receptor sequence is altered and the corresponding protein is locked in an “always active” state thereby constantly promoting a proliferation signal, e.g., *EGFR* mutations in adenocarcinomas of the lung (8,9). Second, the tumor cell acquires an alteration that promotes the over-expression of mRNAs coding for growth factor molecules. These are then released into the intercellular matrix and thereby activate corresponding receptors (10). For example, release of insulin like growth factor 1 following *p21ras* expression in thyroid epithelial cells (11).

3.2.3 The ability to become prone to anti-growth signals

As aforementioned, tumor cells become independent of outside signals promoting proliferation. However, in healthy tissues, cells are kept quiescent in the G0 state until release for controlled cell proliferation. Cell cycle progression is tightly regulated by intrinsic factors, such as cyclin dependent kinases (CDKs), e.g., during the cell cycle checkpoints G1 to S-Phase and G2-Phase to Mitosis. By contrast, in tumor cells these regulating signals are altered, leading to uncontrolled cell cycle progression (2). For example, in healthy cells anti-growth signals predominantly funnel through the retinoblastoma protein (RB). RB interacts with transcription factors of the E2F family, hence altering the expression of genes that promote transition from the G1 into the S-phase of the cell cycle (2). In order to foster the malignant phenotype, tumor cells need to become prone to these inhibitory signals, e.g., by Loss-of-function mutations in the *RB* gene itself (12).

3.2.4 The ability to indefinitely undergo cell division

Physiological proliferation in normal tissues is a highly controlled process. In healthy cells the number of possible cell divisions is defined by the length of telomeres at the end of each chromosome (13). During each mitotic division about 100bp of telomere DNA is lost, hence limiting the number of cell divisions (14). In contrast to tumor cells where the gene *TERT*, that encodes for the catalytic subunit of the telomerase complex is up-regulated and/or amplified. This telomerase complex elongates telomeres at the end of the G2 phase before cell division thereby re-setting the cell division “counter” and enables the tumor cell to divide indefinitely (15).

3.2.5 The ability to initiate blood vessel sprouting

In order to function all cells need a steady supply of nutrients and oxygen that are first transported via the blood stream and later via diffusion. When a tumor extends a size of approx. 0.2mm^3 oxygen diffusion is not sufficient to supply the whole tumor; new blood vessels need to be formed to secure full supply of the inner part of the tumor. Most tumors release Vascular Endothelial Growth Factor (VEGF) protein into the extracellular matrix; initiating sprouting and attracting new blood vessels (2).

3.2.6 The ability to invade into other parts of the body

In all solid tissues, each cell is connected to other cells by integrins or other connecting proteins. These junctions keep the cells close together and also transfer survival signals between cells. Many types of healthy cells that are detached from these connections undergo apoptosis shortly afterwards (2). In the last developmental stage, tumor cells do no longer depend on survival signals from neighboring cells (transferred by e.g., cadherins and integrins), detach from the primary tumor site and are transported via the blood stream or the lymph vessel system to other parts of the body. There, they attach and form new tumors, leading to a secondary tumor site (16).

3.3 (Cell) Biology of Cancer

Cancer is a disease of the genome, where cells that constitute the final tumor have acquired a unique set of abilities. These are acquired by changing the genomic constitution of genes, ultimately changing cell physiology to enable the full malignant phenotype. Advances in high-throughput sequencing technologies enabled a comprehensive view on the genomic changes in cancer. The sheer amount of genomic alterations observed in tumor cells is staggering (17-19) with more than 150 subtle genomic changes observed in one single tumor (17). Thus, it is tempting to conclude that every tumor is absolutely unique on its own suggesting that no effective therapeutic strategy could be developed against molecularly defined classes of tumors. However, a careful analysis of functional cell signaling pathways affected by the multitude of cancer genome alterations has revealed that ultimately, all of these alterations affected only a limited repertoire of pathways that are required for transformation according to the Hanahan and Weinberg dogma (20,21). Therefore, in addition to a genetic "driver"-oriented view of cancer genomics (wherein single alterations functionally support the acquisition of more than one of the Hanahan and Weinberg criteria, e.g., *EGFR* mutations), these observations support a pathway-oriented view, which takes into account multiple genetic possibilities for the activation of each required pathway.

3.3.1 Oncogenic signaling pathways frequently activated in tumor cells

The signaling pathways are composed of several proteins, mostly kinases, which are being activated sequentially (Figure 1). The main function is the transfer from extracellular signals into the cytoplasm and nucleus where they alter the function of proteins and expression of transcription factors or proteins. Signaling pathway functions are frequently altered in tumors, fulfilling most of the Hanahan and Weinberg criteria.

The Mitogen-activated Protein Kinase (MAPK) pathway

Activating signals commonly arise from membrane bound tyrosine kinases (e.g., EGFRs) via adaptor proteins (e.g., Grb2) to Son of Sevenless (SOS) (a guanine exchange factor (GEF)), to the GTPase RAS (Figure 1). Activated RAS protein can phosphorylate and therefore activate the Phospho-Inositol3-Kinase (PI3K) via its RAS binding domain, but also activate the downstream kinase ERK1/2 (MAPK) via the kinases RAF and MEK. The MAPK pathway regulates transcription factors that control proliferation and protein synthesis (2).

The Phosphoinositide 3 Kinase (PI3K) pathway

This pathway signals parallel to the MAPK pathway and is activated similarly (Figure 1). Upon activation of membrane bound RTKs, p85, the regulatory subunit of the PI3K protein complex, is activated and in turn activates the catalytic subunit p110 (PI3CA). Upon activation, p110 phosphorylates phosphatidylinositol (PtdIns) leading to Phosphatidylinositol 3-phosphate (PI(3)P). PI(3)P in turn activates downstream protein kinases in the PI3K pathway. The phosphatase and tensin homolog (pTEN) belongs to the phosphatase protein family and dephosphorylates PI(3)P, thereby antagonizing the PI3K signal (22). Loss of pTEN function in lung tumors confers resistance to abrogation of the EGFR signal by small molecule inhibitors such as erlotinib or gefitinib (23). Following the release of PI(3)P, the tyrosine kinase PDK-1 is recruited to the cell membrane, activated and in turn further activates different substrates. One of the most important substrates activated by PDK-1 is another protein kinase termed Akt (or PKB). Upon activation, Akt mediates anti-apoptotic signals. For example, the pro-apoptotic protein BAD is phosphorylated by Akt on Serin 126 resulting in its deactivation. Moreover, Akt activates anti-apoptotic members of the BCL-2 family, inactivates Caspase 9 and interacts with members of the FOXO transcription factor family, thereby enhancing the transcription of anti-apoptotic proteins (7). The second important role of Akt is the activation of the TORC1 and TORC2 complexes, central regulators of cap-dependent translation and cell metabolism.

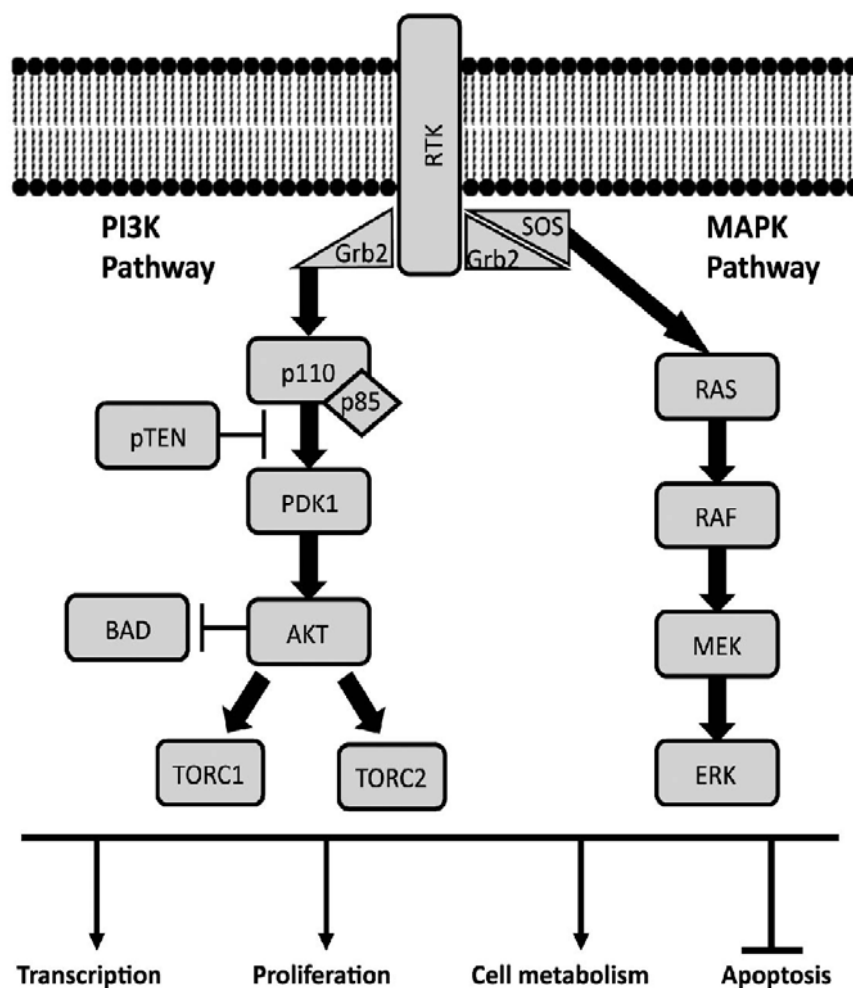


Figure 1: The PI3K and MAPK pathways.

Both pathways are being activated by cell membrane bound tyrosine kinases (RTKs) via Grb2 and SOS. In the case of the MAPK pathway, SOS activates RAS and subsequently RAF, MEK and ERK are being activated sequentially. In the case of the PI3K pathway, GRB2 directly interacts with p85, the regulator subunit of the PI3 kinase complex, thereby activating the kinase itself and subsequent downstream signaling of Akt and TORC1/2. Activation downstream of the PI3K (p110/p85) complex is abrogated by the phosphatase pTEN. Activation of the protein kinase Akt leads to inactivation of the pro-apoptotic factor BAD.

3.3.2 Tumor suppressor genes frequently mutated in cancer

The p53 protein complex

The p53 complex is a key regulator of stress response in cells. Under normal conditions, p53 is locked in an inactive state in the cytoplasm and becomes activated in response to severe cell stress triggered by e.g., DNA damage, oncogene signaling or hypoxia. Upon activation, p53 acts as a transcription factor for proteins regulating the cell cycle, thereby causing a stop in cell cycle progression. Following such an event, two outcomes are possible. First, if the cell or DNA damage is too severe to be repaired, and p53 activates the apoptotic cascade leading to cell death and second, after DNA damage is repaired, p53 releases its blockade and cell cycle progression occurs again (2). P53 is a main regulator to monitor aberrant cell intrinsic signaling and DNA damage. Loss of p53 results in more tolerance to aberrant cell signaling and DNA damage thereby fostering tumor development. This role is reflected by the observation that p53 is one of the most frequent mutated genes in cancer (<http://www.sanger.ac.uk/genetics/CGP/cosmic/>).

The Retinoblastom Protein (RB)

The RB protein functions as a tumor suppressor and is frequently mutated in many types of cancer (<http://www.sanger.ac.uk/genetics/CGP/cosmic/>). RB controls the transit from the G1 to the S phase of the cell cycle by binding to and thereby inhibiting transcription factors of the E2F family (24). As long as E2F transcription factors are blocked, the cell is arrested in the G1 phase of the cell cycle. In healthy cells, RB is deactivated via members of the CDK family, when the cells ready to proceed to a new mitotic cycle. Whereas tumor cells, where RB function is lost, uncontrolled cell cycle progression occurs.

3.3.3 Oncogenes in cancer

RAS as an example of Small GTPases

The members of the RAS family belong to the group of small GTPases. Similar to kinases, GTPases transfer signals by direct interaction with other proteins upon phosphorylation. Unlike kinases (which use Adenosin Tri-Phosphate (ATP)), GTPases use Guanine Tri-Phosphate (GTP) as a substrate. RAS family members become activated by RTKs and subsequently activate various signaling pathways, including the PI3K pathway by direct interaction with PIK3CA, the MAPK pathway by activating the serin/threonine kinase RAF and the Ral-GEF pathway which enables cellular motility through interaction with the cytoskeleton (2). Thus, mutations that foster RAS activity are frequently found in tumors, unfortunately to this point GTPases could not be pharmacologically inhibited. However, we and others have recently identified dependency of RAS-mutant tumors primarily on the MAPK signaling pathway, which can be therapeutically targeted by small molecule kinase inhibitors (25).

Kinases altered in tumors

Sequence alterations in genes coding for kinases are the most frequent way to alter the protein function forcing the protein kinase in an “always-on” state. This leads to a permanent activation of cell internal signaling pathways and fulfillment of many of the cancer criteria proposed by Hanahan and Weinberg (6). Prominent examples are mutations in the *EGF Receptor* (9,26), the *PDGF* and *cKit* receptor tyrosine kinases in GIST tumors (27). Alternatively, kinases can be activated by amplification of the gene encoding the respective protein (e.g., *ERBB2* (28) and the proto-oncogene *MET* (29)). Fusion of a functional kinase domain of one protein to a regulatory subunit of another protein can also render a kinase domain in an “always on” state. Prominent examples are the fusion of the *ALK* kinase domain to *NPM* in anaplastic large cell lymphomas (30) and to *EML4* in lung adenocarcinomas (31). In contrast to GTPases, kinases can be pharmacologically inhibited and some are already being used today to treat cancer patients in the clinic. Examples for these “targeted drugs” are the Abl inhibitor imatinib that is being used to treat patients suffering from *BCR-Abl* positive chronic myeloid

leukemia and rare cases of *cKIT* or *PDGFRa* mutated GIST tumors (27). And also the usage of erlotinib and gefitinib, inhibitors of the *EGF receptor*, for the treatment of *EGF Receptor* mutated adenocarcinomas of the lung (9).

The family of Fibroblast Growth factors receptors (FGFRs)

FGFRs belong to the class of membrane located receptor tyrosine kinases (RTKs) and the family consists of four members (termed *FGFR1* to 4). *FGFRs* are expressed in the variety of tissues, play an important role during embryonic development and, in later live, during all major tissue regeneration processes (32). *FGFRs* are activated upon binding of fibroblast growth factors (FGFs), followed by dimerisation of *FGFR* monomers and activation of downstream signaling proteins, such as *FRS2* (32). Following activation, the *MAPK* pathway gets predominately activated and transfers signals throughout the cell, controlling differentiation, proliferation and anti-apoptosis. *FGFRs* mutations have been predominantly found in breast carcinomas (<http://www.sanger.ac.uk/genetics/CGP/cosmic/>), but also in various other cancer types. Recent studies of *FGFRs* in ovarian (33), Breast (34) and squamous cell lung tumors (35) have clearly evidenced a role for *FGFRs* in cancer development.

3.4 The Oncogene dependency model

In most tumors, a plethora of genomic alterations synergistically cause the malignant phenotype. In most cases inhibition of one gain-of-function aberration alone is therefore not sufficient to inhibit tumor progression. However, in a fraction of tumors, one genomic aberration is driving the whole malignant phenotype and rendering the whole tumor solely dependent on this one aberration (36). These alterations are mostly gain-of-function mutations of tyrosine kinases (e.g., *EGFR*, *PDGFRa* or *cKit* mutations), as well as fusion of two protein parts (e.g., *BCR-Abl* or *EML4-Alk*). Unfortunately, all oncogenic driver oncogenes identified so far are only active in tumors originating from tissues where these genes harbor a physiological function. Therefore, extensive research is necessary to identify driver genes for each single tumor type. Examples of oncogenes, already being used in the clinic as molecular targets, include the fusion proteins *BCR-ABL* (37) and *EML4-Alk* (38) as well as mutated *EGFR* (9). The presence of such targets further demonstrates the necessity to examine the tumor of each patient for alterations of known oncogenes that are predictive to certain treatments. Clinically, dependency on the function of a single protein alone opens a unique therapeutic opportunity since inhibition of this protein has a severe effect on the tumor, but much less so on healthy cells in the body. For example, patients suffering from *EGFR* mutated lung adenocarcinomas that are being treated with targeted therapeutics show a significant longer overall survival when compared to treatment with standard chemotherapy (39).

Taken together, each tumor harbors a unique set of genomic alterations leading to a set of abilities a tumor requires to become fully transformed. Although many mutations are found in tumors, only a handful of oncogenes and tumor suppressor genes are affected. In some cases even one mutation is sufficient to enable the specific malignant phenotype. These observations lead to the following conclusions: First, more research for each tumor type is necessary to identify genes that can drive the malignant phenotype. Second, intensive research is necessary to identify downstream pathway usage in tumors; that would lead to an enhanced understanding of tumor biology and also for novel treatment option in the clinic.

3.5 The pathology of lung cancer

Lung cancer is a disease of tumor formation in the lung, eventually followed by metastazation into the body. It is the leading cause of cancer-related death worldwide (1.4 million in 2008, <http://globocan.iarc.fr>). Histologically, lung cancer is separated in two major subtypes; non-small cell (NSCLC) and small cell (SCLC) lung cancer. This classification was originally based on the size of cells seen by microscopic examination and mitotic cell division rate.

SCLC typically arises from airway bronchioles and rapidly increases in size due to an average tumor doubling time of 81 days (40,41). SCLC tumors initially respond dramatically to chemotherapy and radiation treatment but almost all patients suffer from a recurrence; a re-grown tumor being mostly resistant to the initial treatment (41). Five-year overall survival rate for extensive disease SCLCs is below 5 % (42).

NSCLC is further divided into several subtypes, depending on the tissue of origin; with adenocarcinomas and squamous-cell carcinomas being the most common subtypes (42). Adenocarcinomas arise from epithelial cells, forming glandular tissue in the periphery of the alveolar system. They account for approximately 40% (43) of all lung cancer cases, whereas squamous-cell lung carcinomas arise from epithelial cells that form a layer covering the main bronchus. They account for 30 to 35% of all lung cancer cases (43) and are almost invariably associated with smoking (44). Large-cell carcinoma is another histological subtype. In rare cases, these tumors a neuroendocrine differentiation and are thus called large-cell neuroendocrine lung cancer.

Other tumors occurring in the lung include carcinoids, sarcomas and metastases from tumors originating from other sites (e.g., colonic adenocarcinomas).

Of all lung cancer cases, about 90% are most likely being caused by exposure to tobacco smoke (44). In addition to smoking further carcinogens were described such as (Asbestos, Radon, and passive smoking). In about 10 percent of patients with lung cancer no environmental influence causative for lung cancer can be detected. As shown below, lung tumors in these patients are mainly driven by specific oncogenic lesions. Overall, the five year survival rate of all lung cancer patients strongly depends on the stage they are diagnosed at and varies from 80% (stage I) to less than 1% (stageIV, Table 1, (42)).

Table 1. Survival rate strongly correlates with stage at diagnosis (Schmoll 4th Edition,2005)

Stage	5 year survival rate with treatment	
	SCLC	Non SCLC
Limited disease	10-15%	
Extensive disease	5%	
Stage Ia		75-80%
Stage Ib+IIa		55-60%
Stage IIb		35-45%
Stage IIIa		~25%
Stage IIIb		5%
Stage IV		<1%

3.6 Treatment of lung cancer

The identification of the exact tumor type from each patient is mandatory to choose the optimal treatment strategy. Patients suffering from a SCLC tumor are initially treated with chemotherapy and radiation of the affected area (42). As mentioned above, these tumors inevitably recur after an initial response and lead to rapid death of the patient. Patients with non-small cell lung tumors (stage I to IIIa) undergo surgery, frequently in combination with chemotherapy (45) leading to a stage-dependent median overall survival of up to 80% for stage I and ~23% for stage IIIa patients (Table1). Most patients present with advanced stage lung cancer (IIIb/IV) and cannot undergo complete resection with a curative intention. For these patients palliative chemotherapy is the only therapeutic option and the five-year survival rate is very low (<5%)(42).

Recent advances in the understanding of the molecular biology of lung adenocarcinomas have led to the identification of genomic alterations with therapeutic implications. In 2004 mutations in the Epidermal Growth Factor Receptor (*EGFR*) were discovered in tumors of patients that responded to the *EGFR* inhibitor gefitinib (9,26). Depending on ethnicity, gender and smoking status *EGFR* mutant

tumors account for up to 20-30% of all lung adenocarcinomas. *EGFR* mutations are strongly enriched in tumors of never-smokers, females or patients of Asian origin (46,47). Treatment of these patients with the *EGFR* inhibitors erlotinib or gefitinib leads to significantly prolonged progression-free survival time compared to treatment with standard chemotherapy (39,48) leading to a long overall survival of greater than 2 years (49). More recently, the first recurrent translocation in a solid tumor involving a tyrosine kinase was identified in lung cancer. In a subset of lung adenocarcinomas (around 3%) a chimeric transcript was discovered that encodes a fusion protein involving the *EML4* and *ALK* proteins (31). The chimeric protein exhibits constitutive kinase activity leading to malignant transformation *in-vitro* (31) and *in-vivo* (50) and induces dependency on *ALK* kinase activity. Of note, patients harboring *EML4-ALK* translocated tumors, dramatically respond to the small molecule inhibitor crizotinib (38). Unfortunately, overtime, all tumors become resistant to treatment with *EGFR*-TKIs and crizotinib. Several resistance mechanisms have been identified in *EGFR* mutant lung cancer. For example 50% of all *EGFR* mutant lung tumors acquire a secondary mutation in gene sequence coding for the *EGFR* protein, leading to an aminoacid change from tyrosine to methionine at position 790 in the kinase domain. As a result, *EGFR* inhibitors are unable to gain access to the ATP binding pocket and abrogate the emerging signal (51,52). Other resistance mechanisms identified so far, include the amplification of the proto-oncogene *MET* (29), enabling the cells to rely on another RTK-survival signal and loss of the tumor suppressor *pTEN*, enabling the cells to prolong the activation of PI3K signal (23). Therefore, more research is necessary to identify and understand the biology of resistance mechanisms and transfer this knowledge into clinical relevant treatment options.

Taken together, these findings show that - although not the most effective - chemo and radiation therapy is still the first treatment option for most lung cancer tumor (42,45). Recent breakthroughs in the field of tumor biology lead to the identification of genomic alterations, which render a tumor sensitive to its abrogation. It is imperative to screen patients for the presence of such alterations and stratify treatment accordingly.

Unfortunately, these discoveries have so far been limited to the rare adenocarcinoma subtype of lung cancer occurring in patients who had never smoked. In squamous-cell lung cancer, frequent amplifications of the *SOX2* lineage transcription factor gene were recently discovered by high-resolution genomic profiling of primary lung cancer specimens (53). However, at this point, therapeutic interdiction of transcription factor function is not chemically feasible. Thus, therapeutically tractable genetic alterations had so far been missing in this lung cancer subtype that is invariably associated with smoking and characterized by resistance to therapy and lethality.

3. Aims of the thesis

The Ph.D thesis presented here, aims to answer two major questions.

1. To identify novel dependencies of lung cancers on genetically activated oncoproteins

Primarily, this goal will be pursued by screening of genomically annotated lung cancer cell lines against large libraries of inhibitors of various oncogenic signaling pathways. We will determine the primary driving genetic alteration by computational prediction, followed by functional cell biology validation. To this end, orthogonal cellular and mouse models of cancer will be employed involving various types of genetic and pharmacological manipulation.

2. To characterize functionally, both qualitatively and quantitatively, the signaling pathways engaged by mutant oncoproteins in lung cancer

The availability of genetically defined cellular models as well as genetically manipulated isogenic cell lines enables us to study in detail the functional consequences of oncogenic addiction through oncogene activation. We will apply both gene knockdown techniques (lentiviral RNA interference by hairpin RNAs) as well as a chemical genetics method exploiting structure-based predictions of compound binding. Herein, engineered resistant variants of the target protein will be employed to formally validate the impact of a given compound on a predicted target. These experiments will be complemented by conventional signaling studies involving biochemical techniques.

4. Publications with own contributions

4.1 PTEN Loss Contributes to Erlotinib Resistance in EGFR-Mutant Lung Cancer by Activation of Akt and EGFR

Martin L. Sos, Mirjam Koker, Barbara A. Weir, Stefanie Heynck, Rosalia Rabinovsky, Thomas Zander, Jens M. Seeger, Jonathan Weiss, Florian Fischer, Peter Frommolt, Kathrin Michel, Martin Peifer, Craig Mermel, Luc Girard, Michael Peyton, Adi F. Gazdar, John D. Minna, Levi A. Garraway, Hamid Kashkar, William Pao, Matthew Meyerson and Roman K. Thomas

Original abstract of the publication

Clinical resistance to epidermal growth factor receptor (EGFR) inhibition in lung cancer has been linked to the emergence of the EGFR T790M resistance mutation or amplification of *MET*. Additional mechanisms contributing to EGFR inhibitor resistance remain elusive. By applying combined analyses of gene expression, copy number, and biochemical analyses of EGFR inhibitor responsiveness, we identified heterozygous loss of *PTEN* to segregate EGFR dependent and EGFR-independent cells. We show that in EGFR-dependent cells, *PTEN* loss partially uncouples mutant EGFR from downstream signaling and activates EGFR, thereby contributing to erlotinib resistance. The clinical relevance of our findings is supported by the observation of *PTEN* loss in 1 out of 24 primary EGFR-mutant non-small cell lung cancer (NSCLC) tumors. These results suggest a novel resistance mechanism in EGFR-mutant NSCLC tumors.

Own contributions

In this project, my responsibility was to validate the activation of Akt as one of the required effectors of *PTEN* loss in the setting of acquired erlotinib resistance. These experiments involved packaging the cDNA encoding the Akt protein fused to a myristilation tag into replication incompetent retroviruses. The myr-tag forces the localization to the cell membrane and thereby rendering Akt to be constitutively active. I subsequently performed transduction of H3255 cells with these retroviral particles, followed by Puromycin selection to obtain stable clones. I further treated these cells with different concentrations of erlotinib, prepared protein lysates and westernblots to determine the phosphorylation levels of EGFR and Akt, demonstrating that in parental and transduced H3255 cells phosphorylation of EGFR is lost upon treatment with erlotinib. As expected, phosphorylation of Akt is lost in parental, but not in H3255 cells expressing myristilated Akt. These results clearly showed that, in H3255 cells, EGFR signals downstream to Akt and furthermore that this signal could be rescued by expressing the constitutive active version of Akt. I further prepared the figure 4c as seen in the publication.

Concluding remarks

Understanding resistance mechanisms to tumor therapies is mandatory to explore new treatment options for patients in a relapsed clinical setting and important to gain new insights into tumor biology. In this study, *PTEN* deletions were identified as a possible mechanism for acquired EGFR inhibitor resistance by a prolonged and stronger activation of the PI3K pathway. This finding suggests to analyze primary patient tumors for pre-existing or, in a relapsed situation, acquired *PTEN* deletions. Moreover, our finding strongly suggests to treat these patients with PI3K pathway inhibitors in order to circumvent the effect of *PTEN* deletions.

PTEN Loss Contributes to Erlotinib Resistance in EGFR-Mutant Lung Cancer by Activation of Akt and EGFR

Martin L. Sos,¹ Mirjam Koker,¹ Barbara A. Weir,⁵ Stefanie Heynck,¹ Rosalia Rabinovsky,⁶ Thomas Zander,² Jens M. Seeger,³ Jonathan Weiss,¹ Florian Fischer,¹ Peter Frommolt,⁴ Kathrin Michel,¹ Martin Peifer,¹ Craig Mermel,^{5,6} Luc Girard,⁹ Michael Peyton,⁹ Adi F. Gazdar,^{9,10} John D. Minna,^{9,11} Levi A. Garraway,^{5,6,7} Hamid Kashkar,³ William Pao,¹² Matthew Meyerson,^{5,6,7,8} and Roman K. Thomas^{1,2,13}

¹Max-Planck-Institute for Neurological Research with Klaus-Joachim Zülch Laboratories of the Max-Planck-Society and the Medical Faculty of the University of Köln, ²Department I of Internal Medicine and Center of Integrated Oncology, University of Köln, ³Institute for Medical Microbiology, Immunology and Hygiene, and ⁴Institute for Medical Statistics, Informatics and Epidemiology, Köln, Germany; ⁵The Broad Institute of Harvard and MIT, Cambridge, Massachusetts; ⁶Department of Medical Oncology and ⁷Center for Cancer Genome Discovery, Dana-Farber Cancer-Institute, and ⁸Department of Pathology, Harvard Medical School, Boston, Massachusetts; ⁹Hamon Center for Therapeutic Oncology Research, and Departments of ¹⁰Pathology and ¹¹Internal Medicine and Pharmacology, University of Texas Southwestern Medical Center, Dallas, Texas; ¹²Human Oncology and Pathogenesis Program, Memorial Sloan-Kettering Cancer Center, New York, New York; and ¹³Chemical Genomics Center of the Max-Planck-Society, Dortmund, Germany

Abstract

Clinical resistance to epidermal growth factor receptor (EGFR) inhibition in lung cancer has been linked to the emergence of the EGFR T790M resistance mutation or amplification of *MET*. Additional mechanisms contributing to EGFR inhibitor resistance remain elusive. By applying combined analyses of gene expression, copy number, and biochemical analyses of EGFR inhibitor responsiveness, we identified homozygous loss of *PTEN* to segregate EGFR-dependent and EGFR-independent cells. We show that in EGFR-dependent cells, *PTEN* loss partially uncouples mutant EGFR from downstream signaling and activates EGFR, thereby contributing to erlotinib resistance. The clinical relevance of our findings is supported by the observation of *PTEN* loss in 1 out of 24 primary EGFR-mutant non-small cell lung cancer (NSCLC) tumors. These results suggest a novel resistance mechanism in EGFR-mutant NSCLC involving *PTEN* loss. [Cancer Res 2009;69(8):3256–61]

Introduction

Activating mutations in the epidermal growth factor receptor (EGFR) are present in ~10% of non-small cell lung cancers (NSCLC) in Caucasian patients and in up to 40% of East-Asian patients. By contrast, EGFR mutations are much more rare in African Americans. These mutations lead to the “addiction” of mutant cells to the oncogenic signals driven by mutant EGFR. This dependency is thought to be the cause of the clinical observations that EGFR-mutant tumors shrink when treated with EGFR inhibitors (1, 2). Eventually, these tumors recur; in ~60% to 70% (3) of cases, this has been linked to the emergence of either the T790M resistance mutation of EGFR or amplification of *MET* (2–4). However, a mechanistic explanation for acquired resistance in the remaining cases is lacking.

Note: Supplementary data for this article are available at Cancer Research Online (<http://cancerres.aacrjournals.org/>).

Requests for reprints: Roman K. Thomas, Max-Planck-Institute for Neurological Research, Gleueler Street 50, Cologne 50931, Germany. Phone: 49-221-472-6259; Fax: 49-221-472-6298; E-mail: nini@nf.mpg.de.

©2009 American Association for Cancer Research.
doi:10.1158/0008-5472.CAN-08-4055

Here, we used a large collection of genomically characterized NSCLC cell lines in order to derive genomic features that segregate EGFR-dependent from EGFR-independent EGFR-mutant lung tumor cells. We combined computational, biochemical, and cellular approaches to identify novel, clinically relevant mechanisms uncoupling EGFR-dependent tumors from downstream signaling.

Materials and Methods

A detailed description of all methods is given in the Supplementary Methods. As part of a larger effort to characterize the genomes of NSCLC, we have collected 84 NSCLC cell lines, which we analyzed for chromosomal gene copy number alterations, mutations, as well as transcriptional changes. The detailed description of this collection will be published elsewhere. Here, a subset of 53 of these cell lines was studied (Supplementary Table S1). Hierarchical clustering was performed using dCHIP. Genomic lesions differentiating between erlotinib-sensitive and erlotinib-insensitive cells were analyzed by inferring the mean copy number of chromosomal windows from five contiguous loci. Statistical analyses were performed using R.

Results and Discussion

In order to analyze oncogene dependencies in lung cancer, we used a collection of 84 NSCLC cell lines that we have recently characterized in-depth genomically and phenotypically (Supplementary Table S1).¹⁴

We performed hierarchical clustering of gene expression data of 53 of these lines. In this analysis, the EGFR-mutant cell line, H1650, did not share a cluster with all other EGFR-mutant cell lines (Fig. 1A). This cell line has previously been reported to be erlotinib-resistant, despite lacking known resistance mechanisms (Fig. 1A; ref. 5).

Confirming these observations, H1650 cells were erlotinib-resistant with a half-maximal inhibitory concentration (IC₅₀) of 2.13 μmol/L (Fig. 1B). As previously reported, EGFR-mutant HCC827 cells were erlotinib-sensitive (IC₅₀, 0.02 μmol/L), whereas H1975 cells expressing both the erlotinib-sensitizing L858R mutation and the T790M resistance mutation were resistant (IC₅₀ > 10 μmol/L; Fig. 1B; refs. 5, 6). Treatment with 100 nmol/L of

¹⁴M.L. Sos et al., under revision.

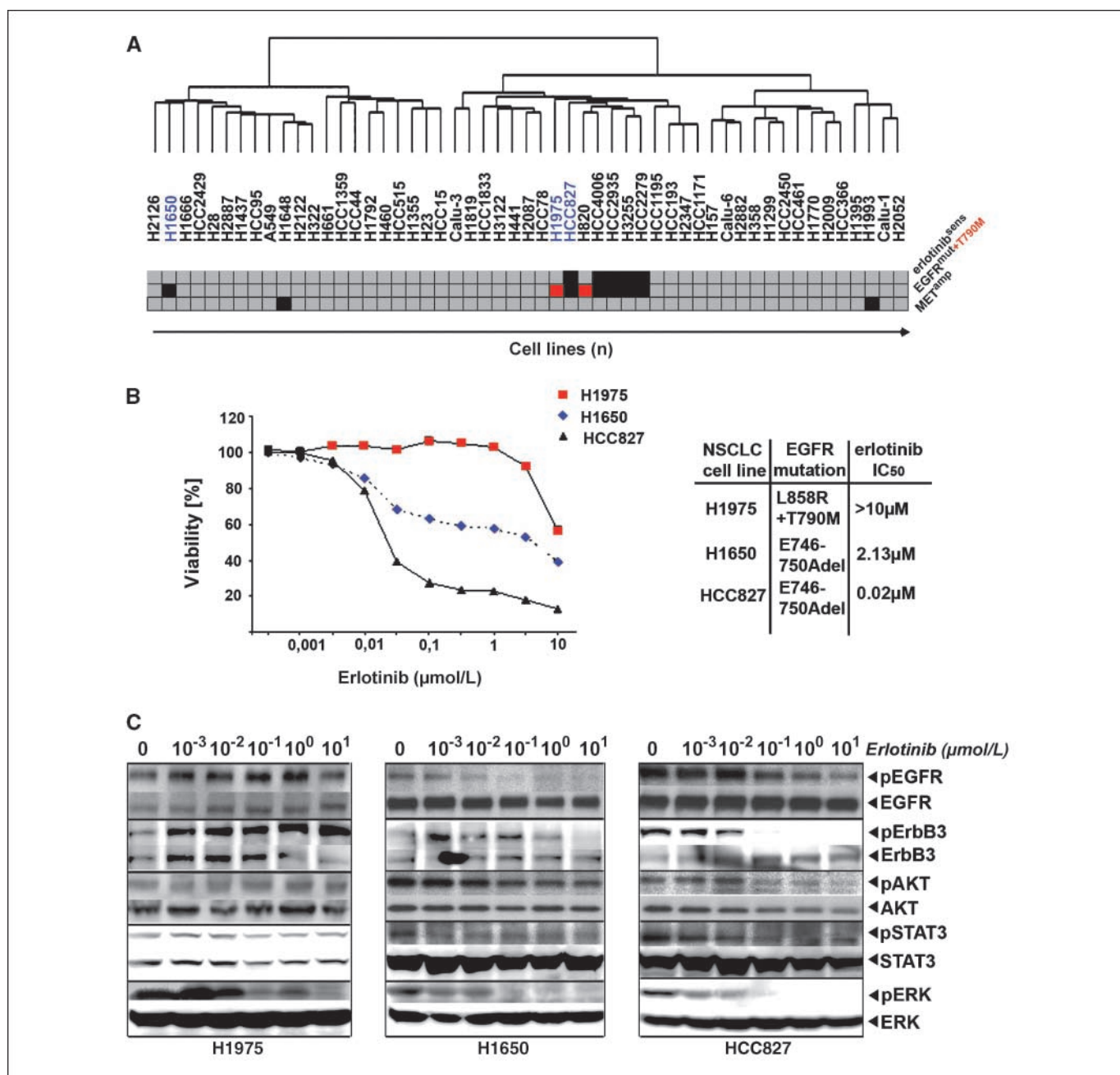


Figure 1. An EGFR independence signature in H1650 cells. *A*, hierarchical clustering of 53 NSCLC cells according to gene expression. Erlotinib sensitivity ($IC_{50} < 1 \mu\text{mol/L}$, red; $IC_{50} > 1 \mu\text{mol/L}$, gray) and EGFR mutations (EGFR-mutant, black; T790M, red; EGFR wild-type, gray) as well as MET amplification (black). *B*, left, cellular viability as a function of erlotinib dose for all three cell lines studied. Right, mutation status and IC_{50} values. *C*, cells were treated with different doses of erlotinib. Activation of EGFR and downstream signaling pathways was determined by analyzing the amount of phosphorylated versions of the respective proteins in comparison with their total levels using phosphorylation-specific antibodies.

erlotinib led to the dephosphorylation of EGFR in H1650 and HCC827 but not in H1975 cells (Fig. 1C). However, although the dephosphorylation of EGFR was accompanied by a reduction in p-Akt levels in erlotinib-sensitive HCC827 cells, H1650 cells retained high levels of p-Akt despite inhibition of EGFR (Fig. 1C). By contrast, erlotinib-mediated inhibition of known signal transducers of the EGFR such as ErbB3, STAT3, and ERK was similar to the levels observed in HCC827, consistent with the uncoupling of mutant EGFR from downstream survival signaling at the level of Akt (Fig. 1C).

We speculated that chromosomal aberrations might be causatively involved in this phenotype and sought for chromosomal regions displaying differential copy numbers between H1650 cells and the EGFR-mutant and erlotinib-sensitive cell lines. We identified 13 H1650-specific chromosomal loci harboring nine known genes, including a chromosomal region affected by homozygous deletion 3' to the locus containing the tumor suppressor gene PTEN (Fig. 2A; ref. 7). Furthermore, when analyzing the transcription of IGFBP2, a marker predictive of PTEN loss in glioblastoma (8), H1650 was the highest scoring line

in our panel (data not shown). PTEN counteracts Akt activation by dephosphorylating phosphatidylinositol-3,4,5-triphosphate (PIP3), the product of class I phosphoinositide-3-kinases (7, 9). Because *PTEN* loss has been shown to be involved in EGFR inhibitor resistance in some tumor cell lines (10, 11) and in glioblastoma patients (12), we reasoned that *PTEN* loss might also be involved in the EGFR-independent phenotype of H1650. Furthermore, lack of PTEN protein expression has previously been speculated to be involved in erlotinib resistance in H1650 cells (13, 14).

To determine whether loss of PTEN protein in H1650 cells (13, 14) might be caused by genomic loss, we mapped the *PTEN* locus by quantitative PCR. Fine-mapping followed by long-distance PCR revealed that the homozygous deletion (spanning 16.8 kb) leads to the deletion of the 3' part of exon 8 and the entire exon 9 (Fig. 2B). The deletion results in a COOH-terminally truncated protein that could only be detected using antibodies against NH₂-terminal

epitopes (Fig. 2C). Previous functional genetics experiments have shown a critical role of the COOH-terminal part of PTEN (15). Thus, the COOH-terminal deletion in H1650 cells might be causally involved in uncoupling mutant EGFR from downstream Akt survival signaling.

We next analyzed a panel of 140 primary lung adenocarcinomas (predominantly Caucasian patients), annotated for copy number alterations and mutations in 623 genes, for the presence of co-occurring lesions in *PTEN* and *EGFR* (16, 17). We found co-occurrence of homozygous deletion of *PTEN* and *EGFR* mutation in 1 out of 24 samples with *EGFR* mutations (Fig. 2D). Thus, primary resistance of EGFR-mutant NSCLC might, in rare cases, be due to homozygous loss of *PTEN*. Furthermore, we found hemizygous loss of chromosome 10 to be significantly enriched in *EGFR*-mutant patients in the cohort of 140 primary samples ($P = 0.012$; data not shown). Loss of the other allele by mutation

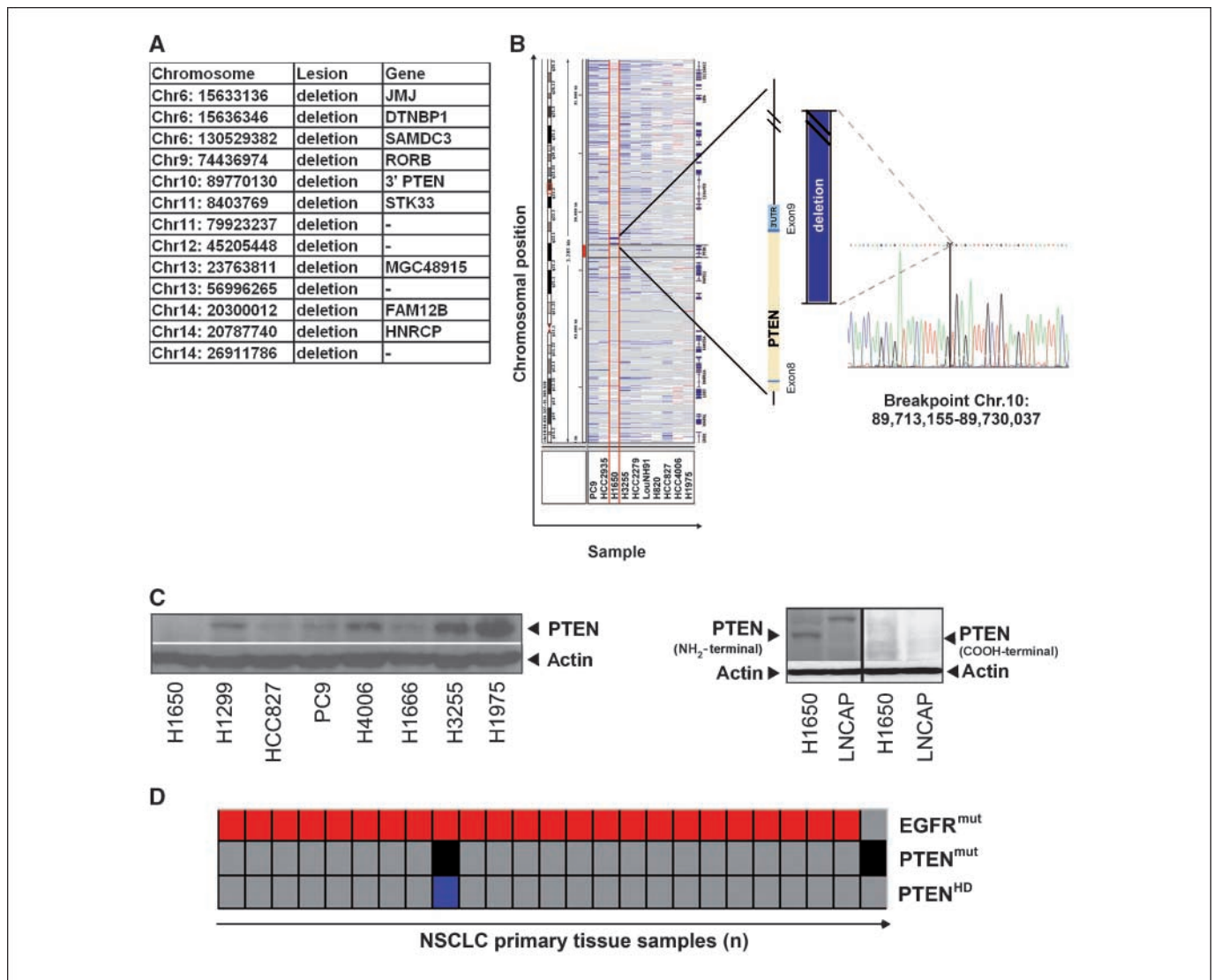


Figure 2. Genomic characterization of *PTEN* loss in H1650 cells. **A**, list of genes affected by differential lesions between H1650 cells and EGFR-mutant and erlotinib-sensitive cell lines. **B**, left, screenshot showing chromosomal aberrations at chromosome 10 (Integrative Genomics Viewer; <http://www.broad.mit.edu/igv/>) of all *EGFR*-mutant cells. Middle, 3'-region mapping of *PTEN* using quantitative PCR reveals a homozygous deletion deleting parts of exon 8 and the entire exon 9. Right, the sequence bridging the breakpoint. **C**, left, PTEN protein status determined using immunoblotting in different NSCLC cell lines. Right, NH₂-terminal and COOH-terminal PTEN detection by immunoblotting. LNCAP cells, known to express a truncated version of *PTEN*, served as controls. **D**, analysis of *EGFR* mutations (red) and homozygous deletions of *PTEN* (black) and *PTEN* mutations (blue) in 140 lung cancer biopsy specimens.

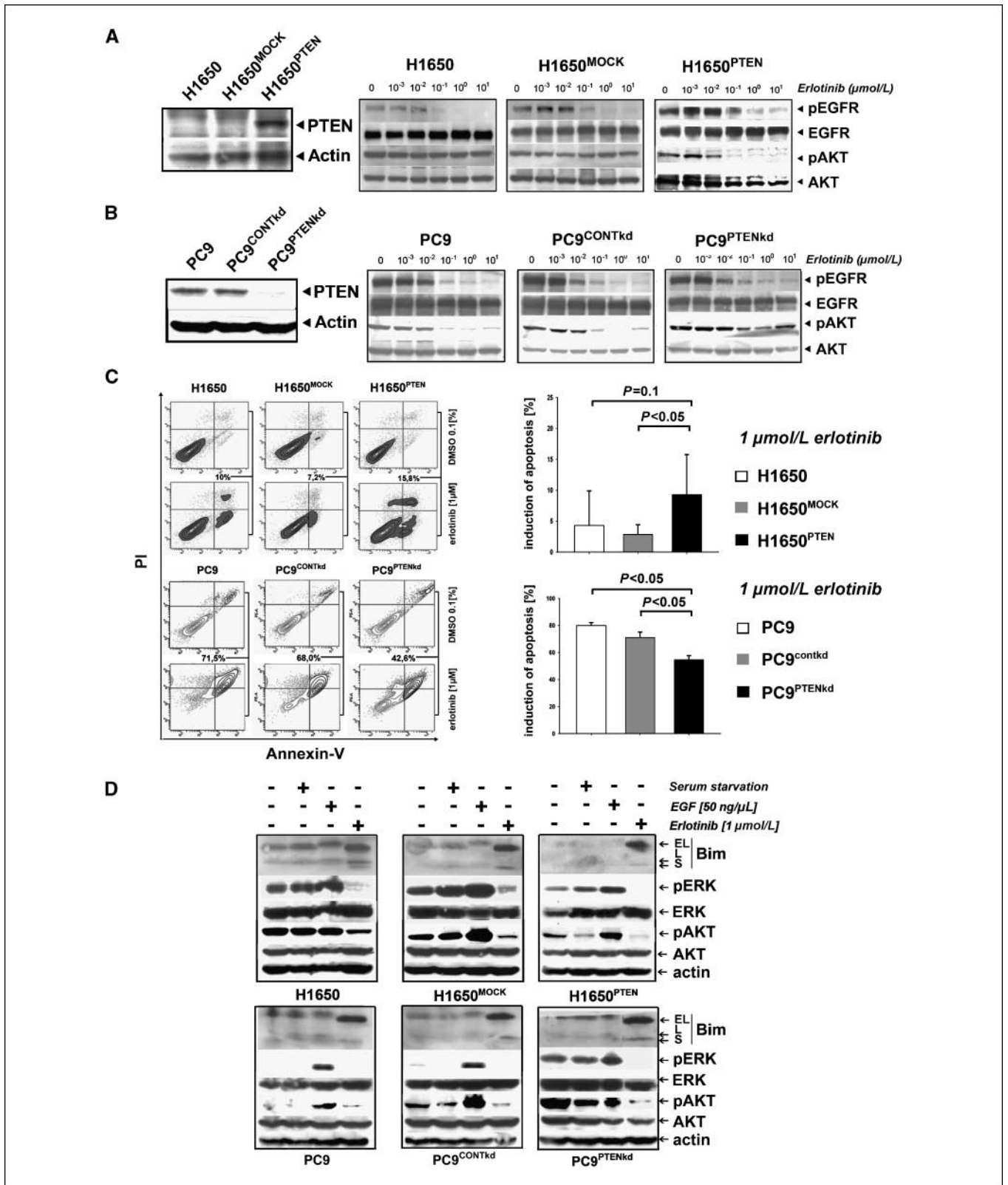


Figure 3. Erlotinib resistance in *EGFR*-mutated NSCLC with PTEN loss. *A, left*, in H1650^{PTEN} cells, PTEN levels were determined by immunoblotting. *Right*, levels of phospho-EGFR and phospho-AKT were assessed by immunoblotting in H1650, H1650^{MOCK}, and H1650^{PTEN} cells treated with erlotinib. *B, left*, in PC9^{PTENkd} cells, PTEN levels were determined by immunoblotting. *Right*, levels of phospho-EGFR and phospho-AKT were assessed in PC9, PC9^{CONTkd}, and PC9^{PTENkd} cells treated with erlotinib. *C, left*, percentage of apoptotic cells (in %, analyzed by measuring the fraction of cells positive for Annexin V and/or propidium iodide by flow cytometry) after treatment with either erlotinib (1 μmol/L) or control. *Right*, cumulative histograms of apoptosis induction. *D*, levels of Bim (EL, extra long; L, long; S, short), phospho-ERK, phospho-pAKT, and actin were measured after serum starvation (serum starvation "+"), EGF stimulation (EGF "+"), or treatment with erlotinib (1 μmol/L erlotinib "+") for 24 h.

might thus confer acquired resistance in patients initially responding to EGFR inhibition. This notion is also supported by a previous study reporting favorable survival of *EGFR*-mutant patients with high expression of PTEN (18).

We reconstituted wild-type *PTEN* in H1650 cells by stable retroviral expression (Fig. 3A). Reconstitution of *PTEN* restored coupling of the EGFR signal to downstream Akt signaling as evidenced by dephosphorylation of both EGFR and Akt upon erlotinib treatment (Fig. 3A). Cellular proliferation of H1650^{PTEN} cells treated with erlotinib was virtually identical to that seen in the parental cells (data not shown) but combinatorial treatment of H1650 cells with erlotinib and an AKT inhibitor led to a reduction of viability when compared with cells treated with erlotinib alone (Supplementary Fig. S1). However, when analyzing the fraction of cells undergoing apoptosis upon treatment with erlotinib, we observed an increase of apoptotic H1650^{PTEN} cells when compared with the parental and the mock-transduced cells (Fig. 3C). Thus, *PTEN* reconstitution increases the susceptibility to erlotinib-induced apoptosis in H1650 cells.

We next silenced *PTEN* in *EGFR*-mutant and erlotinib-sensitive PC9 cells by lentiviral short hairpin RNAs (Fig. 3B). Similar to our observation in the parental H1650 cells, *PTEN* loss in PC9 cells (PC9^{PTENkd}) induced the uncoupling of EGFR and downstream Akt signaling as shown by continuous Akt phosphorylation under

erlotinib treatment (Fig. 3B). Again, recapitulating our observations in H1650 cells, silencing of *PTEN* expression in PC9 cells led to a significant decrease in the fraction of apoptotic cells when treated with erlotinib (Fig. 3C). Induction of apoptosis in both *PTEN*-proficient and *PTEN*-deficient cells was paralleled by activation of the proapoptotic protein Bim, recently shown to play a key role in erlotinib-induced apoptosis in *EGFR*-mutant NSCLC (refs. 19, 20; Fig. 3D). Thus, the differential induction of apoptosis is not mediated through modulation of Bim levels. Interestingly, in PC9^{PTENkd} cell lines, we observed the activation of Erk under steady-state and serum-starved conditions, whereas *PTEN*-proficient cells hardly showed Erk activity (Fig. 3D). Thus, *PTEN* loss partially uncouples EGFR signaling from downstream Akt survival signaling, activates ERK, and contributes to EGFR inhibitor resistance.

While analyzing the activity of Akt in *PTEN*-deficient H1650 and PC9^{PTENkd} *EGFR*-mutant cells, we observed an increase in phospho-EGFR when compared with *PTEN*-proficient cells. In PC9^{PTENkd} cells, complete deactivation of EGFR was achieved at 750 nmol/L of erlotinib, whereas in parental and control PC9 cells, 250 nmol/L of erlotinib was sufficient to fully dephosphorylate the receptor (Fig. 4A). Thus, the resistance phenotype observed in *PTEN*-deficient H1650 cells may be partially explained by the prolonged activation of EGFR under treatment with EGFR tyrosine

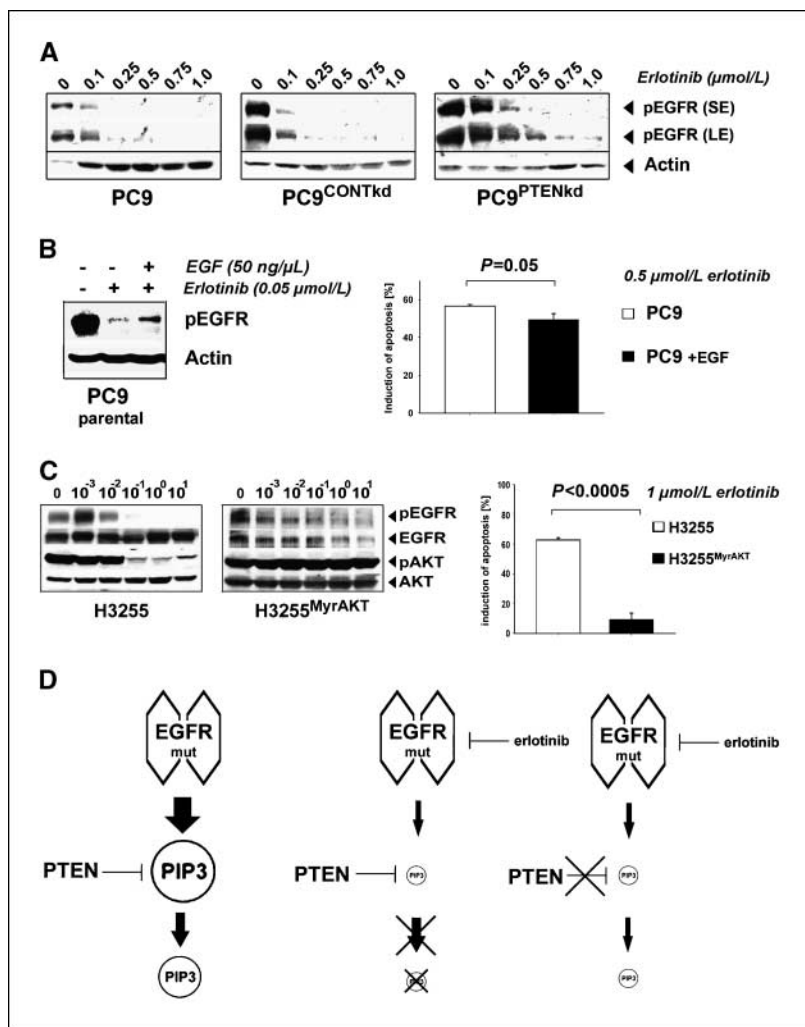


Figure 4. *PTEN* loss activates EGFR. **A**, phospho-EGFR was detected by immunoblotting after short exposure (*SE*) and long exposure (*LE*) in PC9, PC9^{CONTkd}, and PC9^{PTENkd} cells. Actin levels served as a loading control. **B, left**, levels of phospho-EGFR of PC9^{PTENkd} and PC9 cells treated with erlotinib were determined (+/- EGF) under serum starvation. **Right**, apoptosis (%) after erlotinib treatment (0.5 μmol/L) in the given cells. **C, left**, phospho-EGFR and phospho-AKT in H3255 and H3255^{MyrAKT} cells were assessed by immunoblotting. **Right**, the fraction of apoptotic cells (in %) in the given cells. **D**, a simplified model explaining our observations: in *EGFR*-mutant cells, EGFR is the sole input for production of PIP3. Inhibiting EGFR dramatically reduces the input into PIP3 production. Therefore, the lack of negative regulation of PIP3 production by loss of *PTEN* is limited.

kinase inhibitors. To test whether *PTEN* loss-induced EGFR activation may be mimicked by stimulation of EGFR in *PTEN*-proficient PC9 cells, we treated parental PC9 cells with a combination of erlotinib and EGF (Fig. 4B). We observed an induction of phospho-EGFR by dual EGF stimulation and EGFR inhibition resembling the situation in *PTEN*-deficient cells (Fig. 4B). Confirming the functional relevance of *PTEN* loss-induced EGFR activation, this treatment also led to a reduction of the fraction of apoptotic cells (Fig. 4B).

Finally, we asked whether survival signaling activated by loss of *PTEN* is equivalent to immediate activation of Akt. We introduced a constitutively active allele of Akt (MyrAkt) into *EGFR*-mutant and erlotinib-sensitive H3255 cells. As expected, levels of phospho-Akt but not of phospho-EGFR levels remained elevated in H3255^{MyrAkt} cells under erlotinib treatment (Fig. 4C). Furthermore, this pronounced Akt activity was associated with erlotinib resistance ($P < 0.0005$) of H3255^{MyrAkt} cells when measuring apoptosis (Fig. 4C). Thus, immediate and constitutive activation of Akt is more effective than *PTEN* loss to induce erlotinib resistance in *EGFR*-mutant NSCLC cells.

Others have recently shown that *PTEN* loss leads to robust EGFR inhibitor resistance in cells lacking *EGFR* mutations (10, 11). Our findings in *EGFR*-mutant NSCLC cells differ from these observations, as the phenotype elicited by *PTEN* loss was less dominant. This discrepancy may be explained by the fact that *EGFR*-mutant NSCLC cells are exclusively dependent on EGFR signaling for their survival. Thus, erlotinib-mediated inhibition of EGFR as the sole input of PIP3 production may only partially be rescued by *PTEN* loss (Fig. 4D).

In summary, we have shown that in-depth genomic and phenotypic analyses of large cell line collections can be applied to identify a novel cell biology phenotype. Here, computational genomic analyses implied homozygous deletion of *PTEN* as a candidate for EGFR inhibitor resistance. Functional studies revealed that *PTEN* loss induces a significant reduction in apoptosis sensitivity in *EGFR*-mutant cells by activation of Akt and EGFR. We speculate that activation of Erk in *PTEN*-deficient cells (Fig. 3D) may lead to transcriptional up-regulation of EGFR ligands, such as amphiregulin (21). Moreover, *PTEN* loss and *EGFR* mutation co-occurred in 1 out of 24 *EGFR*-mutant patients in a genomic analysis of 140 lung adenocarcinomas, thus confirming the clinical relevance of our findings. Thus, *PTEN* loss may represent an additional mechanism of initial or acquired resistance to erlotinib-induced apoptosis in *EGFR*-mutant NSCLC.

Disclosure of Potential Conflicts of Interest

No potential conflicts of interest were disclosed.

Acknowledgments

Received 10/21/08; revised 2/20/09; accepted 2/24/09; published OnlineFirst 4/7/09.

Grant support: R.K. Thomas is a fellow of the International Association for the Study of Lung Cancer; and is supported by the Deutsche Krebshilfe (107954), the Fritz-Thyssen-Stiftung (10.08.2.175), and the NGFN-Plus Program of the German Ministry of Science and Education (BMBF, 01GS08100). J.D. Minna is supported by grants from the Specialized Programs of Research Excellence P50CA70907, DOD PROSPECT, and the Longenbaugh Foundation.

The costs of publication of this article were defrayed in part by the payment of page charges. This article must therefore be hereby marked *advertisement* in accordance with 18 U.S.C. Section 1734 solely to indicate this fact.

We thank Dr. Ingo Mellinghoff for sharing unpublished results.

References

- Sharma SV, Fischbach MA, Haber DA, Settleman J. "Oncogenic shock": explaining oncogene addiction through differential signal attenuation. *Clin Cancer Res* 2006;12:4392-5.
- Thomas RK, Greulich H, Yuza Y, et al. Detection of oncogenic mutations in the EGFR gene in lung adenocarcinoma with differential sensitivity to EGFR tyrosine kinase inhibitors. *Cold Spring Harb Symp Quant Biol* 2005;70:73-81.
- Engelman JA, Janne PA. Mechanisms of acquired resistance to epidermal growth factor receptor tyrosine kinase inhibitors in non-small cell lung cancer. *Clin Cancer Res* 2008;14:2895-9.
- Bean J, Brennan C, Shih JY, et al. MET amplification occurs with or without T790M mutations in EGFR mutant lung tumors with acquired resistance to gefitinib or erlotinib. *Proc Natl Acad Sci U S A* 2007;104:20932-7.
- Guo A, Villen J, Kornhauser J, et al. Signaling networks assembled by oncogenic EGFR and c-Met. *Proc Natl Acad Sci U S A* 2008;105:692-7.
- Sos ML, Zander T, Thomas RK, Staratschek-Jox A, Claassen J, Wolf J. Expression of signaling mediators downstream of EGF-receptor predict sensitivity to small molecule inhibitors directed against the EGF-receptor pathway. *J Thorac Oncol* 2008;3:170-3.
- Stambolic V, Suzuki A, de la Pompa JL, et al. Negative regulation of PKB/Akt-dependent cell survival by the tumor suppressor PTEN. *Cell* 1998;95:29-39.
- Mehrian-Shai R, Chen CD, Shi T, et al. Insulin growth factor-binding protein 2 is a candidate biomarker for PTEN status and PI3K/Akt pathway activation in glioblastoma and prostate cancer. *Proc Natl Acad Sci U S A* 2007;104:5563-8.
- Sansal I, Sellers WR. The biology and clinical relevance of the PTEN tumor suppressor pathway. *J Clin Oncol* 2004;22:2954-63.
- Yamasaki F, Johansen MJ, Zhang D, et al. Acquired resistance to erlotinib in A-431 epidermoid cancer cells requires down-regulation of MMAC1/PTEN and up-regulation of phosphorylated Akt. *Cancer Res* 2007;67:5779-88.
- She QB, Solit DB, Ye Q, O'Reilly KE, Lobo J, Rosen N. The BAD protein integrates survival signaling by EGFR/MAPK and PI3K/Akt kinase pathways in PTEN-deficient tumor cells. *Cancer Cell* 2005;8:287-97.
- Mellinghoff IK, Wang MY, Vivanco I, et al. Molecular determinants of the response of glioblastomas to EGFR kinase inhibitors. *N Engl J Med* 2005;353:2012-24.
- McDermott U, Sharma SV, Dowell L, et al. Identification of genotype-correlated sensitivity to selective kinase inhibitors by using high-throughput tumor cell line profiling. *Proc Natl Acad Sci U S A* 2007;104:19936-41.
- Rikova K, Guo A, Zeng Q, et al. Global survey of phosphotyrosine signaling identifies oncogenic kinases in lung cancer. *Cell* 2007;131:190-203.
- Georgescu MM, Kirsch KH, Akagi T, Shishido T, Hanafusa H. The tumor-suppressor activity of PTEN is regulated by its carboxyl-terminal region. *Proc Natl Acad Sci U S A* 1999;96:10182-7.
- Weir BA, Woo MS, Getz G, et al. Characterizing the cancer genome in lung adenocarcinoma. *Nature* 2007;450:893-8.
- Ding L, Getz G, Wheeler DA, et al. Somatic mutations affect key pathways in lung adenocarcinoma. *Nature* 2008;455:1069-75.
- Endoh H, Yatabe Y, Kosaka T, Kuwano H, Mitsudomi T. PTEN and PIK3CA expression is associated with prolonged survival after gefitinib treatment in EGFR-mutated lung cancer patients. *J Thorac Oncol* 2006;1:629-34.
- Gong Y, Somwar R, Politi K, et al. Induction of BIM is essential for apoptosis triggered by EGFR kinase inhibitors in mutant EGFR-dependent lung adenocarcinomas. *PLoS Med* 2007;4:e294.
- Deng J, Shimamura T, Perera S, et al. Proapoptotic BH3-only BCL-2 family protein BIM connects death signaling from epidermal growth factor receptor inhibition to the mitochondrion. *Cancer Res* 2007;67:11867-75.
- Toulany M, Baumann M, Rodemann HP. Stimulated PI3K-AKT signaling mediated through ligand or radiation-induced EGFR depends indirectly, but not directly, on constitutive K-Ras activity. *Mol Cancer Res* 2007;5:863-72.

4.2 Predicting drug susceptibility of non–small cell lung cancers based on genetic lesions

Martin L. Sos, Kathrin Michel, Thomas Zander, Jonathan Weiss, Peter Frommolt, Martin Peifer, Danan Li, Roland Ullrich, Mirjam Koker, Florian Fischer, Takeshi Shimamura, Daniel Rauh, Craig Mermel, Stefanie Fischer, Isabel Stückrath, Stefanie Heynck, Rameen Beroukhim, William Lin, Wendy Winckler, Kinjal Shah, Thomas LaFramboise, Whei F. Moriarty, Megan Hanna, Laura Tolosi, Jörg Rahnenführer, Roel Verhaak, Derek Chiang, Gad Getz, Martin Hellmich, Jürgen Wolf, Luc Girard, Michael Peyton, Barbara A. Weir, Tzu-Hsiu Chen, Heidi Greulich, Jordi Barretina, Geoffrey I. Shapiro, Levi A. Garraway, Adi F. Gazdar, John D. Minna, Matthew Meyerson, Kwok-Kin Wong, and Roman K. Thomas

Abstract of the publication

Somatic genetic alterations in cancers have been linked with response to targeted therapeutics by creation of specific dependency on activated oncogenic signaling pathways. However, no tools currently exist to systematically connect such genetic lesions to therapeutic vulnerability. We have therefore developed a genomics approach to identify lesions associated with therapeutically relevant oncogene dependency. Using integrated genomic profiling, we have demonstrated that the genomes of a large panel of human non–small cell lung cancer (NSCLC) cell lines are highly representative of those of primary NSCLC tumors. Using cell-based compound screening coupled with diverse computational approaches to integrate orthogonal genomic and biochemical data sets, we identified molecular and genomic predictors of therapeutic response to clinically relevant compounds. Using this approach, we showed that v-Ki-ras2 Kirsten rat sarcoma viral oncogene homolog (KRAS) mutations confer enhanced Hsp90 dependency and validated this finding in mice with KRAS driven lung adenocarcinoma, as these mice exhibited dramatic tumor regression when treated with an Hsp90 inhibitor. In addition, we found that cells with copy number enhancement of v-abl Abelson murine leukemia viral oncogene homolog 2 (ABL2) and ephrin receptor kinase and v-src sarcoma (Schmidt-Ruppin A-2) viral oncogene homolog (avian) (SRC) kinase family genes were exquisitely sensitive to treatment with the SRC/ABL inhibitor dasatinib, both in vitro and when it xenografted into mice. Thus, genomically annotated cell-line collections may help translate cancer genomics information into clinical practice by defining critical pathway dependencies amenable to therapeutic inhibition.

Own contributions

For this study, I collected data for main figure 3 where I screened half of the cell lines displayed against the small molecule inhibitor dasatinib. Together with Roman Thomas, I developed the algorithm that led to the identification of the human *avian sarcoma (Schmidt-ruppin A-2) viral oncogene (cSRC)* gene as the putative target of dasatinib in the H322M cell line. I was also leading the team's efforts to validate this finding that was critical for the resulting manuscript. To confirm this finding, I packaged pLKO vectors containing either no insert or a shRNA construct targeting the mRNA encoding the tyrosine kinase SRC into lentiviral particles. I next transduced H322M cells with these particles and confirmed that knockdown of SRC in this cell line leads to a profound reduction in proliferation. I also confirmed loss of SRC protein by westernblot analysis. Furthermore, I performed site-directed mutagenesis (SDM) to alter the aminoacid sequence of the SRC protein from a tyrosine at position 341 to a methionine. The methionine at this position clashes with dasatinib and hinders the entrance into the ATP-binding pocket, hence rendering this SRC version resistant to dasatinib. I packaged the cDNA encoding either wildtype or T341M mutated SRC into retroviral particles, transduced H322M cells and selected with Puromycin to obtain stable insert expressing cells. I further treated these cells with dasatinib and could show that expressing T341M but not wildtype SRC protein rescues the dasatinib induced phenotype. Together, these results proved that SRC was the relevant target of dasatinib in the cells carrying the SRC gene amplification. Moreover, I packaged lentiviral particles containing a shRNA construct targeting the mRNA of KRAS, and subsequently

performed KRAS knockdown in A549 cells, which I also confirmed by western blots (Supplementary figure 7 B). For supplementary figure 9, I performed treatment of H322M cell with increasing doses of dasatinib and subsequently determined the level of phosphorylated SRC protein. My data directly lead to figures 6 B and C in the main part and figures 7 B and 9 B. I prepared figures 3, 6 (B and C) and also supplementary figures 7B and 9B as seen in the manuscript. I also was involved in writing and editing of the manuscript prior to submitting to the Journal of Clinical Investigation.

Unpublished data

I further treated H322M cells expressing either wildtype or mutated SRC with different concentrations of dasatinib. Westernblot analysis confirmed the absence of phosphorylated SRC protein in H322M cells expressing wildtype, but not in H322M cells expressing T314M mutated SRC. Additionally, I sequenced *EPHA3*, one of the top dasatinib targets, in the five most dasatinib sensitive cell lines. However, we did not observe any mutation as a cause of sensitivity, suggesting that amplification rather than mutation of *EPHA3* was associated with sensitivity to dasatinib.

Concluding remarks

This study aimed at the establishment of a cell line-based screening platform that allows a systematical search for potential novel drug targets in non-small cell lung cancer. First we confirmed that a large panel of lung tumor derived cell lines adequately reflects the genomic landscape of primary lung tumors. In a proof-of-concept experiment by using the above mentioned screening platform, we identified genomic *EGFR* aberrations in conjunction with absent *KRAS* mutations as the most significant predictor for EGFR inhibitor sensitivity, as also been shown by other groups in the field. In addition we identified two possible therapeutic targets in non-small cell lung cancer. First, we identified *KRAS* mutant cell lines to be more susceptible towards HSP90 inhibitors and second, we identified solitary *SRC* amplifications in a cell line as being a predictive marker and the functional relevant target of dasatinib. Taken together, screening of large numbers of lung tumor derived cell lines can be utilized to identify novel oncogenes in this deadly disease.



Predicting drug susceptibility of non–small cell lung cancers based on genetic lesions

Martin L. Sos,¹ Kathrin Michel,¹ Thomas Zander,² Jonathan Weiss,¹ Peter Frommolt,³ Martin Peifer,¹ Danan Li,⁴ Roland Ullrich,¹ Mirjam Koker,¹ Florian Fischer,¹ Takeshi Shimamura,⁴ Daniel Rauh,⁵ Craig Mermel,^{4,6} Stefanie Fischer,¹ Isabel Stückerath,¹ Stefanie Heynck,¹ Rameen Beroukhi,^{4,6} William Lin,^{4,6} Wendy Winckler,^{4,6} Kinjal Shah,^{4,6} Thomas LaFramboise,⁷ Whei F. Moriarty,^{4,6} Megan Hanna,^{4,6} Laura Tolosi,⁸ Jörg Rahnenführer,⁹ Roel Verhaak,^{4,6} Derek Chiang,^{4,6} Gad Getz,⁶ Martin Hellmich,³ Jürgen Wolf,² Luc Girard,¹⁰ Michael Peyton,¹⁰ Barbara A. Weir,^{4,6} Tzu-Hsiu Chen,^{4,6} Heidi Greulich,^{4,6} Jordi Barretina,^{4,6,11} Geoffrey I. Shapiro,⁴ Levi A. Garraway,^{4,6,11,12} Adi F. Gazdar,^{10,13} John D. Minna,^{10,14} Matthew Meyerson,^{4,6,11,12} Kwok-Kin Wong,^{4,15} and Roman K. Thomas^{1,2,5}

¹Max Planck Institute for Neurological Research, Klaus-Joachim-Zülch Laboratories of the Max Planck Society, and University of Köln Medical Faculty, ²Department I of Internal Medicine and Center of Integrated Oncology Köln-Bonn, and ³Institute of Medical Statistics, Informatics and Epidemiology, University of Köln, Cologne, Germany. ⁴Department of Medical Oncology, Dana-Farber Cancer Institute, Harvard Medical School, Boston, Massachusetts, USA. ⁵Chemical Genomics Center of the Max Planck Society, Dortmund, Germany. ⁶Broad Institute of MIT and Harvard, Cambridge, Massachusetts, USA. ⁷Department of Genetics, Case Western Reserve University School of Medicine, Cleveland, Ohio, USA. ⁸Max Planck Institute for Informatics, Saarbrücken, Germany. ⁹Department of Statistics, Technical University of Dortmund, Dortmund, Germany. ¹⁰Hamon Center for Therapeutic Oncology Research, University of Texas Southwestern Medical Center, Dallas, Texas, USA. ¹¹Center for Cancer Genome Discovery, Dana-Farber Cancer Institute, Harvard Medical School, Boston, Massachusetts, USA. ¹²Department of Medicine, Brigham and Women's Hospital and Harvard Medical School, Boston, Massachusetts, USA. ¹³Department of Pathology and ¹⁴Departments of Internal Medicine and Pharmacology, University of Texas Southwestern Medical Center, Dallas, Texas, USA. ¹⁵Ludwig Center, Dana-Farber Cancer Institute, Harvard Medical School, Boston, Massachusetts, USA.

Somatic genetic alterations in cancers have been linked with response to targeted therapeutics by creation of specific dependency on activated oncogenic signaling pathways. However, no tools currently exist to systematically connect such genetic lesions to therapeutic vulnerability. We have therefore developed a genomics approach to identify lesions associated with therapeutically relevant oncogene dependency. Using integrated genomic profiling, we have demonstrated that the genomes of a large panel of human non–small cell lung cancer (NSCLC) cell lines are highly representative of those of primary NSCLC tumors. Using cell-based compound screening coupled with diverse computational approaches to integrate orthogonal genomic and biochemical data sets, we identified molecular and genomic predictors of therapeutic response to clinically relevant compounds. Using this approach, we showed that v-Ki-ras2 Kirsten rat sarcoma viral oncogene homolog (KRAS) mutations confer enhanced Hsp90 dependency and validated this finding in mice with KRAS-driven lung adenocarcinoma, as these mice exhibited dramatic tumor regression when treated with an Hsp90 inhibitor. In addition, we found that cells with copy number enhancement of v-abl Abelson murine leukemia viral oncogene homolog 2 (ABL2) and ephrin receptor kinase and v-src sarcoma (Schmidt-Ruppin A-2) viral oncogene homolog (avian) (SRC) kinase family genes were exquisitely sensitive to treatment with the SRC/ABL inhibitor dasatinib, both in vitro and when it xenografted into mice. Thus, genomically annotated cell-line collections may help translate cancer genomics information into clinical practice by defining critical pathway dependencies amenable to therapeutic inhibition.

Introduction

The dynamics of ongoing efforts to fully annotate the genomes of all major cancer types are reminiscent of those of the Human Genome Project. The analysis of somatic gene copy number alterations and gene mutations associated with cancer (both

here referred to as *lesions*) will thus provide the genetic landscape of human cancer in the near future. The medical implications of these endeavors are exemplified by the success of molecularly targeted cancer therapeutics in genetically defined tumors: the ERBB2/Her2-targeted (where ERBB2 is defined as *v-erb b2 eryth-*

Authorship note: Martin L. Sos, Kathrin Michel, Thomas Zander, Peter Frommolt, and Jonathan Weiss contributed equally to this work.

Conflict of interest: R.K. Thomas has received research support from AstraZeneca. J. Wolf has received research support from Novartis and Roche. A.F. Gazdar has served as a consultant/lecturer for AstraZeneca, Genentech, and Boehringer Mannheim. L.A. Garraway has received research support from and served as a consultant for Novartis. M. Meyerson is a consultant for and received research funding from Novartis. M. Meyerson is an inventor on a patent describing EGFR mutation testing as a diagnostic test.

Nonstandard abbreviations used: 17-AAG, 17-(allylamino)-17-demethoxygeldanamycin; ABL2, v-abl Abelson murine leukemia viral oncogene homolog 2; BCR, breakpoint cluster region; BRAF, v-raf murine sarcoma viral oncogene homolog B1; 17-DMAG, 17-(dimethylaminoethylamino)-17-demethoxygeldanamycin; ERBB2, v-erb b2 erythroblastic leukemia viral oncogene homolog 2, neuro/glioblastoma-derived oncogene homolog (avian); GI₅₀, half-maximal growth inhibitory concentrations; GISTIC, Genomic Identification of Significant Targets in Cancer; KIT, v-kit Hardy-Zuckerman 4 feline sarcoma viral oncogene homolog; KNN, K-nearest-neighbor; KRAS, v-Ki-ras2 Kirsten rat sarcoma viral oncogene homolog; LOH, loss of heterozygosity; NSCLC, non–small cell lung cancer; PIK3CA, phosphoinositide-3-kinase, catalytic, α polypeptide; SRC, v-src sarcoma (Schmidt-Ruppin A-2) viral oncogene homolog (avian); TESP, Target-Enriched Sensitivity Prediction.

Citation for this article: *J. Clin. Invest.* 119:1727–1740 (2009). doi:10.1172/JCI37127.



roblastik leukemia viral oncogene homolog 2, neuro/glioblastoma-derived oncogene homolog [avian]) antibody trastuzumab shrinks tumors in women with *ERBB2*-amplified breast cancer (1); the *ABL/KIT*/*PDGFR* (where *ABL* is defined as *v-abl* *Abelson murine leukemia viral oncogene homolog* and *KIT* is defined as *v-kit* *Hardy-Zuckerman 4 feline sarcoma viral oncogene homolog*) inhibitor imatinib induces responses in patients with chronic myeloid leukemia carrying the *BCR/ABL* (where *BCR* is defined as *breakpoint cluster region*) translocation (2, 3) as well as in patients with gastrointestinal stromal tumors and melanomas bearing mutations in *KIT* (4) or *PDGFRA* (5); and finally, *EGFR*-mutant lung tumors are highly sensitive to the *EGFR* inhibitors gefitinib and erlotinib (6–8). In most cases, such discoveries were made after the completion of clinical trials; as yet no robust mechanism currently exists that permits systematic identification of lesions causing therapeutically relevant oncogene dependency prior to initiation of such clinical trials.

The use of cancer cell lines allows systematic perturbation experiments *in vitro*, yet the validity and clinical interpretability of these widely used models have been questioned. In some notable instances, pathways may lose function when grown in culture (9). In addition, cell lines are frequently thought to be genomically disarrayed and unstable and therefore likely poorly representative of primary tumors. Furthermore, the genetic diversity of histopathologically defined classes of tumors is often substantial, e.g., the clinical tumor entity non-small cell lung cancer (NSCLC) comprises *EGFR*- and *KRAS*-mutant (where *KRAS* is defined as *v-Ki-ras2 Kirsten rat sarcoma viral oncogene homolog*) lung adenocarcinomas as well as *KRAS*-mutant squamous-cell lung cancers. Thus, any representative preclinical model would need to capture the nature of lesions of primary tumors as well as their distribution in the histopathologically defined cohort.

Recent reports have credentialed the use of cancer cell lines in preclinical drug target validation experiments (10–13). Building on the foundation of these studies, we have now established a cell-line collection that enables systematic prediction of drug activity using global profiles of genetic lesions in NSCLC. Given the genomic diversity of a particular cancer type, we reasoned that in-depth preclinical analyses of activity of cancer therapeutics in tumor cells would require *both* thorough genomic analysis of a large cell-line collection of a single tumor entity *and* high-throughput cell-line profiling, followed by genomic prediction of compound activity.

We set out to systematically annotate the genomes of a large panel of NSCLC cell lines in order to determine whether such a collection reflects the genetic diversity of primary NSCLC tumors. We further determined the phenotypic validity of this collection and analyzed drug activity as a function of genomic lesions in a systematic fashion. Finally, we confirmed the validity of our predictors *in vitro* and in lung cancer mouse models. Such complementary efforts may provide a framework for future preclinical analyses of compound activity, taking into account the multitude of genetic lesions in histopathologically defined cancer types.

Results

A genomically validated collection of NSCLC cell lines. Eighty-four NSCLC cell lines were collected from various sources (Supplemental Table 1; supplemental material available online with this article; doi:10.1172/JCI37127DS1) and formed the basis for all subsequent experiments. Cell lines were derived from tumors representing all major subtypes of NSCLC tumors, including adenocarcinoma, squamous-cell carcinoma, and large-cell carcinoma.

The genomic landscape of these cell lines was characterized by analyzing gene copy number alterations using high-resolution SNP arrays (250K Sty1). We used the statistical algorithm Genomic Identification of Significant Targets in Cancer (GISTIC) to distinguish biologically relevant lesions from background noise (14). The application of GISTIC revealed 16 regions of recurrent, high-level copy number gain (inferred copy number > 2.14) and 20 regions of recurrent copy number loss (inferred copy number < 1.86) (Supplemental Tables 2 and 3). Overall, we identified focal peaks with a median width of 1.45 Mb (median 13.5 genes/region) for amplifications and 0.45 Mb for deletions (median 1 gene/region). These regions contained lesions known to occur in NSCLC (e.g., deletion of *LRP1B* [2q], *FHIT* [3p], *CDKN2A* [9p]; amplification of *MYC* [8q], *EGFR* [7p] and *ERBB2* [17q]; Figure 1A and Supplemental Table 2). Furthermore, within broad regions of copy number gain, we also identified amplification of *TTF1* (14q) and *TERT* (5p) (Figure 1A and Supplemental Table 2), recently identified by large-scale genomic profiling of primary lung adenocarcinomas (15–17).

Analysis of homozygous deletions as well as loss of heterozygosity (LOH) is typically hampered by admixture of nontumoral cells in primary tumors. The purity of cell-line DNA permitted identification of previously unknown homozygous deletions and regions of LOH, including LOH events resulting from uniparental disomy (e.g., copy-neutral events) (Supplemental Table 4). In this analysis, known genes such as *MTAP* (9p) and *LATS2* (13q) were altered by homozygous deletions (18, 19) and we found what we believe are novel homozygous deletion of genes such as *TUBA2* (Supplemental Table 4). Of note, most of these regions could also be identified in primary NSCLC tumors as deleted (15); however, inferred copy numbers only inconstantly showed LOH or homozygous deletions, indicating admixture of normal diploid DNA (Supplemental Table 4). Thus, while a recent large-scale cancer profiling study (15) enabled insight into the genomic landscape of lung adenocarcinoma, the use of pure populations of tumor cells further afforded discovery of previously unrecognized regions of homozygous deletions and LOH.

We next compared the profile of significant amplifications and deletions in this cell-line collection with that of a set of 371 primary lung adenocarcinomas (15). This comparison revealed a striking similarity between the 2 data sets (Figure 1A) but not between NSCLC cell lines and gliomas or melanomas (Supplemental Figure 1, A and B). A quantitative analysis of similarity by computing correlations of the false discovery rate (*q* value) confirmed the similarity of primary lung cancer and lung cancer cell lines ($r = 0.77$) and the lack of similarity of lung cancer cell lines and primary gliomas (14) ($r = 0.44$), melanoma cell lines (11) ($r = 0.44$), or ovarian tumors ($r = 0.38$; Supplemental Figure 1C). As a control, repeated random splitting of the lung cancer cell-line data and computation of internal similarity resulted in correlation coefficients between 0.82 and 0.86, whereas we found no correlation with normal tissue ($r = 0.0195$; Supplemental Figure 1C). These results demonstrate that the genomic copy number landscape of NSCLC cell lines reflects that of primary NSCLC tumors, while tumors or cell lines of other lineages show a much lower degree of similarity (20, 21). Furthermore, the distribution of oncogene mutations in the cell lines (Supplemental Table 5) was similar to that in primary NSCLC tumors, with a high prevalence of mutations in the *KRAS* and *EGFR* genes (22–25) and rare occurrence of phosphoinositide-3-kinase, catalytic, α polypeptide (*PIK3CA*) and v-raf murine sarcoma viral oncogene homolog B1 (*BRAF*) mutations (Figure 1B). These results further validate our cell-line collection on a genetic level.

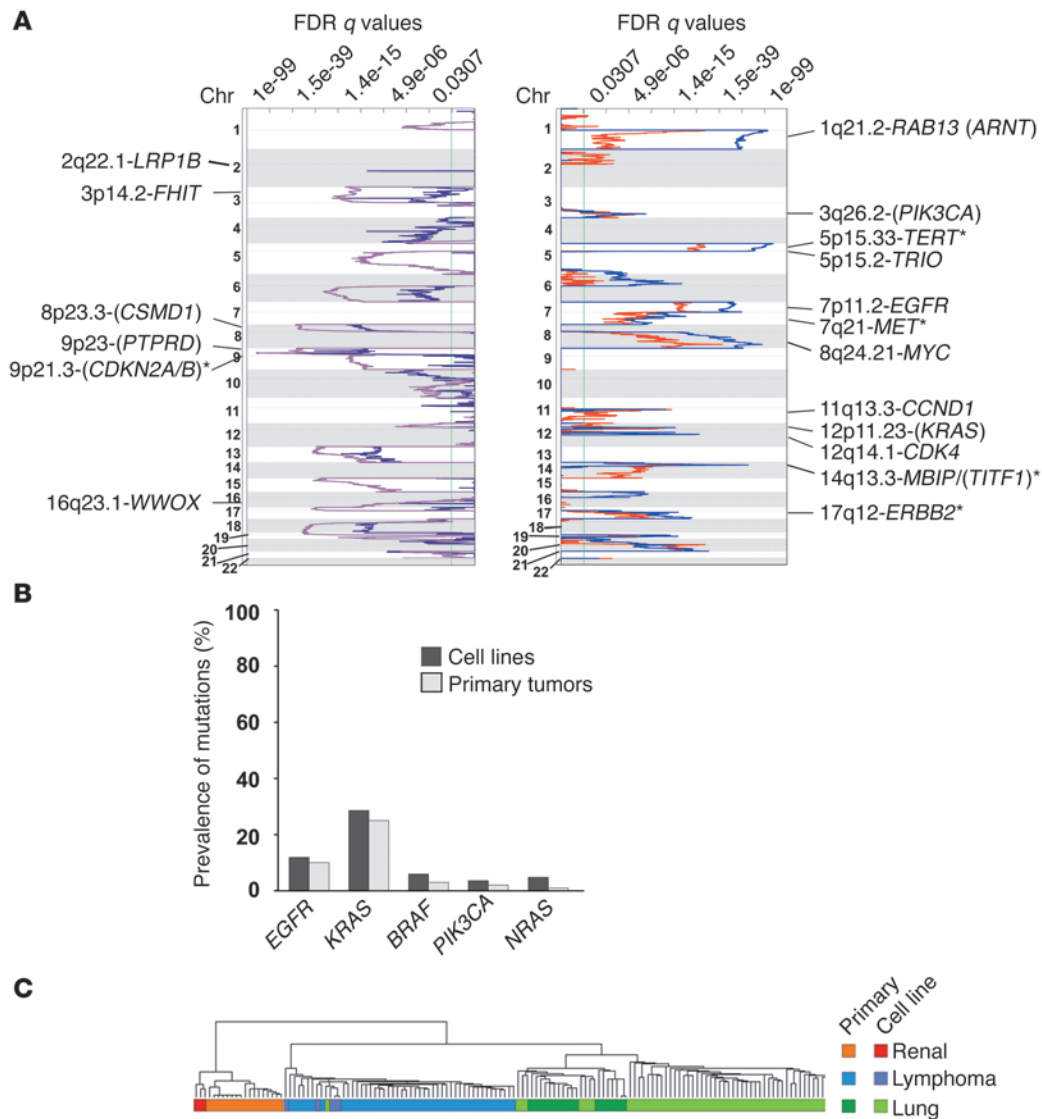


Figure 1

Genomic validation of 84 NSCLC cell lines. **(A)** Chromosomal copy number changes of NSCLC cell lines are plotted against those of 371 primary NSCLC tumors. The q values (false discovery rates) for each alteration (x axis) are plotted at each genome position (y axis). Left panel shows chromosomal losses (cell lines, purple; primary tumors, dark blue); right panel shows chromosomal gains (cell lines, red; primary tumors, blue). Genomic positions corresponding to even-numbered chromosomes are shaded; dotted lines indicate centromeres; green lines, q value cutoff (0.25) for significance. Genes represent known targets of mutation in lung adenocarcinomas. Putative targets near peaks are given in parentheses. Genes identified by GISTIC using stringent filtering criteria for peak border detection are marked by asterisks. **(B)** Oncogene mutations present in NSCLC cell lines (black bars) are plotted according to their relative frequencies in comparison with primary lung tumors (gray bars) (22–25). **(C)** Transcriptional profiles of primary renal cell carcinomas (orange) and corresponding cell lines (red); primary lung tumors (dark green) and lung cancer cell lines (light green); primary lymphomas (blue) and lymphoma cell lines (purple) were analyzed by hierarchical clustering. To reduce noise, probe sets were filtered prior to clustering (coefficient of variation from 1.0 through -10.0 , present call rate, 20%; absolute expression greater than 100 in more than 20% of samples).

The availability of both copy number alteration and oncogene mutation data of the NSCLC cell lines enabled us to analyze the interactions of both types of lesions (Supplemental Figure 2). Hierarchical clustering of lesions robustly grouped both mutations and amplification of *EGFR* in 1 subcluster (ratio Q of observed vs. expected cooccurrence: $Q = 4.38$, $P = 0.001$), while *KRAS* mutations consistently grouped in a distinct cluster. These findings corroborate prior observations in vivo in which mutations in *KRAS* and *EGFR* were mutually exclusive while *EGFR* mutation and *EGFR* amplification

frequently cooccurred (23, 26, 27). Moreover, these results suggest that these mutations influence the particular signature of genomic alterations in the affected tumors. Finally, in unsupervised hierarchical cluster analyses of gene expression data, primary lung cancer specimens (28) and lung cancer cell lines shared 1 cluster (Figure 1C), while renal cell carcinomas (29) and lymphomas (30) as well as the corresponding cell lines clustered in a separate group.

In summary, in-depth comparative analysis of orthogonal genomic data sets of a large panel of NSCLC cell lines and primary

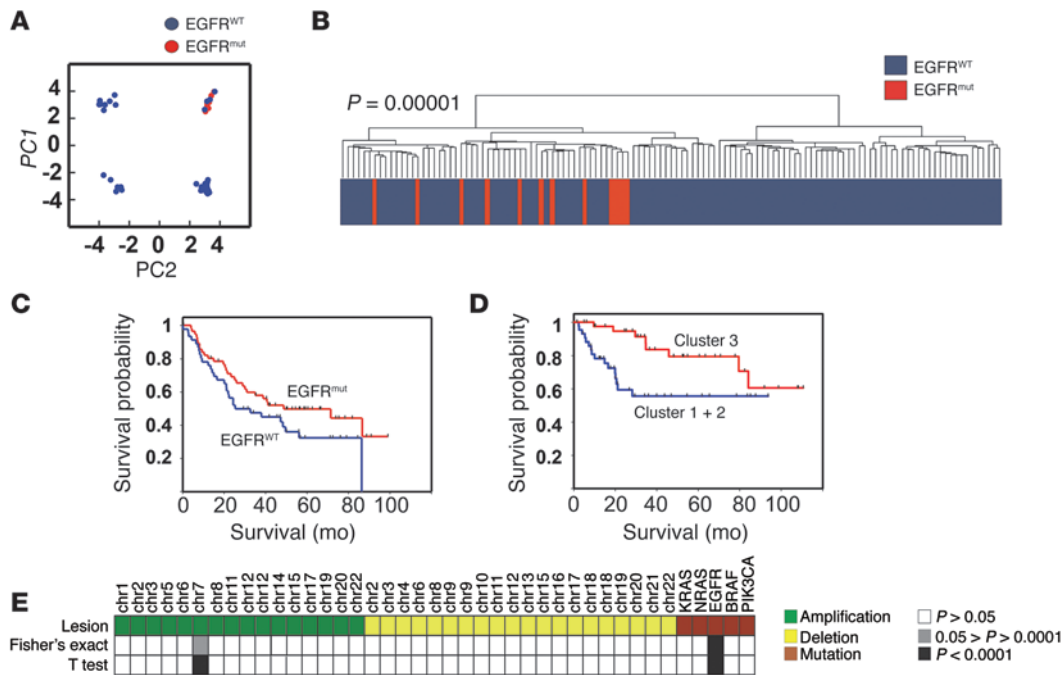


Figure 2

Robustness of phenotypic properties of EGFR-mutant lung cancer cells in vivo. (A) The first 2 principal components (PC1 and PC2) distinguish cell lines with mutated (mut) *EGFR* (red dots) and WT *EGFR* (blue dots) ($n = 54$). (B) The signature (fold change greater than 2; absolute difference, 100; $P < 0.01$) of *EGFR*-mutant cell lines ($n = 8/54$) was used for hierarchical clustering of 123 primary adenocarcinomas (35) annotated for the presence (*EGFR*^{mut}, red bars) or absence (*EGFR*^{WT}, dark blue bars) of *EGFR* mutations. (C) Probability of survival was estimated for all 123 primary adenocarcinomas with known *EGFR* mutation status following grouping according to relative abundance of 337 RNA transcripts identified as differentially expressed between *EGFR*-mutant and *EGFR* WT cell lines. *EGFR*-mutant tumors ($n = 13$) were excluded from survival analyses. Survival probabilities are depicted as Kaplan-Meier survival estimate curves. (D) The same analysis was performed using 86 lung tumors from Beer et al. (37) with available survival data. Two groups were formed according to relative abundance of the *EGFR* mutation-specific genes, and survival analysis was performed as in D. (E) The association between presence (amplification, green; mutation, red; deletion, yellow) of genetic lesions identified in the cell lines and sensitivity of the respective cell lines to treatment with the *EGFR* inhibitor erlotinib was analyzed by Welch's *t* test and Fisher's exact test. Significant lesions are marked by gray ($P < 0.05$) or black ($P < 0.0001$) boxes.

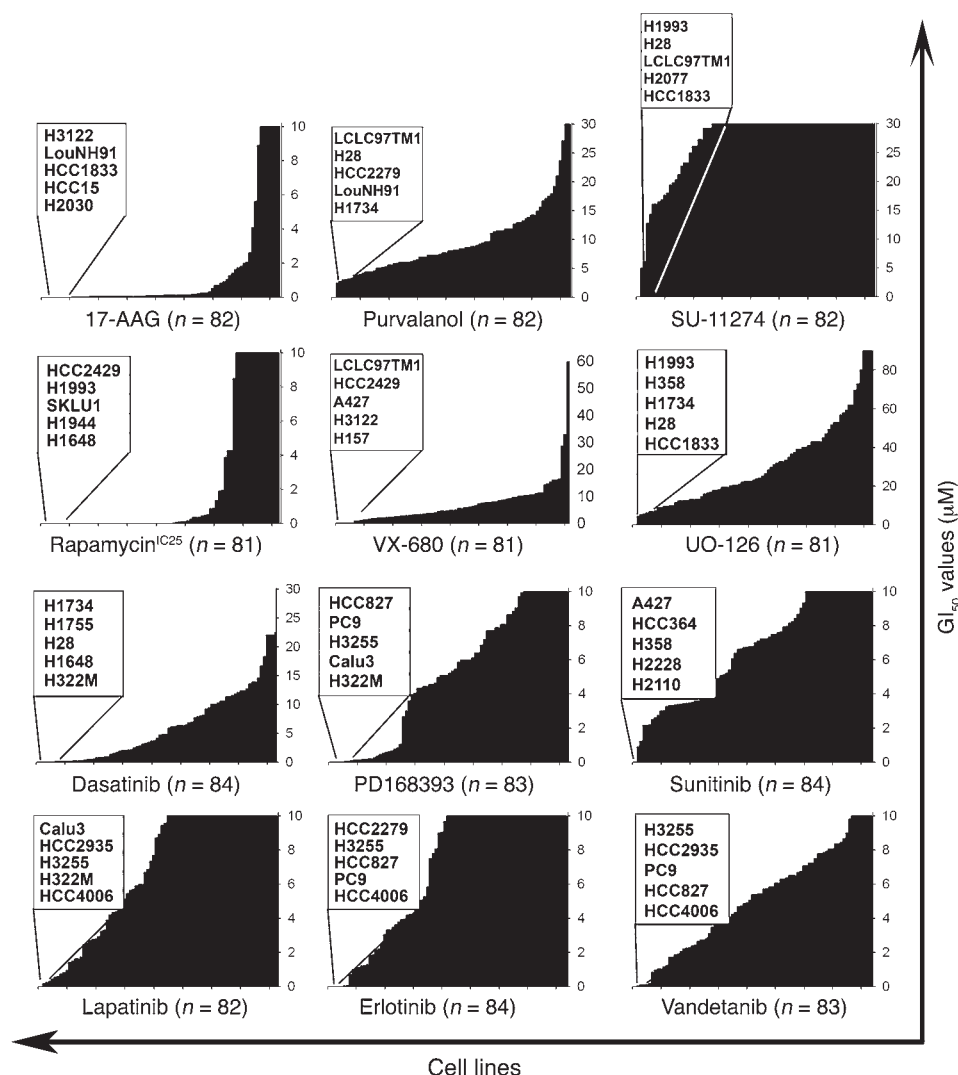
tumors demonstrates that these cell lines reflect the genetic and transcriptional landscape of primary NSCLC tumors.

EGFR mutations define phenotypic properties of lung tumors in vitro and in vivo. Activated oncogenes typically cause a transcriptional signature that can be used to identify tumors carrying such oncogenes (31, 32). However, we consistently failed to identify a gene expression signature characteristic of *EGFR*-mutant tumors (33, 34) using a gene expression data set of 123 primary lung adenocarcinomas (35) annotated for mutations in *EGFR* (data not shown). We therefore reasoned that the cellular purity of our cell lines ($n = 54$ analyzed on U133A) might enable the determination of such a signature and the application of this signature in primary tumors. We applied principal component analyses on the variable genes and found a remarkable grouping of all *EGFR* mutated cell lines ($n = 8/54$), with a significant dissociation already in the first principal component (Welch's *t* test on the distribution of eigenvalues: $P = 0.0005$) contributing 14.5% to the overall variance (Figure 2A). Similar results were obtained by hierarchical clustering (data not shown). Using genes differentially expressed in *EGFR*-mutant cell lines (including T790M) as a surrogate feature (Supplemental Table 6), all of the *EGFR*-mutant primary tumors (35) were grouped in a distinct cluster ($P = 0.00001$) when performing hierarchical clustering (Figure 2B). This result was also recapitulated when selecting genes differentially expressed in erlotinib-sensitive

($GI_{50} < 0.1 \mu M$, $n = 5/54$ vs. $GI_{50} > 2 \mu M$, $n = 45$, where GI_{50} indicates half-maximal growth inhibitory concentration) cell lines (Supplemental Figure 3A). Furthermore, patients with tumors expressing the signature of *EGFR* mutated cell lines had better overall survival than those whose tumors did not (Figure 2C) (36). The power of our *EGFR*^{mut} signature to predict survival was confirmed, employing the data published by Beer and colleagues (Figure 2D) (37). This effect was even observed when excluding *EGFR*-mutant tumors ($n = 13$) from the analysis (Figure 2C). Thus, expression signatures extracted in vitro can be used to identify biologically diverse tumors in vivo (38).

Others have recently characterized a transcriptional signature of *EGFR*-mutant NSCLC using a small set of cell lines (39). However when analyzing primary lung adenocarcinomas with the signature described by Choi et al., *EGFR*-mutant samples were randomly distributed across the data set (Supplemental Figure 3B). This finding further highlights the importance of using large cell-line collections in order to represent the overall genomic diversity of primary tumors.

Recent studies have linked the presence of *EGFR* mutations in lung adenocarcinomas to clinical response to the *EGFR* inhibitors erlotinib and gefitinib (6–8). However, retrospective studies aimed at determining predictive markers for *EGFR* inhibition yielded heterogeneous results, implicating *EGFR* mutations and/or

**Figure 3**

Sensitivity profiles of compounds determined by high-throughput cell-line screening. GI_{50} values (y axes) for 12 compounds are shown for the successfully screened (Supplemental Table 5) cell lines (x axes show individual cell lines). Due to the fact that rapamycin typically fails to completely abrogate cellular proliferation (79), the 25% inhibitory concentration is shown for these compounds. Bars represent GI_{50} (GI_{25} values in the case of rapamycin, y axis) throughout the cell-line collection (x axis) ranked according to sensitivity. The maximum concentration is adapted to the GI_{50} value (GI_{25} values in the case of rapamycin; 10 μ M for 17-AAG, erlotinib, vandetanib, lapatinib, sunitinib, rapamycin, and PD168393; 30 μ M for SU-11274, dasatinib, and purvalanol; 60 μ M for VX-680; 90 μ M for UO126) of resistant cell lines. The 5 most sensitive cell lines for each compound are highlighted in table form.

EGFR amplifications among others as predictive of response or patient outcome (40–42). We set out to systematically identify genetic lesions associated with sensitivity to erlotinib by including all global lesion data from our genomics analyses rather than focusing on *EGFR*-associated lesions. We established a high-throughput cell-line screening pipeline that enables systematic chemical perturbations across the entire cell-line panel followed by automated determination of GI_{50} values (43) to determine erlotinib sensitivity for all cell lines. We next analyzed the distribution of genetic lesions in erlotinib-sensitive compared with insensitive cell lines (Supplemental Tables 5 and 7) and further compared the mean sensitivity of cell lines with and without the respective genetic lesions. In both analyses, *EGFR* mutations were the best single-lesion predictor of erlotinib sensitivity (Figure 2E and Supplemental Table 7; Fisher's exact test; $P = 6.9 \times 10^{-8}$). Furthermore, we found a less stringent association with amplification of *EGFR* (Fisher's exact test; $P = 1.4 \times 10^{-4}$); however, only *EGFR* mutations were significant predictors of erlotinib sensitivity when we adjusted for multiple hypothesis testing using Bonferroni's correction (data not shown). We next used signal-to-noise-based feature selection combined with the

K-nearest-neighbor (KNN) algorithm (44, 45) to build a multilesson predictor of erlotinib sensitivity. The best performing multilesson predictor comprised *EGFR* mutations, amplification of *EGFR*, and lack of *KRAS* mutations (Figure 2E and Supplemental Table 7), which have all been implicated in determining responsiveness of NSCLC patients to *EGFR* inhibitors (6–8, 27, 40, 41, 46). We note that in our data set, as in previously published reports (6–8, 27, 40, 41, 46), *EGFR* amplification and mutation were correlated, whereas *KRAS* mutations were mutually exclusive with either lesion (Supplemental Figure 2). Thus, our observation confirms the overall predominant role of *EGFR* mutations in predicting responsiveness to *EGFR* inhibition, and it provides an explanation for the finding of *EGFR* amplification as being predictive of response as well. Our findings also corroborate prior clinical reports establishing *KRAS* mutations as a resistance marker for *EGFR* inhibition therapy. Together, these results imply that essential transcriptional and biological phenotypes of the original tumors are preserved in the cell lines, a necessary requirement for application of such collections as proxies in preclinical drug target validation efforts.

Differential activity of compounds in clinical development in NSCLC cell lines. Having validated the cell-line collection by demonstrating its

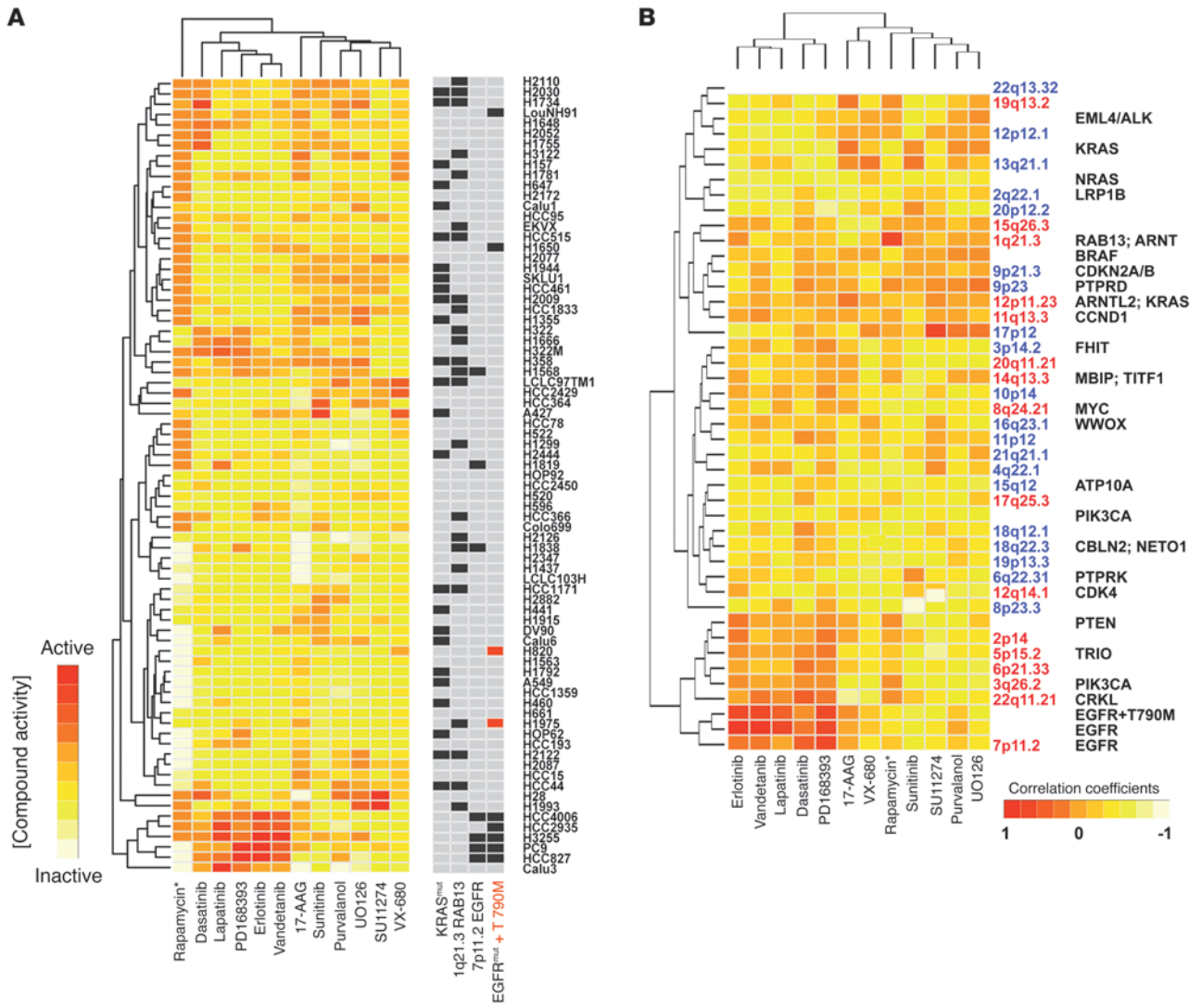


Figure 4

Hierarchical clustering of compound activity uncovers mutated *EGFR* as a target for dasatinib activity. **(A)** Displayed is a hierarchical cluster of cell lines and compounds, clustered according to GI_{50} values (red, high compound activity; white, low compound activity) after logarithmic transformation and normalization. 77 cells reached full compound coverage. The presence (black) or absence (gray) of selected lesions is annotated in the right panel. **(B)** Correlation of activity of compounds to presence of amplifications (red) and deletions (blue) as well as oncogene mutations (mut) was used for hierarchical clustering. Putative target genes inside and bordering (*) the region defined by GISTIC are annotated. **(C)** Upper panel shows that binding mode of erlotinib (white) to WT *EGFR*. Dasatinib (pink) is modeled into the ATP-binding site of *EGFR*. The 2-amino-thiazole forms 2 hydrogen bonds with the hinge region of the kinase. Lower panel shows that the chloro-methyl-phenyl ring of dasatinib binds to a hydrophobic pocket near the gatekeeper Thr790 and helix C and will clash with the Met side chain of the *EGFR* drug-resistance mutation T790M. **(D)** Upper panel shows that Ba/F3 cells ectopically expressing mutant *EGFR* with (delEx19 + T790M) or without (delEx19) the T790M mutation were treated for 12 hours with either dasatinib or erlotinib, and phospho-*EGFR* and *EGFR* levels were detected by immunoblotting. Lower panel shows that the same cells were treated for 96 hours with either dasatinib or erlotinib and viability was assessed. Growth inhibition relative to untreated cells (y axis) is shown as a function of compound concentrations.

genomic and phenotypic similarity to primary NSCLC tumors, we reasoned that adding complex phenotypic data might elicit additional insights into the impact cancer genotypes have on cell biology phenotypes. In our initial pilot screening experiment, we profiled all cell lines against erlotinib and subsequently extended our assay to 11 additional inhibitors that were either under clinical evaluation or showed high activity in preclinical models; these compounds target a wide spectrum of relevant proteins in cancer (Supplemental Figure 4). We treated all cell lines with these compounds and determined GI_{50} values (GI_{25} respectively; Supplemental Table 5). The resulting sensitivity patterns (Figure 3) revealed that while some of the compounds exhibited a pronounced cytotoxic activity in a small subset of cell lines (e.g., erlotinib, vandetanib, VX-680), others were active in most of the cell lines, with only a minority being resistant [e.g., 17-(allylamino)-17-demethoxygeldanamycin (17-AAG)]. Only 2 cell lines (<2%) were resistant to all of the compounds (Supplemental Table 5), suggesting that most NSCLC tumors might be amenable to targeted treatment. Overall, these observations are highly reminiscent of patient responses in clinical trials in which limited subsets of patients experience partial and, rarely, complete response while the majority of patients exhibit stable disease, no change, or progression.

Identification of relevant compound targets by similarity profiling. As an initial approach to identification of shared targets of inhibitors, we performed hierarchical clustering based on the similarity of sensitivity profiles (Figure 4A) and based on the correlation between sensitivity and genomic lesion profiles (Figure 4B). Erlotinib and vandetanib exhibited the highest degree of similarity, pointing to mutant *EGFR* as the critical target of vandetanib in NSCLC tumor cells (Figure 4, A and B) (47, 48). The high degree of correlation ($r = 0.91$; $P < 0.001$) of cell-line GI_{50} values for both compounds as well as structural modeling of vandetanib binding in the *EGFR* kinase domain, which revealed a binding mode identical to that of erlotinib, further corroborate this notion (Supplemental Figure 5A). This model predicted that binding of both compounds would be prevented by the T790M resistance muta-

tions of *EGFR* (48–50); accordingly, murine Ba/F3 cells ectopically expressing erlotinib-sensitizing mutations of *EGFR* together with T790M (51) were completely resistant to erlotinib and vandetanib (Supplemental Figure 5, B and C).

In addition to the ERBB2/*EGFR* inhibitor lapatinib, vandetanib, and the irreversible *EGFR* inhibitor PD168393 (52), the SRC/*ABL* (where SRC is defined as *v-src sarcoma [Schmidt-Ruppin A-2] viral oncogene homolog [avian]*) inhibitor dasatinib (53) shared a cluster with the *EGFR* inhibitor erlotinib, although at a much lower potency than erlotinib (Figure 4, A and B). Molecular modeling of dasatinib binding to *EGFR* predicted a binding mode similar to that of erlotinib (Figure 4C), with a steric clash of erlotinib and dasatinib with the erlotinib resistance mutation T790M (49, 50, 54, 55) (Figure 4C). We therefore formally validated *EGFR* as a relevant dasatinib target in tumor cells by showing cytotoxicity as well as *EGFR* dephosphorylation (56) elicited by this compound in Ba/F3 cells ectopically expressing mutant *EGFR* but not in those coexpressing the T790M resistance allele (Figure 4D). Thus, large-scale phenotypic profiling coupled to computational prediction formally validated a relevant tumor-cell target of an FDA-approved drug using a systematic unbiased approach. It is noteworthy that a trial of dasatinib in patients with acquired erlotinib resistance is currently ongoing (trial ID: NCT00570401; <http://clinicaltrials.gov/ct2/show/NCT00570401?term=NCT00570401&rank=1>; based on previously reported biochemical findings (54) and our results, we predict limited clinical activity in those patients in whom erlotinib resistance is due to the *EGFR* resistance mutation T790M.

Supervised learning identifies predictors for inhibitor responsiveness. We have shown that hierarchical clustering can identify compounds with overlapping target specificities within a screening experiment. We now set out to extend our analyses to additional computational approaches to predict inhibitor responsiveness from global lesion data in a systematic fashion. To this end, we applied supervised learning methods as we did for erlotinib (see above). Applying this method, we identified robust, genetic lesion-based predictors for the majority of the tested compounds (Supplemental Table 7).

UO126 is a MEK inhibitor that also showed enhanced activity in a subset of the lung cancer cell-line collection. Here, the supervised approach identified chromosomal gains of 1q21.3 affecting the genes *ARNT* and *RAB13* as being robustly associated with UO126 sensitivity (Fisher's exact test, copy number threshold 2.14, $P = 0.02$; Supplemental Figure 6 and Supplemental Table 7). In order to validate this finding in an independent data set, we made use of the NCI-60 cancer cell-line panel (57) in which hypothemycin was used as a MEK inhibitor (12). This cross-platform validation revealed that 1q21.3 gain predicted sensitivity to MEK inhibition in both data sets (Fisher's exact test, $P = 0.03$, NCI-60 collection; Supplemental Figure 6).

In our initial cluster analysis, we found that *KRAS* mutations correlated with sensitivity to the Hsp90 inhibitor 17-AAG, a geldanamycin derivative (Figure 4B). Recapitulating this observation, we found *KRAS* mutations to be predictive of 17-AAG sensitivity, even when applying our KNN-based prediction approach (Fisher's exact test, $P = 0.029$; Figure 5A and Supplemental Table 7). Confirming this observation in an independent cell-line model, we found the distribution of geldanamycin sensitivity and *KRAS* mutation in the NCI-60 cell-line collection to be strikingly similar to that observed in our panel ($P = 0.049$; Figure 5A).

In 17-AAG-sensitive cells, Hsp90 inhibition led to robust induction of apoptosis (Supplemental Figure 7A). In order to gain mech-

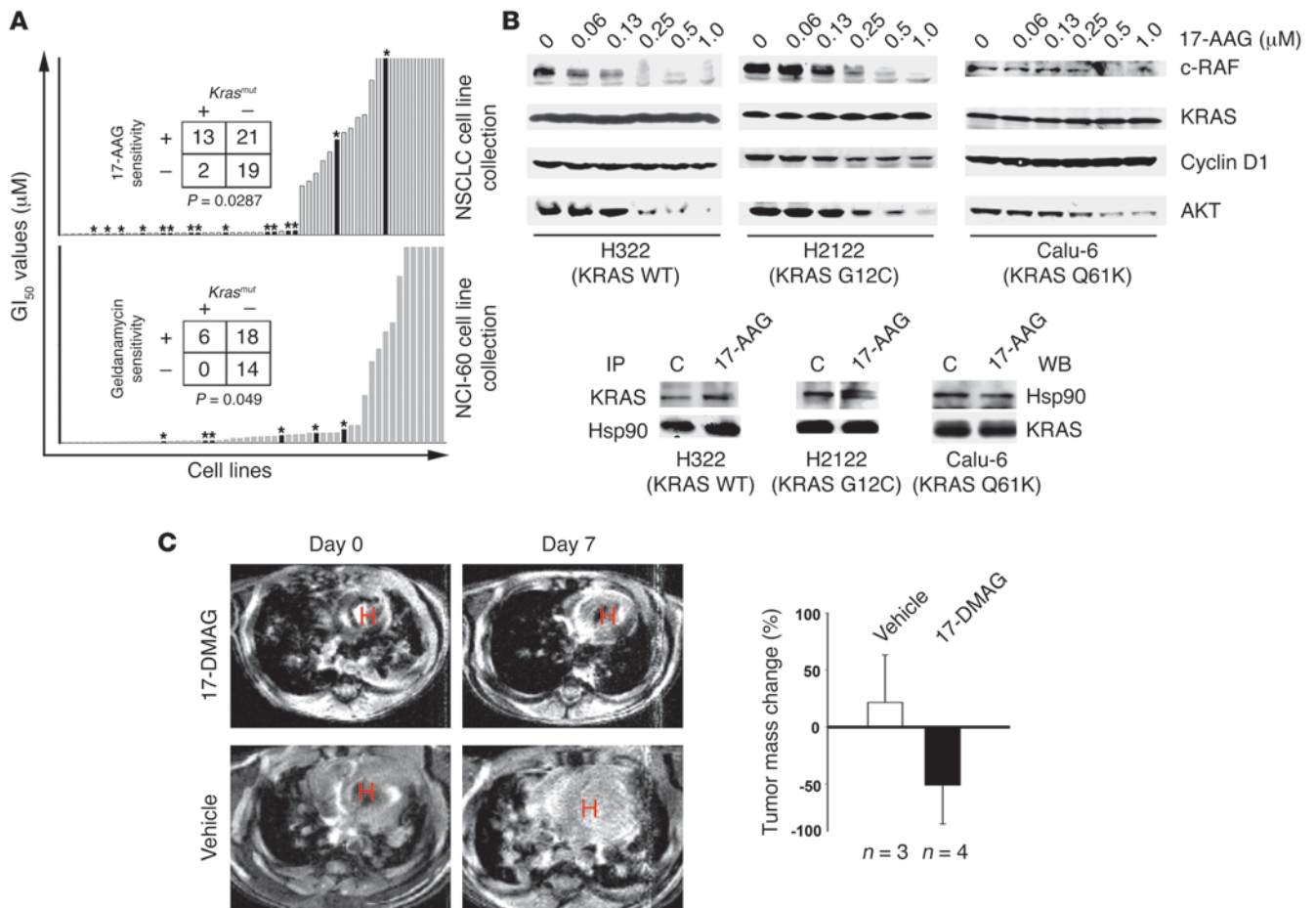
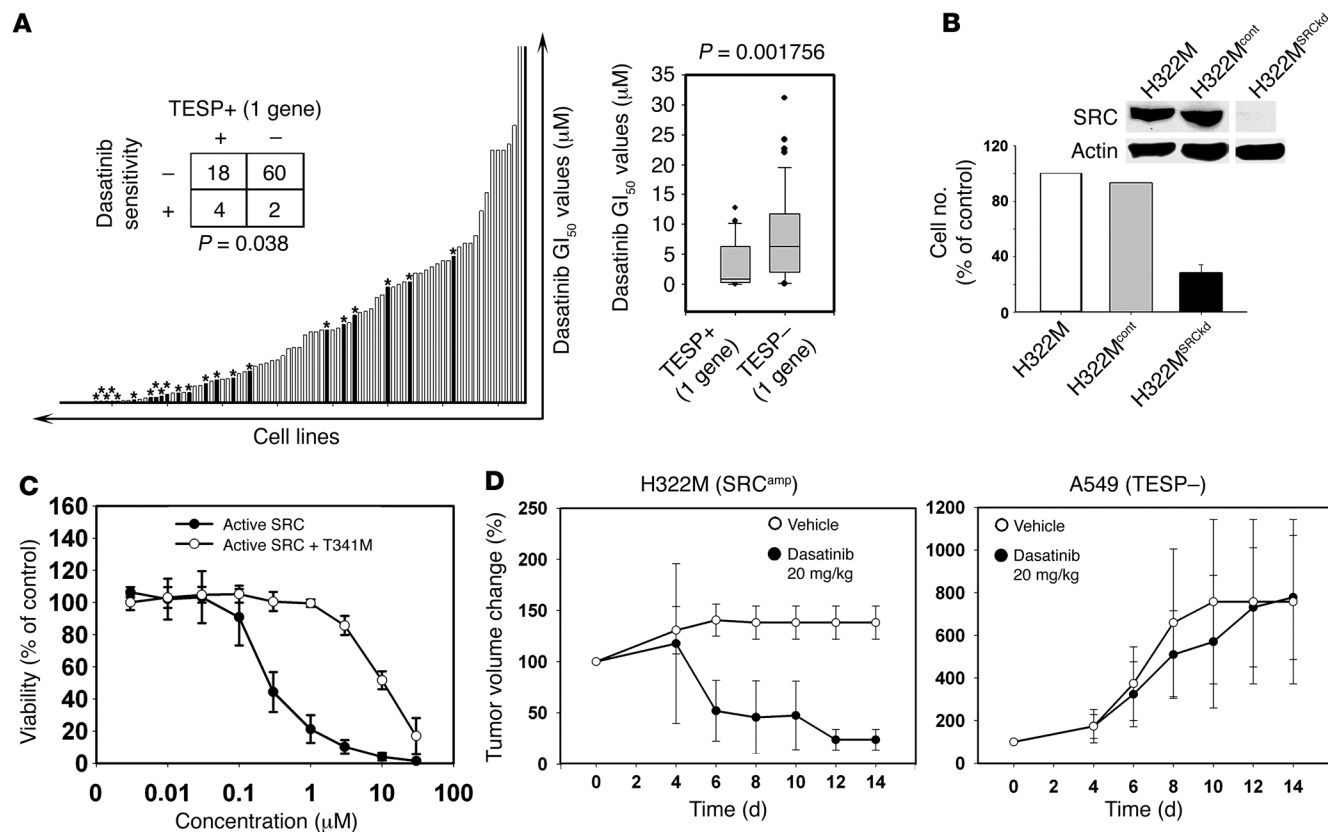


Figure 5 *KRAS* mutations predict response to inhibition of Hsp90 in vitro and in vivo. **(A)** The sensitive and resistant cell lines were sorted according to their GI_{50} values and annotated for the presence of *KRAS* mutations (asterisks and black columns). Bar height represents the respective GI_{50} values. The association of *KRAS* mutations and 17-AAG sensitivity ($GI_{50} < 0.07 \mu M =$ sensitive; $GI_{50} > 0.83 \mu M =$ resistant; according to the lower and upper 25th percentiles) was calculated by Fisher's exact test for the lung cancer data set (upper panel) and for the NCI60 data set (lower panel). **(B)** Upper panel shows that whole-cell lysates of the indicated *KRAS* WT and *KRAS* mutated cell lines treated with different concentrations of 17-AAG were analyzed for levels of c-RAF, KRAS, cyclin D1, and AKT by immunoblotting. Lower panel shows that extracts of the indicated cells treated with either control (C) or 0.5 μM (H322 and Calu-6) or 1 μM (H2122) of 17-AAG were subjected to coimmunoprecipitation with antibodies to either KRAS (top) or Hsp90 (bottom); immunoprecipitates were analyzed for levels of Hsp90 (top) or KRAS (bottom) by immunoblotting. Noncontiguous bands run on the same gel are separated by a black line (H2122). WB, Western blot. **(C)** Displayed are coronal MRI scans of *lox-stop-lox^{KRASG12D}* mice before and after 7 days of treatment with either 17-DMAG or vehicle. The areas of lung tumors were manually segmented and measured on each magnetic resonance slice, and total tumor volume reduction was calculated for all mice treated with 17-DMAG ($n = 4$) and placebo ($n = 3$). SD of tumor volume in the cohort of treated and untreated mice was calculated and is depicted as error bars.

anistic insight into *KRAS* dependency on Hsp90 chaperonage, we first confirmed the specificity of our *KRAS* antibody (Supplemental Figure 7C). Using conditions under which EGFR coprecipitated with Hsp90 in *EGFR*-mutant cells (Supplemental Figure 7B) (58), we found *KRAS* to be bound to Hsp90 as well (Figure 5B). However, while 17-AAG treatment depleted mutant EGFR from Hsp90 (Supplemental Figure 7B), *KRAS* binding to Hsp90 was not affected by this treatment (Figure 5B). Furthermore, cellular *KRAS* protein levels were also not reduced by 17-AAG (Figure 5B). These findings are surprising, as other oncogenes, such as EGFR or BRAF, known to be dependent on Hsp90 chaperonage are depleted from the complex after treatment with 17-AAG (58, 59). However, reduction of viability of *KRAS*-mutant cells treated with 17-AAG is accompanied by depletion of c-RAF and AKT (60) (Figure 5B). Since both c-RAF

and AKT are known Hsp90 clients (59, 61), we hypothesize that this observation might rely on the activation of the AKT and RAF/MEK/ERK signaling pathways by mutant *KRAS* (62, 63).

To further validate the power of *KRAS* mutations to predict response to Hsp90 inhibition, we employed a *lox-stop-lox^{KRASG12D}* mouse model that enables the study of *KRAS*-driven lung adenocarcinomas in vivo (64). Mice with established lung tumors induced by nasal inhalation of adenoviral *Cre* (64) were either treated with the water-soluble geldanamycin Hsp90 inhibitor 17-(dimethylaminoethylamino)-17-demethoxygeldanamycin (17-DMAG) or placebo. Whereas no tumor shrinkage was observed in the placebo-treated mice after 1-week treatment (Figure 5C and Supplemental Figure 8), substantial regression of established tumors was observed in 3 out of 4 mice receiving 17-DMAG, with a tumor volume reduction

**Figure 6**

Identification of functionally relevant targets for dasatinib activity. **(A)** Left panel shows that cell lines with copy number gain involving at least 1 gene encoding dasatinib target are labeled with asterisks and black columns. The probability of these cells being dasatinib sensitive was calculated by Fisher's exact test. In right panel, dasatinib GI_{50} values are shown as box plots (representing the 25th to 75th percentile; whisker representing the 95th percentile; dots representing outliers) for cell lines with (TESP+ 1 gene) and without (TESP- 1 gene) copy number gain of dasatinib target genes (Wilcoxon test). **(B)** H322M cells harboring amplified *SRC* were either left untreated or transduced with an empty vector control (H322M^{cont}) or with shRNA targeting *SRC* (H322M^{SRCKd}). After puromycin selection, levels of *SRC* in H322M cells transduced with the indicated vectors were analyzed by immunoblotting (top). The H322M^{SRCKd} lanes were run on the same gel but were noncontiguous, as indicated by the white line. Viability was quantified by cell counting. Error bars represent SD between different experiments. **(C)** H322M cells were transduced with vectors encoding either active *SRC* or active *SRC* with a gatekeeper mutation *SRC* (T341M). Stable cells were treated with dasatinib for 96 hours. Viability is shown as percentage of untreated controls. Error bars indicate SD of 3 independent experiments. **(D)** Dasatinib-sensitive (TESP+; H322M) or -resistant cells (TESP-; A549) were grown s.c. in nude mice. After 14 days of treatment (vehicle, dasatinib), tumor volumes were measured as diameters. SD of tumor volume in the cohort of treated and untreated mice was calculated and is depicted as error bars.

of up to 80% (Figure 5C and Supplemental Figure 8). Although responses were transient as those seen in 17-DMAG-treated transgenic mice with EGFR-driven lung carcinomas (data not shown), these findings validate our observation that *KRAS* mutation predicts response to Hsp90 inhibition in vivo.

Compound target gene enrichment predicts sensitivity. We have used similarity profiling and supervised learning approaches that led to the identification of predictive markers based on significant lesions found in our data set as defined by GISTIC. However, the advantage of statistically defining relevant lesions in a given data set limits the utility of lesions occurring at low frequency and/or amplitude to be used as predictors for compound sensitivity. We therefore developed an additional approach, denoted *Target-Enriched Sensitivity Prediction (TESP)*, which enables inclusion of statistically underrepresented yet biologically relevant lesions.

Amplification of drug-target genes has been demonstrated to predict vulnerability to target-specific compounds in *ERBB2*-

amplified breast cancer and *EGFR*-amplified lung cancer (1, 46). We therefore speculated that chromosomal copy number alterations of biochemically defined drug targets could be used for prediction of sensitivity to other tyrosine kinase inhibitors as well. To this end, we used tyrosine kinase inhibitor targets defined by the quantitative dissociation constant as determined in quantitative kinase assays (65). As a proof of principle, we determined whether copy number gain in *EGFR* is associated with sensitivity to erlotinib (40). In our systematic approach, cell lines inhibited by erlotinib at clinically achievable dosages (up to 1 μ M) were highly enriched for amplification of *EGFR* ($P = 0.00023$; Supplemental Figure 9A). We next tested our prediction model for lapatinib, a specific inhibitor of *ERBB2* and *EGFR*, clinically approved for *ERBB2*-positive breast cancer (66). Again, we observed cell lines inhibited by lapatinib ($n = 82$) below clinically achievable dosage of 1 μ M to be significantly enriched in the subgroup of cell lines with amplification of



ERBB2 or *EGFR* (Fisher's exact test, $P = 0.009$; data not shown). Thus, TESP enables discovery of clinically relevant genotype-phenotype relationships.

Encouraged by these findings, we set out to test our approach for compounds inhibiting a wide range of kinases, such as dasatinib (65). We determined the distribution of GI_{50} values of cell lines with chromosomal copy number gain (copy number > 3) affecting at least 1 or 2 of either one of the genes encoding the most biochemically sensitive dasatinib targets and compared these to the distribution of GI_{50} values of cells without copy number gain at these genomic positions (Figure 6A, Supplemental Table 8, and Supplemental Figure 9B). As hypothesized, these groups were significantly distinct in the distribution of GI_{50} values ($P = 1.8 \times 10^{-3}$ when 1 gene was affected and $P = 4.6 \times 10^{-3}$ when 2 of the target genes were affected by copy number gain; Figure 6A and Supplemental Figure 9B). In particular, this predictor comprised copy number gain at the loci of gene family members of ephrin receptor kinases (*EPHA3*, *EPHA5*, and *EPHA8*), SRC kinases (*SRC*, *FRK*, *YES1*, *LCK*, and *BLK*), and *ABL2*, suggesting that NSCLC cells harboring such lesions might be exquisitely sensitive to therapeutic inhibition of the encoded proteins. The probability that cell lines with copy number gain at either 1 or 2 of these genes will be sensitive to dasatinib treatment ($GI_{50} < 100$ nM) increases up to 5.6-fold (gain of 1 gene) and 15.8-fold (gain of 2 genes), respectively, when compared with cells without copy number gain at these loci (Figure 6A and Supplemental Figure 9B). In contrast, copy number gain involving loci encoding biochemically less sensitive dasatinib targets failed to show enrichment of sensitive cell lines (data not shown).

In cells with copy number gain of biochemically defined dasatinib target genes, dasatinib treatment led to robust induction of apoptosis (data not shown). Importantly, copy number gain of at least one of either of these genes is present in 12.9% (copy number > 3) of several hundred primary lung adenocarcinomas (15) (data not shown), thus emphasizing the potential clinical relevance of our predictor.

In the dasatinib-sensitive cell-line H322M harboring amplified *SRC*, dasatinib treatment led to dephosphorylation of *SRC* at low nanomolar doses, paralleling growth inhibition at similar concentrations (Supplemental Figure 9C). In order to determine whether the genes in our dasatinib predictor are causatively linked with the activity of dasatinib, we silenced *SRC* by lentiviral shRNA in H322M cells (Figure 6B). When compared with parental cells or cells expressing the control vector, H322M-*SRC*-knockdown (*H322M^{SRCKd}*) cells showed a massive reduction in cellular proliferation (Figure 6B) and increase in cell death (data not shown). In order to further validate activated *SRC* as the relevant dasatinib target in H322M cells, we expressed an activated allele of *SRC* together with a sterically demanding mutation at the gatekeeper position of the ATP-binding pocket (T341M) (67); this mutation and the analogous mutations in Bcr-Abl and *EGFR* (see above) induce on-target drug resistance (67) by displacing the compound from the ATP-binding pocket. As hypothesized, expression of the T341M gatekeeper mutation but not of *SRC* alone rescued dasatinib-induced cell death in H322M cells (Figure 6C). These results formally validate *SRC* as the relevant dasatinib target in *SRC*-amplified NSCLC cells.

We also validated *EPHA3* as a relevant target in H28 cells with gain of *EPHA3* by showing decreased viability of these cells upon stable knockdown of *EPHA3* (Supplemental Figure 10).

We next transplanted cells with or without copy number gain of *SRC* into nude mice. Mice were treated with either dasatinib or placebo on a daily application schedule. Again confirming our

in-vitro observations, robust tumor shrinkage was observed in mice transplanted with cells harboring copy number gain of *SRC* (H322M) (Figure 6D) receiving dasatinib. In contrast, no tumor shrinkage was observed in mice transplanted with cells predicted to be resistant against dasatinib (A549) and in all mice treated with placebo (Figure 6D). We consistently failed to grow *EPHA3*-amplified H28 cells in nude mice; HCC515 cells were therefore chosen as another model of NSCLC with gain of *EPHA3*. Dasatinib treatment of established HCC515 tumors also induced significant tumor shrinkage (data not shown).

Together, these results show that in NSCLC, copy number gain of ephrin receptor or *SRC* family member genes and *ABL2* may render tumor cells dependent on these kinases, thus exposing a vulnerability to therapeutic inhibition with dasatinib.

Discussion

Here, we show that diverse analytical approaches of multiple orthogonal genomic and chemical perturbation data sets pertinent to a large collection of cancer cell lines afford insights into how somatic genetic lesions impact cell biology and therapeutic response in cancer. Such data sets provide a rich source for different computational approaches that each yield complementary, accurate, and valid predictors of inhibitor sensitivity. The basis for such predictions is a panel of genomically annotated NSCLC cell lines that is representative of the genetic diversity, the transcriptional profile, and the phenotypic properties of primary NSCLC tumors. The overall functional biological validity of our approach is supported by the observation that *EGFR* mutations are the strongest predictor of sensitivity to the *EGFR* inhibitor erlotinib. Others have similarly observed high activity of *EGFR* inhibitors in *EGFR*-mutant NSCLC cell lines (6, 13, 68), supporting the validity of our unbiased computational approach employing systematic global measurements of genetic lesions.

Applying systematic similarity profiling using computationally defined significant genetic lesions, we also identified predictors for compounds currently in clinical use or trials. Specifically, in an unbiased manner, we confirmed *EGFR* mutations not only to predict sensitivity to *EGFR* inhibitors (erlotinib, PD168393, vandetanib) (6–8, 47, 52) but also to the *SRC*/*ABL* inhibitor dasatinib (54, 56). We formally demonstrated that *EGFR* is the *relevant* target of dasatinib in *EGFR*-mutant cells by showing the lack of activity of this compound in Ba/F3 cells expressing the T790M resistance allele of *EGFR*. Thus, exploring multiple orthogonal genomic and chemical data sets enabled the formal definition of a *relevant* tumor-cell target of an FDA-approved drug.

In addition, we performed supervised identification of predictors for drug sensitivity. A noteworthy finding is the role of *KRAS* mutation as a predictor of sensitivity to 17-AAG. Independent validation of the predictor for an Hsp90 inhibitor in a transgenic murine lung cancer model strengthens the robustness of our approach. Given the high prevalence of cancer patients with mutated *KRAS* and their unfavorable prognosis, this finding might be of clinical importance, as Hsp90 inhibitors (e.g., 17-AAG, IPI-504, NVP-AUY922) are currently under clinical evaluation.

Finally, our compound target-enrichment approach for prediction of sensitivity led to the observation of exquisite vulnerability of cells with copy number gain of ephrin receptor and *SRC* family genes as well as *ABL2* to dasatinib treatment. As a proof of principle we validated our prediction model in great depth for the relevance of *SRC* amplification for dasatinib activity in vitro



and *in vivo*. Thus, copy number gain affecting one of these genes may render tumor cells dependent on the encoded kinases, thereby defining potential biomarkers for successful treatment of NSCLC patients with dasatinib, an FDA-approved drug.

In summary, we have established a genomically, phenotypically, and functionally validated tool for studying drug activity mechanisms in the laboratory. Our results strengthen the notion that multiple orthogonal data sets pertinent to large cancer cell-line collections may offer an as-yet-unmatched potential for exploring the cell-biological impact of novel compounds in genomically defined cancer types. Such cell-line collections may advance molecularly targeted treatment of cancer by providing a tool for preclinical molecular drug target validation on the basis of the genetic lesion signature characteristic of individual tumors.

Methods

Cells. The cell-line collection generated by A.F. Gazdar, J. Minna, and colleagues (69, 70) formed the basis of this collection. Further cell lines were obtained from ATCC, DSMZ (German Collection of Microorganisms and Cell Cultures, Germany), and our own or other cell culture collections. Details on all cell lines are listed in Supplemental Table 1, including providers and culture conditions. Cells were routinely controlled for infection with mycoplasma by MycoAlert (Cambrex) and were treated with antibiotics according to a previously published protocol (71) in case of infection.

SNP arrays. Genomic DNA was extracted from cell lines using the Puregene kit (QIAGEN) and hybridized to high-density oligonucleotide arrays (Affymetrix) interrogating 238,000 SNP loci on all chromosomes except Y, with a median intermarker distance of 5.2 kb (mean 12.2 kb). Array experiments were performed according to the manufacturer's instructions. SNPs were genotyped by the Affymetrix Genotyping Tools software, version 2.0. SNP array data of 371 primary samples were obtained from the Tumor Sequencing Project (processed data file viewable in GenePattern's SNP viewer: dataset.snp; <http://www.broad.mit.edu/cancer/pub/tsp/>) (15). We applied what we believe is a novel and general method for GISTIC (14) to analyze the data sets. In brief, each genomic marker was scored according to an integrated measure of the prevalence and amplitude of copy number changes (and only prevalence in the case of LOH), and the statistical significance of each score was assessed by comparison with the results expected from the background aberration rate alone. The GISTIC algorithm was run using 2 different pairs of copy number thresholds: copy number 4 (amplifications); 1 (deletions); and copy number 2.14 (amplifications); 1.87 (deletions) to reflect focal and broad events, respectively. For the sake of simplicity, we refer to these settings using only the amplification threshold.

Detection of homozygous deletions. For identification of homozygous deletions, SNP data were filtered for 5 coherent SNPs exhibiting copy numbers of less than 0.5. The analysis was focused on focal losses, excluding entire chromosomal arms. Information about genes located in a region of homozygous deletion was based on hg17 build of the human genome sequence from the University of California Santa Cruz (<http://genome.ucsc.edu>).

Analysis of cooccurring lesions. The analysis was performed computing ratios of observed versus expected cooccurrence frequency of individual lesions. Hierarchical clustering of mutation data combined to quantitative copy number changes that were dichotomized was performed using the reciprocal cooccurrence ratio as distance measure with average linkage method. As the adequate threshold for occurrence of copy number lesions depends on the overall level of copy number alteration for that specific lesion, the sum of these ratios for 3 distinct thresholds was used.

Mutation detection. Mutation status of known oncogene mutations in the genes *EGFR*, *BRAF*, *ERBB2*, *PIK3CA*, *NRAS*, *KRAS*, *ABLI*, *AKT2*, *CDK4*, *FGFR1*, *FGFR3*, *FLT3*, *HRAS*, *JAK2*, *KIT*, *PDGFR α* , and *RET* was determined

by mass-spectrometric genotyping. Mutation status of these genes for all cell lines was published previously (22). In addition, the genes *EGFR*, *BRAF*, *ERBB2*, *PIK3CA*, *KRAS*, *TP53*, *STK11*, *PTEN*, and *CDKN2A* were bi-directionally sequenced following PCR amplification of all coding exons.

Expression arrays. Expression data for 54 of the cell lines were obtained using Affymetrix U133A arrays. RNA extraction, hybridization, and scanning of arrays were performed using standard procedures (35). CEL files from U133A arrays were preprocessed using the dChip software (<http://biosun1.harvard.edu/complab/dchip/>; built date May 5, 2008). We compared the cell lines with cell lines and primary tumors from lung cancer (28), renal cell carcinomas (29, 72), and lymphoma (30, 73) data sets obtained from GEO (<http://www.ncbi.nlm.nih.gov/geo/>) by hierarchical clustering. Data were processed by standard procedures; normalization was performed in dChip. For comparison of NSCLC cell lines (U133A) and primary tumors, we used data on adenocarcinomas from Bhattacharjee and colleagues generated on U95Av2 arrays (35). We selected genes that we found differentially expressed between cell lines with mutant *EGFR* and WT *EGFR* (fold change between groups >2, 90% CI; absolute difference >100, $P < 0.01$) and between erlotinib-sensitive and erlotinib-resistant cell lines (erlotinib-sensitive [$GI_{50} < 0.1 \mu M$] vs. erlotinib-resistant [$GI_{50} > 2 \mu M$], fold change >2, 90% CI; absolute difference >100, $P < 0.005$). For principal component analysis, the R language for statistical computing was used. Variable transcripts were identified using the following filtering criteria: coefficient of variation 1.9 through 10, 40% present call rate. The first principal component described 14.5% of the overall variance, the second 9.6%, and the third 8.2%. Using a cutoff of 1400 in the eigenvalue, samples were grouped according to the first principal component.

Cell-based screening. All compounds were purchased from commercial suppliers or synthesized in house, dissolved in DMSO, and stored at $-80^{\circ}C$. Cells were plated into sterile microtiter plates using a Multidrop instrument (Thermo Scientific) and cultured overnight. Compounds were then added in serial dilutions. Cellular viability was determined after 96 hours by measuring cellular ATP content using the CellTiter-Glo Assay (Promega). Plates were measured on a Mithras LB 940 Plate Reader (Berthold Technologies). GI_{50} values were determined from the preimage under the growth inhibition curve, where the latter was smoothed according to the logistic function with the parameters appropriately chosen. For these analyses, we have established a semiautomated pipeline as what we believe to be a novel R package (43).

Lesion-based prediction of compound sensitivity. For lesion-based prediction of sensitivity, 3 different approaches were applied. First, the most sensitive and most resistant samples were chosen according to their sensitivity profile. Where the sensitivity profile of the corresponding compound did not allow a clear distinction between resistant and sensitive cell lines, groups were defined by the 25th and 75th percentiles. We used Fisher's exact test to evaluate the association between the activity of the compound and the presence of significant lesions as defined by GISTIC. For this purpose, the cell-line panel was divided according to the presence of each lesion. The logarithmically transformed GI_{50} values pertinent to each group were now compared by a 2-sample Welch's *t* test. In order to avoid an artificially low variance, the Welch's *t* tests were based on a fixed variance determined as the mean of the variances that were clearly distinct from zero (>0.1). Details of this procedure are presented in the publication by Solit and colleagues (12).

In a next step, multilesion predictors of sensitivity were calculated using feature selection, with subsequent validation by a KNN algorithm with a leave-one-out strategy (45), in which the same choice of samples was used as above for Fisher's exact test: For all but 1 sample, genetic lesions strongly discriminating between sensitive and resistant cell lines were selected and the prediction was validated by the remaining left-out sample. Copy number data were dichotomized to ensure a better comparability with the mutation data. Five different thresholds were used to



dichotomize the copy numbers: 2.14, 2.46, 2.83, 3.25, and 4 for amplified loci; and 1.87, 1.62, 1.41, 1.23, and 1 for deletions. The collection of features and the threshold for the dichotomization were selected for which the leave-one-out validation showed best performance and was taken as the best combined predictor to the respective compound. As a measure to select the setting with the largest predictive strength, the Youden index (sensitivity + specificity - 1) was used.

For example, the best erlotinib single gene predictor was obtained when the lesion data were dichotomized using the thresholds 3.25 and 1.23, respectively. Cell lines with a GI_{50} of less than 0.07 μ M were considered sensitive. For the predictor, the same cutoff values were used. Best performance in the leave-one-out cross validation was obtained using 15 features, $k = 3$ neighbors, and the cosine-based metric. Due to the problem of multiple hypothesis testing, the significance of the above Welch's t tests as well as Fisher's exact tests should be understood in an explorative rather than confirmative sense.

The NCI-60 cancer cell-line panel was used for validation of our findings (http://dtp.nci.nih.gov/mtargets/mt_index.html). Since the MEK inhibitor UO126 and the Hsp90 inhibitor 17-AAG were not covered by the collection of pharmacological data, we analyzed the association of the respective lesions to hypothemycin (MEK inhibitor) and to geldanamycin (17-AAG is a geldanamycin derivative) instead. Significance of association was analyzed by Fisher's exact test. Due to strongly discordant GI_{50} values, the cell lines HOP62 and A549 were excluded from the analysis with respect to the Hsp90 inhibitors. The thresholds for 1q21.3 amplification were set according to the overall distribution of copy number changes in the respective data sets (2.7 corresponding to 33% of the NSCLC cell lines; 2.4 corresponding to 33% of the NCI-60 collection).

All Fisher's exact tests, Welch's t tests (all 2-tailed), and Wilcoxon tests were performed using R version 2.7.1 (<http://www.wpic.pitt.edu/WPIC-CompGen/hclust/hclust.htm>). A level of significance of 5% was chosen. For cluster analysis, the R routine "hclust" was used.

Structural modeling of compound binding. The crystal structures of dasatinib bound to ABL kinase (pdb code 2IVU; ref. 74) and vandetanib bound to the RET kinase (pdb code 2IVU; ref. 75) were aligned to the kinase domain of EGFR bound to erlotinib (pdb code 1M17; ref. 76) using PyMOL software, 1.1beta (DeLano Scientific LLC). Based on the structural alignment of ABL with EGFR, the binding mode for dasatinib in EGFR is identical to that of the dasatinib-Abl complex. Figures of the structures were prepared using PyMOL.

Western blot analyses. Whole-cell lysates were prepared in NP40 lysis buffer (50 mmol/l Tris-HCl, pH 7.4, 150 mmol/l NaCl, 1% NP40) supplemented with protease and phosphatase inhibitor I and II cocktails (Merck) and clarified by centrifugation. Proteins were subjected to SDS-PAGE on 12% gels, except where indicated. Western blotting was done as described previously (77). The EGFR (no. 2232), the AKT (no. 9272), and the phospho-SRC (Tyr⁴¹⁶) (no. 2101) antibodies were both purchased from Cell Signaling Technology. The SRC (GD11) antibody was purchased from Millipore. The Hsp90 antibody (16F1) was purchased from Stressgen (Assay Designs). The phospho-EGFR (Tyr¹⁰⁶⁸) antibody was purchased from BioSource (Invitrogen). The cyclin D1 (DCS-6), the c-RAF (C-20), and the actin (C-11) antibody were purchased from Santa Cruz Biotechnology Inc. The KRAS (234-4.2) antibody was purchased from Calbiochem.

Immunoprecipitation. For the detection of complexes of Hsp90 with KRAS or EGFR and vice versa, whole-cell lysate (0.5–1 mg) in NP40 lysis buffer was incubated with Agarose A/G Plus pre-conjugated with the Hsp90 or KRAS antibody (see Western blot analyses). Immunoprecipitates were washed in NP40 lysis buffer, boiled in sample buffer, and subjected to SDS-PAGE followed by Western blotting using an anti KRAS, Hsp90, or EGFR antibody to detect complex formation.

Apoptosis assays. Cells were plated in 6-well plates after 24 hours of incubation, treated with 17-AAG for 72 hours, and finally harvested after trypsinization. Then cells were washed with PBS, resuspended in annexin V binding buffer, and finally stained with annexin V-FITC and propidium iodide. FACS analysis was performed on a FACSCanto flow cytometer (BD Biosciences), and results were calculated using FACSDiva Software, version 5.0.

Transfection and infection. Replication-incompetent retroviruses were produced from pBabe-based vectors by transfection into the Phoenix 293-TL packaging cell line (Orbigen) using the calcium precipitation method. Replication-incompetent lentiviruses were produced from pLKO.1-puro based vectors containing the shRNA insert (<http://www.broad.mit.edu/node/563>) by cotransfection of 293-TL cells with pMD.2 and pCMVd.8.9 helper plasmids using reagent Trans-LT (Mirus). Cells were infected with viral supernatants in the presence of polybrene. After 24 hours, medium was changed and cell lines were selected with 1–2 μ g/ml puromycin, from which stable transduced clonal cell lines were derived.

Site-directed mutagenesis. All mutations (Y530F; T341M) were introduced into the c-SRC ORF with the QuikChange XL II Mutagenesis Kit (Stratagene) following the instructions of the manufacturer. Oligonucleotides covering the mutations were designed with the software provided by Stratagene, and each mutant was confirmed by sequencing.

17-DMAG treatment in LSL-KRAS mice. The lox-stop-lox-KRAS (LSL-KRAS) mouse lung cancer model has been described elsewhere (64). Seven mice were imaged by MRI at 12 to 20 weeks after adeno-CRE treatments to document initial tumor volume. The mice were then divided into 17-DMAG (LC Laboratories) and placebo treatment groups, with 4 and 3 mice in each group, respectively. 17-DMAG was formulated in saline and given through tail-vein injection at 20 mg/kg/d dosing schedule. Mice were imaged by MRI after 1 week of drug treatment and sacrificed for further histological analysis thereafter. The protocol for animal work was approved by the Dana-Farber Cancer Institute Institutional Animal Care and Use Committee, and the mice were housed in a pathogen-free environment at the Harvard School of Public Health.

MRI scanning and tumor volume measurement. Mice were anesthetized with 1% isoflurane; respiratory and cardiac rates were monitored with BioTrig Software, version BT1 (Bruker BioSpin). Animals were imaged in the coronal planes with a rapid acquisition with relaxation enhancement (RARE) sequence ($Tr = 2000$ ms; TE effect = 25 ms, where Tr = pulse repetition time and TE = minimum echo time), using 17×1 mm slices to cover the entire lung. Matrix size of 128×128 and field of view (FOV) of 2.5×2.5 cm² were used for all imaging. The areas of lung tumors were manually segmented and measured using ImageJ software (version 1.33; <http://rsbweb.nih.gov/ij/>) on each magnetic resonance slice. Total tumor volume was calculated by adding tumor areas from all 17 slices (78). Note that MRI cannot clearly distinguish tumor lesions and postobstruction pneumonia that is induced by bronchial tumors of this particular tumor model.

Xenograft models. All animal procedures were in accordance with the German Laws for Animal Protection and were approved by the local animal protection committee and the local authorities (Bezirksregierung Köln). Tumors were generated by s.c. injections of 5×10^6 tumor cells into *nu/nu* athymic male mice. When tumors had reached a size of about 50 mm³, animals were randomized into 2 groups, control (vehicle) and dasatinib-treated mice. All controls were dosed with the same volume of vehicle. Mice were treated daily by oral gavage of 20 mg/kg dasatinib. The vehicle used was propylene glycol/water (1:1). Tumor size was monitored every 2 days by measuring perpendicular diameters. Tumor volumes were calculated from the determination of the largest diameter and its perpendicular diameter according to the equation [tumor volume = $a \times (b^2/2)$], where a = tumor width and b = tumor length].



Acknowledgments

We thank William Pao and William Sellers for helpful discussions and comments on the manuscript. We thank Andreas Janzer for help with immunoblotting experiments and Diana Wagner-Stippich for excellent technical assistance. Roman Thomas is a fellow of the International Association for the Study of Lung Cancer (IASLC). Stefanie Fisher holds a Köln Fortune fellowship. This work was supported by grants from the Deutsche Krebsstiftung (107954 to Roman Thomas) and the German Ministry of Science and Education (BMBF) as part of the German National Genome Research Network (NGFNplus) program (01GS08100 to Roman Thomas). John Minna is supported by grants from SPORE (P50CA70907), DOD PROSPECT, and the Longenbaugh Foundation. Jordi Barretina holds a Beatriu de Pinós fellowship from the Departament d'Educació i Universitats de la Generalitat de Catalunya. K.-K. Wong was supported by NIH grants R01 CA122794 and R01 AG2400401; Dana-Farber/Harvard Cancer Center Lung

Cancer Specialized Program of Research Excellence (SPORE) grant P50 CA090578; and the Cecily and Robert Harris Foundation.

Received for publication August 12, 2008, and accepted in revised form March 25, 2009.

Address correspondence to: Roman Thomas, Max Planck Institute for Neurological Research, Gleueler Str. 50, 50931 Köln, Germany. Phone: 49-221-4726-259; Fax: 49-221-4726-298; E-mail: nini@nf.mpg.de. Or to: Kwok-Kin Wong, Department of Medical Oncology, Dana-Farber Cancer Institute, Harvard Medical School, 44 Binney St., Boston, Massachusetts 02115, USA. Phone: (617) 632-6084; Fax: (617) 582-7839; E-mail: kwong1@partners.org. Or to: Matthew Meyerson, Department of Medical Oncology, Dana-Farber Cancer Institute, Harvard Medical School, 44 Binney St., Boston, Massachusetts 02115, USA. Phone: (617) 632-4768; Fax: (617) 582-7880; E-mail: matthew_meyerson@dfci.harvard.edu.

- Slamon, D.J., et al. 2001. Use of chemotherapy plus a monoclonal antibody against HER2 for metastatic breast cancer that overexpresses HER2. *N. Engl. J. Med.* **344**:783–792.
- Druker, B.J., et al. 2001. Activity of a specific inhibitor of the BCR-ABL tyrosine kinase in the blast crisis of chronic myeloid leukemia and acute lymphoblastic leukemia with the Philadelphia chromosome. *N. Engl. J. Med.* **344**:1038–1042.
- Druker, B.J., et al. 2001. Efficacy and safety of a specific inhibitor of the BCR-ABL tyrosine kinase in chronic myeloid leukemia. *N. Engl. J. Med.* **344**:1031–1037.
- Hodi, F.S., et al. 2008. Major response to imatinib mesylate in KIT-mutated melanoma. *J. Clin. Oncol.* **26**:2046–2051.
- Heinrich, M.C., et al. 2003. Kinase mutations and imatinib response in patients with metastatic gastrointestinal stromal tumor. *J. Clin. Oncol.* **21**:4342–4349.
- Paez, J.G., et al. 2004. EGFR mutations in lung cancer: correlation with clinical response to gefitinib therapy. *Science*. **304**:1497–1500.
- Lynch, T.J., et al. 2004. Activating mutations in the epidermal growth factor receptor underlying responsiveness of non-small-cell lung cancer to gefitinib. *N. Engl. J. Med.* **350**:2129–2139.
- Pao, W., et al. 2004. EGF receptor gene mutations are common in lung cancers from “never smokers” and are associated with sensitivity of tumors to gefitinib and erlotinib. *Proc. Natl. Acad. Sci. U. S. A.* **101**:13306–13311.
- Sasai, K., et al. 2006. Shh pathway activity is down-regulated in cultured medulloblastoma cells: implications for preclinical studies. *Cancer Res.* **66**:4215–4222.
- Neve, R.M., et al. 2006. A collection of breast cancer cell lines for the study of functionally distinct cancer subtypes. *Cancer Cell.* **10**:515–527.
- Lin, W.M., et al. 2008. Modeling genomic diversity and tumor dependency in malignant melanoma. *Cancer Res.* **68**:664–673.
- Solit, D.B., et al. 2006. BRAF mutation predicts sensitivity to MEK inhibition. *Nature*. **439**:358–362.
- McDermott, U., et al. 2007. Identification of genotype-correlated sensitivity to selective kinase inhibitors by using high-throughput tumor cell line profiling. *Proc. Natl. Acad. Sci. U. S. A.* **104**:19936–19941.
- Beoukheim, R., et al. 2007. Assessing the significance of chromosomal aberrations in cancer: Methodology and application to glioma. *Proc. Natl. Acad. Sci. U. S. A.* **104**:20007–20012.
- Weir, B.A., et al. 2007. Characterizing the cancer genome in lung adenocarcinoma. *Nature*. **450**:893–898.
- Kendall, J., et al. 2007. Oncogenic cooperation and coamplification of developmental transcription factor genes in lung cancer. *Proc. Natl. Acad. Sci. U. S. A.* **104**:16663–16668.
- Kwei, K.A., et al. 2008. Genomic profiling identifies TITF1 as a lineage-specific oncogene amplified in lung cancer. *Oncogene*. **27**:3635–3640.
- Schmid, M., et al. 1998. Homozygous deletions of methylthioadenosine phosphorylase (MTAP) are more frequent than p16INK4A (CDKN2) homozygous deletions in primary non-small cell lung cancers (NSCLC). *Oncogene*. **17**:2669–2675.
- Chen, C.F., Yeh, S.H., Chen, D.S., Chen, P.J., and Jou, Y.S. 2005. Molecular genetic evidence supporting a novel human hepatocellular carcinoma tumor suppressor locus at 13q12.11. *Genes Chromosomes Cancer*. **44**:320–328.
- Jong, K., et al. 2007. Cross-platform array comparative genomic hybridization meta-analysis separates hematopoietic and mesenchymal from epithelial tumors. *Oncogene*. **26**:1499–1506.
- Greshock, J., et al. 2007. Cancer cell lines as genetic models of their parent histology: analyses based on array comparative genomic hybridization. *Cancer Res.* **67**:3594–3600.
- Thomas, R.K., et al. 2007. High-throughput oncogene mutation profiling in human cancer. *Nat. Genet.* **39**:347–351.
- Sharma, S.V., Bell, D.W., Settleman, J., and Haber, D.A. 2007. Epidermal growth factor receptor mutations in lung cancer. *Nat. Rev. Cancer*. **7**:169–181.
- Bamford, S., et al. 2004. The COSMIC (Catalogue of Somatic Mutations in Cancer) database and website. *Br. J. Cancer*. **91**:355–358.
- Aviel-Ronen, S., Blackhall, F.H., Shepherd, F.A., and Tsao, M.S. 2006. K-ras mutations in non-small-cell lung carcinoma: a review. *Clin. Lung Cancer*. **8**:30–38.
- Kaye, F.J. 2005. A curious link between epidermal growth factor receptor amplification and survival: effect of “allele dilution” on gefitinib sensitivity? *J. Natl. Cancer Inst.* **97**:621–623.
- Pao, W., et al. 2005. KRAS mutations and primary resistance of lung adenocarcinomas to gefitinib or erlotinib. *PLoS Med.* **2**:e17.
- Lu, Y., et al. 2006. A gene expression signature predicts survival of patients with stage I non-small cell lung cancer. *PLoS Med.* **3**:e467.
- Lenburg, M.E., et al. 2003. Previously unidentified changes in renal cell carcinoma gene expression identified by parametric analysis of microarray data. *BMC Cancer*. **3**:31.
- Hummel, M., et al. 2006. A biologic definition of Burkitt’s lymphoma from transcriptional and genomic profiling. *N. Engl. J. Med.* **354**:2419–2430.
- Lamb, J., et al. 2003. A mechanism of cyclin D1 action encoded in the patterns of gene expression in human cancer. *Cell*. **114**:323–334.
- Bild, A.H., et al. 2006. Oncogenic pathway signatures in human cancers as a guide to targeted therapies. *Nature*. **439**:353–357.
- Balko, J.M., et al. 2006. Gene expression patterns that predict sensitivity to epidermal growth factor receptor tyrosine kinase inhibitors in lung cancer cell lines and human lung tumors. *BMC Genomics*. **7**:289.
- Dziadziszko, R., et al. 2006. Epidermal growth factor receptor messenger RNA expression, gene dosage, and gefitinib sensitivity in non-small cell lung cancer. *Clin. Cancer Res.* **12**:3078–3084.
- Bhattacharjee, A., et al. 2001. Classification of human lung carcinomas by mRNA expression profiling reveals distinct adenocarcinoma subclasses. *Proc. Natl. Acad. Sci. U. S. A.* **98**:13790–13795.
- Eberhard, D.A., et al. 2005. Mutations in the epidermal growth factor receptor and in KRAS are predictive and prognostic indicators in patients with non-small-cell lung cancer treated with chemotherapy alone and in combination with erlotinib. *J. Clin. Oncol.* **23**:5900–5909.
- Beer, D.G., et al. 2002. Gene-expression profiles predict survival of patients with lung adenocarcinoma. *Nat. Med.* **8**:816–824.
- Nevins, J.R., and Porti, A. 2007. Mining gene expression profiles: expression signatures as cancer phenotypes. *Nat. Rev. Genet.* **8**:601–609.
- Choi, K., Creighton, C.J., Stivers, D., Fujimoto, N., and Kurie, J.M. 2007. Transcriptional profiling of non-small cell lung cancer cells with activating EGFR somatic mutations. *PLoS ONE*. **2**:e1226.
- Cappuzzo, F., et al. 2005. Epidermal growth factor receptor gene and protein and gefitinib sensitivity in non-small-cell lung cancer. *J. Natl. Cancer Inst.* **97**:643–655.
- Hirsch, F.R., et al. 2005. Increased epidermal growth factor receptor gene copy number detected by fluorescence in situ hybridization associates with increased sensitivity to gefitinib in patients with bronchioloalveolar carcinoma subtypes: a Southwest Oncology Group Study. *J. Clin. Oncol.* **23**:6838–6845.
- Sequist, L.V., Bell, D.W., Lynch, T.J., and Haber, D.A. 2007. Molecular predictors of response to epidermal growth factor receptor antagonists in non-small-cell lung cancer. *J. Clin. Oncol.* **25**:587–595.
- Frommolt, P., and Thomas, R.K. 2008. Standardized high-throughput evaluation of cell-based compound screens. *BMC Bioinformatics*. **9**:475.
- Reich, M., et al. 2006. GenePattern 2.0. *Nat. Genet.* **38**:500–501.



45. Golub, T.R., et al. 1999. Molecular classification of cancer: class discovery and class prediction by gene expression monitoring. *Science*. **286**:531-537.
46. Tsao, M.S., et al. 2005. Erlotinib in lung cancer - molecular and clinical predictors of outcome. *N. Engl. J. Med.* **353**:133-144.
47. Arao, T., et al. 2004. Small in-frame deletion in the epidermal growth factor receptor as a target for ZD6474. *Cancer Res.* **64**:9101-9104.
48. Ichihara, E., et al. 2008. Emergence of the EGFR T790M mutation in a lung adenocarcinoma cell line after vandetanib treatment. In *Proceedings of the 99th Annual Meeting of the American Association for Cancer Research*. April 12-16. San Diego, California, USA. AACR. Philadelphia, Pennsylvania, USA. 678.
49. Kobayashi, S., et al. 2005. EGFR mutation and resistance of non-small-cell lung cancer to gefitinib. *N. Engl. J. Med.* **352**:786-792.
50. Pao, W., et al. 2005. Acquired resistance of lung adenocarcinomas to gefitinib or erlotinib is associated with a second mutation in the EGFR kinase domain. *PLoS Med.* **2**:e73.
51. Yuza, Y., et al. 2007. Allele-dependent variation in the relative cellular potency of distinct EGFR inhibitors. *Cancer Biol. Ther.* **6**:661-667.
52. Sos, M.L., et al. 2008. Expression of signaling mediators downstream of EGF-receptor predict sensitivity to small molecule inhibitors directed against the EGF-receptor pathway. *J. Thorac. Oncol.* **3**:170-173.
53. Shah, N.P., et al. 2004. Overriding imatinib resistance with a novel ABL kinase inhibitor. *Science*. **305**:399-401.
54. Carter, T.A., et al. 2005. Inhibition of drug-resistant mutants of ABL, KIT, and EGF receptor kinases. *Proc. Natl. Acad. Sci. U. S. A.* **102**:11011-11016.
55. Yun, C.H., et al. 2007. Structures of lung cancer-derived EGFR mutants and inhibitor complexes: mechanism of activation and insights into differential inhibitor sensitivity. *Cancer Cell.* **11**:217-227.
56. Song, L., Morris, M., Bagui, T., Lee, F.Y., Jove, R., and Haura, E.B. 2006. Dasatinib (BMS-354825) selectively induces apoptosis in lung cancer cells dependent on epidermal growth factor receptor signaling for survival. *Cancer Res.* **66**:5542-5548.
57. Shoemaker, R.H. 2006. The NCI60 human tumour cell line anticancer drug screen. *Nat. Rev. Cancer.* **6**:813-823.
58. Shimamura, T., Lowell, A.M., Engelman, J.A., and Shapiro, G.I. 2005. Epidermal growth factor receptors harboring kinase domain mutations associate with the heat shock protein 90 chaperone and are destabilized following exposure to geldanamycins. *Cancer Res.* **65**:6401-6408.
59. Grbovic, O.M., et al. 2006. V600E B-Raf requires the Hsp90 chaperone for stability and is degraded in response to Hsp90 inhibitors. *Proc. Natl. Acad. Sci. U. S. A.* **103**:57-62.
60. Shields, J.M., Pruitt, K., McFall, A., Shaub, A., and Der, C.J. 2000. Understanding Ras: 'it ain't over 'til it's over'. *Trends Cell Biol.* **10**:147-154.
61. Basso, A.D., et al. 2002. Akt forms an intracellular complex with heat shock protein 90 (Hsp90) and Cdc37 and is destabilized by inhibitors of Hsp90 function. *J. Biol. Chem.* **277**:39858-39866.
62. Lim, K.H., and Counter, C.M. 2005. Reduction in the requirement of oncogenic Ras signaling to activation of PI3K/AKT pathway during tumor maintenance. *Cancer Cell.* **8**:381-392.
63. Ji, H., et al. 2007. Mutations in BRAF and KRAS converge on activation of the mitogen-activated protein kinase pathway in lung cancer mouse models. *Cancer Res.* **67**:4933-4939.
64. Jackson, E.L., et al. 2001. Analysis of lung tumor initiation and progression using conditional expression of oncogenic K-ras. *Genes Dev.* **15**:3243-3248.
65. Karaman, M.W., et al. 2008. A quantitative analysis of kinase inhibitor selectivity. *Nat. Biotechnol.* **26**:127-132.
66. Geyer, C.E., et al. 2006. Lapatinib plus capecitabine for HER2-positive advanced breast cancer. *N. Engl. J. Med.* **355**:2733-2743.
67. Du, J., et al. 2009. Bead-based profiling of tyrosine kinase phosphorylation identifies SRC as a potential target for glioblastoma therapy. *Nat. Biotechnol.* **27**:77-83.
68. Tracy, S., et al. 2004. Gefitinib induces apoptosis in the EGFR L858R non-small-cell lung cancer cell line H3255. *Cancer Res.* **64**:7241-7244.
69. Gazdar, A.F., and Minna, J.D. 1996. NCI series of cell lines: an historical perspective. *J. Cell Biochem. Suppl.* **24**:1-11.
70. Phelps, R.M., et al. 1996. NCI-Navy Medical Oncology Branch cell line data base. *J. Cell Biochem. Suppl.* **24**:32-91.
71. Uphoff, C.C., and Drexler, H.G. 2005. Eradication of mycoplasma contaminations. *Methods Mol. Biol.* **290**:25-34.
72. Shankavaram, U.T., et al. 2007. Transcript and protein expression profiles of the NCI-60 cancer cell panel: an integrative microarray study. *Mol. Cancer Ther.* **6**:820-832.
73. Rinaldi, A., et al. 2006. Genomic and expression profiling identifies the B-cell associated tyrosine kinase Syk as a possible therapeutic target in mantle cell lymphoma. *Br. J. Haematol.* **132**:303-316.
74. Tokarski, J.S., et al. 2006. The structure of Dasatinib (BMS-354825) bound to activated ABL kinase domain elucidates its inhibitory activity against imatinib-resistant ABL mutants. *Cancer Res.* **66**:5790-5797.
75. Knowles, P.P., et al. 2006. Structure and chemical inhibition of the RET tyrosine kinase domain. *J. Biol. Chem.* **281**:33577-33587.
76. Stamos, J., Sliwkowski, M.X., and Eigenbrot, C. 2002. Structure of the epidermal growth factor receptor kinase domain alone and in complex with a 4-anilinoquinazoline inhibitor. *J. Biol. Chem.* **277**:46265-46272.
77. Shimamura, T., et al. 2006. Non-small-cell lung cancer and Ba/F3 transformed cells harboring the ERBB2 G776insV_G/C mutation are sensitive to the dual-specific epidermal growth factor receptor and ERBB2 inhibitor HKI-272. *Cancer Res.* **66**:6487-6491.
78. Li, D., et al. 2007. Therapeutic anti-EGFR antibody 806 generates responses in murine de novo EGFR mutant-dependent lung carcinomas. *J. Clin. Invest.* **117**:346-352.
79. O'Reilly, K.E., et al. 2006. mTOR inhibition induces upstream receptor tyrosine kinase signaling and activates Akt. *Cancer Res.* **66**:1500-1508.

4.3 Identifying genotype-dependent efficacy of single and combined PI3K- and MAPK-pathway inhibition in cancer

Martin L. Sos, Stefanie Fischer, Roland Ullrich, Martin Peifer, Johannes M. Heuckmann, Mirjam Koker, Stefanie Heynck, Isabel Stückrath, Jonathan Weiss, Florian Fischer, Kathrin Michel, Aviva Goel, Lucia Regales, Katerina A. Politi, Samantha Perera, Matthäus Getlik, Lukas C. Heukamp, Sascha Ansén, Thomas Zander, Rameen Beroukhim, Hamid Kashkar, Kevan M. Shokat, William R. Sellers, Daniel Rauh, Christine Orr, Klaus P. Hoeflich, Lori Friedman, Kwok-Kin Wong, William Pao, and Roman K. Thomas

Abstract of the publication

In cancer, genetically activated proto-oncogenes often induce “upstream” dependency on the activity of the mutant oncoprotein. Therapeutic inhibition of these activated oncoproteins can induce massive apoptosis of tumor cells, leading to sometimes dramatic tumor regressions in patients. The PI3K and MAPK signaling pathways are central regulators of oncogenic transformation and tumor maintenance. We hypothesized that upstream dependency engages either one of these pathways preferentially to induce “downstream” dependency. Therefore, we analyzed whether downstream pathway dependency segregates by genetic aberrations upstream in lung cancer cell lines. Here, we show by systematically linking drug response to genomic aberrations in non-small-cell lung cancer, as well as in cell lines of other tumor types and in a series of *in vivo* cancer models, that tumors with genetically activated receptor tyrosine kinases depend on PI3K signaling, whereas tumors with mutations in the RAS/RAF axis depend on MAPK signaling. However, efficacy of downstream pathway inhibition was limited by release of negative feedback loops on the reciprocal pathway. By contrast, combined blockade of both pathways was able to overcome the reciprocal pathway activation induced by inhibitor-mediated release of negative feedback loops and resulted in a significant increase in apoptosis and tumor shrinkage. Thus, by using a systematic chemo-genomics approach, we identify genetic lesions connected to PI3K and MAPK pathway activation and provide a rationale for combined inhibition of both pathways. Our findings may have implications for patient stratification in clinical trials.

Own contributions

Here, I screened 20% of the cell lines displayed in figure 3B and conducted the associated data analysis. The cell lines were treated with two different inhibitors alone or in combination. All cells were monitored for occurrence of apoptosis after 48 hours. Overall, I contributed to the design of the experiments and analyzed the data shown in figure 3B.

Concluding remarks

The success of novel molecular therapies is based on the notion that tumors depend on the signals emerging from the protein inhibited by the applied drug. In this study, we investigated the dependency on the MAPK or PI3K pathways in tumor cells with various genomic alterations. We showed that tumors with genomic alterations in receptor tyrosine kinases (RTKs) are more sensitive towards PI3K pathway inhibitors, whereas tumor cells harboring *Ras/Raf* alterations are more sensitive towards MAPK pathway inhibitors, both *in-vitro* and *in-vivo*. In addition, we combined inhibitors for both pathways and show an enhanced induction of apoptosis, as compared to the induction by each compound alone. Importantly, PI3K inhibitors or inhibitor combinations are also active in tumor cells that are resistant to direct RTK inhibition and moreover, these results can lead to novel treatment strategies for patients in the clinic.

Identifying genotype-dependent efficacy of single and combined PI3K- and MAPK-pathway inhibition in cancer

Martin L. Sos^{a,1}, Stefanie Fischer^{a,1}, Roland Ullrich^{a,1}, Martin Peifer^{a,1}, Johannes M. Heuckmann^a, Mirjam Koker^a, Stefanie Heynck^a, Isabel Stückrath^a, Jonathan Weiss^a, Florian Fischer^a, Kathrin Michel^a, Aviva Goel^b, Lucia Regales^b, Katerina A. Politi^b, Samantha Perera^c, Matthäus Getlik^d, Lukas C. Heukamp^e, Sascha Ansén^f, Thomas Zander^f, Rameen Beroukhim^{c,g}, Hamid Kashkar^h, Kevan M. Shokat^{i,j}, William R. Sellers^k, Daniel Rauh^d, Christine Orr^l, Klaus P. Hoeflich^l, Lori Friedman^l, Kwok-Kin Wong^{c,m}, William Paoⁿ, and Roman K. Thomas^{a,d,f,2}

^aMax Planck Institute for Neurological Research and Klaus Joachim Zülch Laboratories, Max Planck Society and Medical Faculty, University of Cologne, Gleueler Strasse 50, 50931 Cologne, Germany; ^bHuman Oncology and Pathogenesis Program, Memorial Sloan-Kettering Cancer Center, 1275 York Avenue, New York, NY 10021; ^cDepartment of Medical Oncology, Dana-Farber Cancer Institute, 44 Binney Street, Boston, MA 02115; ^dChemical Genomics Center, Max Planck Society, Otto Hahn Strasse 15, 44227 Dortmund, Germany; ^eDepartment of Pathology, University Hospital Bonn Medical School, Sigmund Freud Strasse 25, 53127 Bonn, Germany; ^fDepartment I of Internal Medicine and Center of Integrated Oncology Cologne–Bonn and ^gInstitute for Medical Microbiology, Immunology, and Hygiene, Medical Faculty, University of Cologne, 50924 Cologne, Germany; ^hBroad Institute of Harvard and Massachusetts Institute of Technology, 320 Charles Street, Cambridge, MA 02141; ⁱHoward Hughes Medical Institute and Department of Cellular and Molecular Pharmacology, University of California, 600 16th Street, San Francisco, CA 94158; ^jDepartment of Chemistry, University of California, Room 419 Latimer Hall, Berkeley, CA 94720; ^kNovartis Institutes for BioMedical Research, 250 Massachusetts Avenue, Cambridge, MA 02139; ^lDepartment of Cancer Signaling and Translational Oncology, Genentech Inc., 1 DNA Way, South San Francisco, CA 94070; ^mDepartment of Medicine, Brigham and Women's Hospital and Harvard Medical School, 75 Francis Street, Boston, MA 02115; and ⁿVanderbilt-Ingram Cancer Center, 777 Preston Research Building, 2220 Pierce Avenue, Nashville, TN 37232

Edited by Charles R. Cantor, Sequenom, Inc., San Diego, CA, and approved August 27, 2009 (received for review July 6, 2009)

In cancer, genetically activated proto-oncogenes often induce “upstream” dependency on the activity of the mutant oncoprotein. Therapeutic inhibition of these activated oncoproteins can induce massive apoptosis of tumor cells, leading to sometimes dramatic tumor regressions in patients. The PI3K and MAPK signaling pathways are central regulators of oncogenic transformation and tumor maintenance. We hypothesized that upstream dependency engages either one of these pathways preferentially to induce “downstream” dependency. Therefore, we analyzed whether downstream pathway dependency segregates by genetic aberrations upstream in lung cancer cell lines. Here, we show by systematically linking drug response to genomic aberrations in non-small-cell lung cancer, as well as in cell lines of other tumor types and in a series of in vivo cancer models, that tumors with genetically activated receptor tyrosine kinases depend on PI3K signaling, whereas tumors with mutations in the RAS/RAF axis depend on MAPK signaling. However, efficacy of downstream pathway inhibition was limited by release of negative feedback loops on the reciprocal pathway. By contrast, combined blockade of both pathways was able to overcome the reciprocal pathway activation induced by inhibitor-mediated release of negative feedback loops and resulted in a significant increase in apoptosis and tumor shrinkage. Thus, by using a systematic chemo-genomics approach, we identify genetic lesions connected to PI3K and MAPK pathway activation and provide a rationale for combined inhibition of both pathways. Our findings may have implications for patient stratification in clinical trials.

cancer genomics | combination therapy | high-throughput cell line screening | oncogene dependency

The past decade has witnessed the advent of targeted cancer therapeutics targeting mutationally activated proto-oncogenes. When targeted to the right patient population, such approaches have proven efficacious with, sometimes dramatic, responses and improvement in survival (1–3). Given the pace of the currently ongoing efforts to fully characterize cancer genomic aberrations, a comprehensive genetic compendium of all human cancers is within reach. Although initial studies suggested that most human tumors are dominated by an array of individual, or “private” mutations (4), more recent studies imply that most human cancer genome aberrations converge on activation of a limited repertoire of “downstream” oncogenic signaling pathways (5–8). Importantly, among

the most heavily affected oncogenic pathways were the PI3K and the MAPK signaling pathways. Thus, rather than providing therapeutic strategies for each individual mutation, targeting key modulators of downstream pathways appears increasingly attractive. Importantly, small synthetic molecules targeting these pathways have been developed and are currently undergoing clinical testing.

Previously, mutations in *BRAF* have been linked to downstream dependency on MEK (9), the kinase phosphorylating MAPK (or ERK), *KRAS*-mutant lung cancers depend on both PI3K and MAPK signaling (10), and resistance to EGFR inhibition appears to involve mechanisms that maintain PI3K signaling (11, 12). However, in the vast majority of the cases, the inhibition of either the PI3K or the MAPK pathway alone is not sufficient to robustly induce tumor shrinkage (13), in part explained through release of negative feedback loops resulting in the activation of the alternate pathway (14–18). By contrast, studies analyzing combinations of pathway inhibitors showed favorable results (13, 14). Thus, a genetically defined framework that would allow predicting which of these pathways is primarily affected and whether the combinatorial inhibition of both pathways is superior to single-agent treatment would greatly impact future clinical strategies in trials involving such therapeutics.

A major hurdle in the transition from preclinical drug discovery to clinical trials lies in the genomic diversity of human tumors and the lack of preclinical models that capture this diversity. Given the impact of genomic aberrations on therapeutic response, such mod-

Author contributions: M.L.S., S.F., R.U., M.P., M.K., S.H., I.S., J.W., K.M., A.G., L.R., K.A.P., S.P., L.C.H., T.Z., R.B., H.K., C.O., K.P.H., L.F., K.-K.W., W.P., and R.K.T. designed research; M.L.S., S.F., R.U., J.M.H., M.K., S.H., I.S., J.W., F.F., K.M., A.G., L.R., K.A.P., S.P., H.K., C.O., and K.P.H. performed research; M.G., K.M.S., D.R., and L.F. contributed new reagents/analytic tools; M.L.S., S.F., R.U., M.P., J.M.H., M.K., S.H., J.W., F.F., K.M., A.G., L.R., K.A.P., S.P., M.G., L.C.H., S.A., T.Z., R.B., H.K., K.M.S., W.R.S., D.R., C.O., K.P.H., L.F., K.-K.W., W.P., and R.K.T. analyzed data; and M.L.S., S.F., M.P., S.A., W.R.S., D.R., K.-K.W., W.P., and R.K.T. wrote the paper.

Conflict of interest statement: R.K.T. has received research support from AstraZeneca and Novartis. W.R.S. is an employee of Novartis. C.O., K.P.H., and L.F. are employees of Genentech.

This article is a PNAS Direct Submission.

Freely available online through the PNAS open access option.

¹M.L.S., S.F., R.U., and M.P. contributed equally to this work.

²To whom correspondence should be addressed. E-mail: nini@nf.mpg.de.

This article contains supporting information online at www.pnas.org/cgi/content/full/0907325106/DCSupplemental.

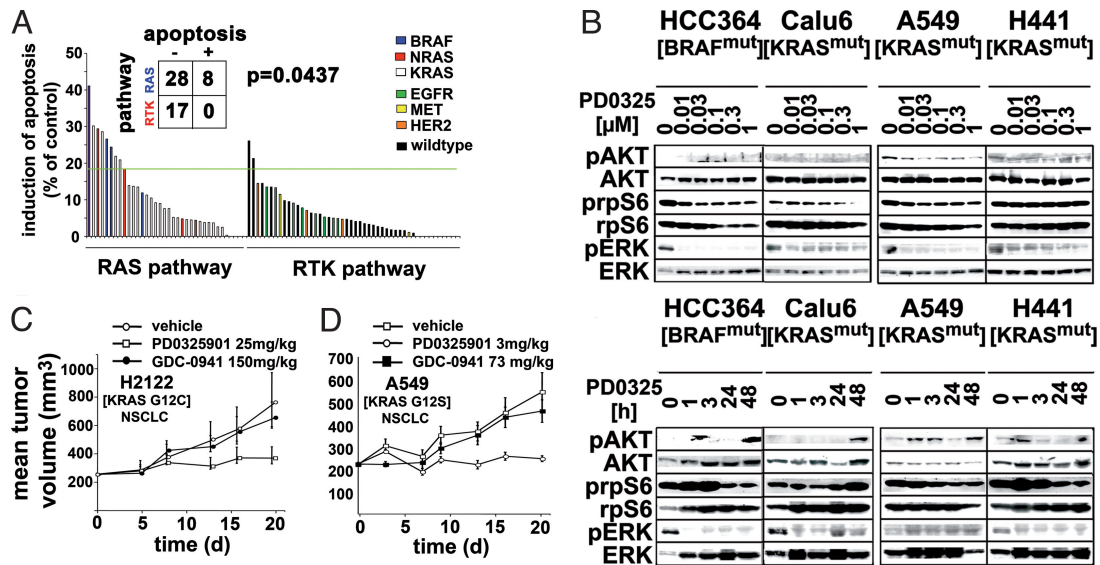


Fig. 2. Inhibition of MAPK signaling in cancer. (A) All cell lines were screened for induction of apoptosis using Annexin-V/PI staining after 72 h of treatment with PD0325901. Bars represent the fraction of apoptotic cells and are sorted from the most sensitive cell line (Left) to the most resistant cell line (Right), and grouped according to the presence of RTK- (EGFR, ERBB2, MET) or RAS-lesions (KRAS, NRAS, BRAF). Two-by-two table highlights the distribution of apoptotic cell lines in the two different genetically defined groups (RTK, RAS). (B) Two PD0325901 sensitive (HCC364, Calu6) and two less sensitive cell lines (A549, H441) were treated with PD0325901 either in a dilution series (Left) or over time at a fixed concentration (0.5 μM ; Right). Pharmacodynamic markers (pAKT, AKT, pS6, S6, pERK, ERK) were assessed by immunoblotting for all cell lines and all conditions. (C) Nude mice were s.c. engrafted with H2122 and A549 cells, and tumors were treated with either the vehicle control, GDC-0941 or PD0325901 at the indicated concentration. Both compounds were administered every other day in the case of H2122 or every day in the case of A549. Similar results were obtained with other doses and other schedules (Fig. 4 D and E). The mean tumor volumes (y axis) are plotted over time (x axis).

induced apoptosis (Fig. S3). Also, hierarchical clustering of the activity of compounds with enhanced selectivity against the different isoforms of PI3K, as well as of the mTOR inhibitor rapamycin across all of the cell lines validated p110 α as the critical target of PI-103 (Fig. S4 A and B) (25, 26). Also, these experiments revealed a high degree of synergy between PI3K and mTOR inhibition, as previously reported (Fig. S4C) (26).

In sensitive cells, PI-103 induced sustained suppression of phosphorylated (p-)Akt at submicromolar concentrations (Fig. 1B; Fig. S3). In resistant cells, p-Akt levels were also extinguished, but returned to almost baseline levels after 24–48 h of treatment. By contrast, in all cell lines tested, levels of p-ERK were either induced or failed to be reduced by PI-103 treatment (Fig. 1B; Fig. S3), presumably due to release of negative feedback loops (15–17). Thus, although RTK-driven cancers exhibit a therapeutically exploitable dependency on PI3K signaling, treatment-induced activation of the MAPK signaling pathway may limit the overall activity of single-agent PI3K inhibition.

We next transplanted a series of cell lines of different tumor types onto nude mice (SI Methods) and treated the mice with GDC-0941, a pharmlalog of PI-103 with superior pharmacokinetic properties (27). The panel studied in vivo comprised cell lines derived from *EGFR*-mutant lung cancer, *MET*-amplified gastric cancer, and *FGFR2*-mutant endometrial cancer. Tumor growth was halted when treated with 150 mg/kg of GDC-0941, and resulted in tumor shrinkage in the case of the *MET*-amplified gastric cancer cell line MKN45 and the *EGFR*-mutant lung cancer cell line HCC827, in the latter case even when only 75 mg/kg of GDC-0941 were administered (Fig. 1C). Tumor growth inhibition was paralleled by decreased phosphorylation of AKT, as evidenced by immunohistochemical analysis of explanted tumors (Fig. S5). Remarkably, even the growth of tumors expressing the T790M resistance mutation of *EGFR* was inhibited by single-agent treatment with GDC-0941 (H1975; Fig. 1C Upper Right). By contrast, mice receiving placebo exhibited massive growth of all tumors (Fig. 1C). We next assessed the efficacy of GDC-0941 in two transgenic mouse models of RTK-driven NSCLC. In one model (28), lung cancer is driven by

inducible expression of the insertion mutation YVMA of *ERBB2* (Her2/neu). In the other model (29), lung-specific induction of the double-mutant *EGFR*^{L858R/T790M} (LTM) leads to erlotinib-resistant lung cancer growth in mice. In the *ERBB2*^{YVMA} mice, treatment with 150 mg/kg of GDC-0941 led to pronounced tumor shrinkage, whereas the lower dose (75 mg/kg) induced inhibition of tumor growth compatible with stable disease (Fig. 1D; Fig. S6A). In the LTM mice, 150 mg/kg of GDC-0941 halted tumor growth in four out of five mice, compatible with stable disease (Fig. S6B). These findings validate PI3K signaling as the predominant downstream signaling pathway regulating survival in RTK-driven cancers. However, in some cases, tumor growth was only stopped, compatible with release of negative feedback loops limiting the single agent activity of PI3K inhibition.

Dissecting MAPK Dependency in Cancer. To identify MAPK signaling dependency in NSCLC, we systematically screened our cell line panel for apoptosis induction after treatment with the potent and selective MEK1/2 inhibitor PD0325901 at clinically achievable doses of 0.25 μM (Fig. S7) and 0.1 μM (Fig. S2 and Table S1) (30). Due to its high potency and selectivity, the MEK inhibitor PD0325901 was used to interrogate the MAPK pathway. This analysis indicated enrichment of cell lines with RAS pathway mutations among the top scoring cell lines displaying robust induction of apoptosis ($P = 0.0165$) (Fig. S7). We next grouped the cells according to their genotype and the fraction of apoptotic cells after treatment with PD0325901 and observed an enrichment of cells with MAPK lesions among the top scoring cell lines ($P = 0.0437$) (Fig. 2A). Interestingly, *BRAF*- and *NRAS*-mutant cells were predominantly found among the top 10 sensitive cell lines, but did not reach statistical significance due to the low prevalence of *BRAF*- and *NRAS*-mutations in our cell line panel (*BRAF*^{mut}, 6%; *NRAS*^{mut}, 5%).

Again, treatment with an inhibitor of a single downstream pathway, PD0325901, led to induction of the other signaling pathway: p-Akt was induced both in highly sensitive and cells of limited sensitivity (Fig. 2B). Thus, our findings confirm and extend previ-

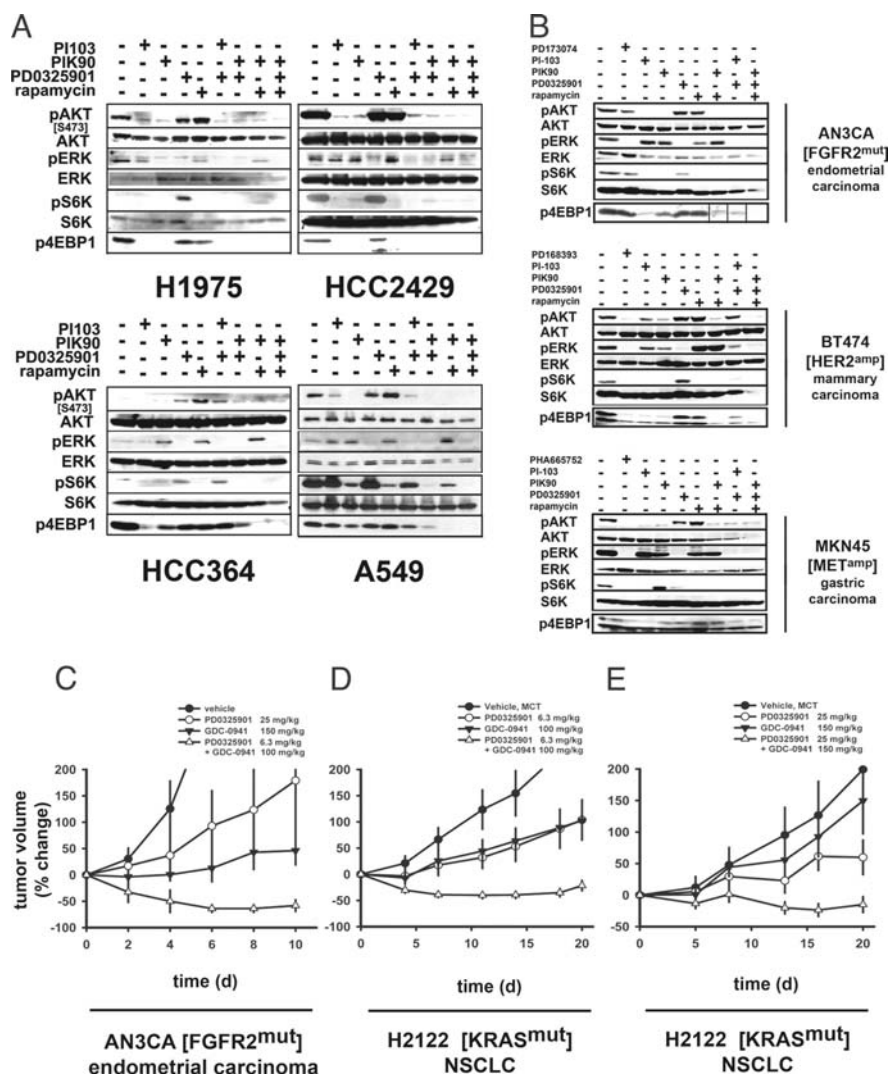


Fig. 4. Suppression of feedback loops by dual PI3K/MAPK-inhibition enhances tumor shrinkage in vivo. (A) Four NSCLC cell lines (H1975, HCC2429, HCC364, A549) with different genetic lesions were treated for 24 h with PI-103, PIK90, PD0325901 and rapamycin, in various combinations at fixed concentrations (PI-103, 1 μ M; PIK90, 5 μ M; PD0325901, 0.5 μ M; rapamycin, 0.01 μ M). Pharmacodynamic markers (pAKT, AKT, pS6K, S6K, pERK, ERK, p4EBP1) were assessed by immunoblotting. (B) Three different cell lines of non-NSCLC cancer type (AN3CA, BT474, MKN45) with different genetic lesions were treated for 6 h with PI-103, PIK90, PD0325901 and rapamycin, in different combinations at fixed concentrations (PI-103 1 μ M; PIK90 5 μ M; PD0325901 0.5 μ M; rapamycin 0.01 μ M). Pharmacodynamic markers (pAKT, AKT, pS6K, S6K, pERK, ERK, p4EBP1) were assessed by immunoblotting. The biochemical response to specific inhibitors targeting the primary genetic lesion in the respective cell line is shown as a reference (PD173074 targets FGFR, PD168393 targets ERBB2, PHA665752 targets MET). Black bars indicate splicing of noncontiguous bands run on the same gel. (C and D) Nude mice were s.c. engrafted with AN3CA or H2122 cells, and tumors were treated daily with vehicle control, GDC-0941, PD0325901, or a combination of both at the indicated dose. The tumor volumes (y axis) are plotted over time (x axis). (E) H2122 tumors were grown on nude mice as in D, and mice were treated with an intermittent schedule of the combination of GDC-0941 and PD0325901, both dosed at their MTD (the combination was administered every fourth day; GDC-0941 dose, 150 mg/kg; PD0325901 dose, 25 mg/kg).

Suppression of Feedback Loop-Mediated Pathway Reactivation by Combined Blockade of MAPK and PI3K Pathways. We hypothesized that enhanced cell killing by dual pathway inhibition (Fig. 3) might be due to suppression of release of negative feedback loops and analyzed the impact of these combinations on pathway activation. Biochemical analyses of response indicated that although the dual PI3K/mTOR inhibitor, PI-103, the p110 α inhibitor, PIK-90, the mTOR inhibitor, rapamycin, and the MEK inhibitor, PD0325901, all led to inhibition of signaling downstream of the respective targets, all of these inhibitors led to induction of at least one signaling mediator in the alternate pathway (Fig. 4A and B). By contrast, combined blockade of both PI3K and MAPK signaling potentially suppressed activation of the other pathway in all cell lines tested (Fig. 4A and B). Thus, combined inhibition of both PI3K and MAPK signaling pathways can suppress feedback loop-induced activation of other oncogenic signaling pathways, resulting in more potent induction of apoptosis.

Last, we transplanted the *FGFR2*-mutant cell line AN3CA into nude mice. Although single-agent treatment with the MEK inhibitor PD0325901 had no impact on tumor growth and the treatment with the PI3K inhibitor GDC-0941 halted tumor growth (Fig. 1C), only the combination of both compounds led to robust tumor shrinkage (Fig. 4C). We next analyzed the *KRAS*-mutant cell line H2122. As expected, only the combination treatment and not single-agent treatment led to significant tumor size reduction in vivo (Fig. 4D). Also, an alternating schedule where both the MEK

inhibitor PD0325901 and the PI3K inhibitor GDC-0941 were administered at their MTD every fourth day was similarly effective (Fig. 4E), potentially being more tolerable.

Discussion

A critical determinant for the success of molecularly targeted drugs will be to identify those tumors that are connected with a therapeutically amenable dependency and to define the optimal therapeutic strategy for treating these tumors. Here, we applied a chemo-genomics approach to link dependency on the PI3K and MAPK pathways to subsets of genomic aberrations in cancer using an NSCLC, as well as non-NSCLC cell line model. Notably, we found RTK-driven tumors to largely depend on PI3K and RAS-/RAF-driven tumors to be addicted to the MAPK signaling pathways, respectively. However, in all settings tested, release of negative feedback loops led to activation of the alternate pathway. Similar to recent studies in breast cancer (14), combined inhibition of both pathways potentially suppressed release of negative feedback loops; thereby, resulting in enhanced induction of apoptosis in tumor cells and tumor shrinkage in vivo. Thus, patients whose tumors harbor genomic aberrations in RTKs or any of the RAS-/RAF-oncogenes might benefit from treatment with a combination of a PI3K inhibitor and a MEK inhibitor.

It has been generally assumed that the engagement of both the MAPK and PI3K pathways by mutant RTKs is essential (1, 34). Our results, by contrast, suggest that the primary *downstream* depen-

dependency of such tumors is on the PI3K pathway, whereas activation of the MAPK pathway may primarily be the result of inhibition of the PI3K pathway. This finding might be of particular interest for treatment of patients whose RTK-driven cancer has acquired secondary resistance after an initial response (e.g., EGFR-mutant lung cancer treated with EGFR inhibitors). In these tumors, secondary resistance mechanisms arise that either abrogate the binding of the kinase inhibitor (35, 36), or that substitute the primary signaling input by activation of additional kinases that reactivate the same *downstream* pathway (12, 37, 38). Notably, we found H1975 cells that express the T790M resistance mutation of EGFR to be sensitive to PI3K inhibition. Similarly, HCC827 GR cells (12) that acquired EGFR inhibitor resistance by amplification of *MET* retained the high sensitivity to PI3K inhibition of the parental HCC827 cell line. Thus, the primary signaling dependency encoded by an activated mutation in a receptor tyrosine kinase remains exploitable by PI3K inhibition alone, or better, in combination with a MAPK pathway inhibitor.

BRAF-mutant tumors were found in previous studies to be addicted to *downstream* activation of MEK (9). Our findings corroborate these observations; however, they further indicate that these and *RAS*-mutant tumors exhibit the highest degree of susceptibility to combined PI3K/MAPK pathway inhibition. Thus, as is the case with RTK-driven tumors, suppression of feedback-mediated PI3K activation is still synergistic, even in the case of a direct *downstream* dependency. We further found *NRAS*-mutant NSCLC tumors to be exquisitely sensitive to MEK inhibition; thereby, adding these genotypes to the growing list of genetic lesions that might be amenable to specific therapeutic intervention (13).

Of note, we found that intermittent administration of a combination of a MEK inhibitor and a PI3K inhibitor at their respective MTD was similarly effective as the daily administration at lower doses. This observation suggests that noncontinuous, but potent inhibition of these pathways might be sufficient for tumor growth inhibition, a finding reminiscent of BCR-ABL inhibition in chronic

myeloid leukemia (39). Thus, rather than administering continuously lower doses of inhibitors targeting *downstream* signaling pathways, intermittent high dosing of such drug combinations might be better tolerated and allow for more potent target inhibition, induction of apoptosis, and tumor control.

In summary, we have defined the role of PI3K and MAPK signaling in genetically defined cancers, and provide strong evidence that combined inhibition of both pathways might be clinically beneficial. More broadly, our chemical-genomics approach may be useful for the study of novel therapeutics and might help to direct future drug development and patient stratification in clinical trials.

Materials and Methods

The cell line panel described previously (19) was used for cell-based screening against various inhibitors using CellTiterGlo as a growth inhibition assay or using Annexin-V and propidium iodide staining of cells as a measure of apoptosis. The accuracy of the measurement of apoptosis was assessed in nine representative cell lines (Fig. S10). Cell-based screening was performed as described (19). This cell line panel has been shown to represent the distribution of genetic aberrations present in primary lung tumors (19). Other cell lines representing additional non-NSCLC tumor types were included to test whether observations were general features of tumors with the respective genotypes. Calculation of the *P* values was performed using a two-tailed *t* test implemented in "R" and, where appropriate, corrected for testing of multiple hypotheses. Pharmacodynamic response of signaling was measured by immunoblotting of cellular lysates of treated cells using phospho-specific antibodies. Mouse experiments were performed under approval of the respective animal care review board. Mice were treated with inhibitors by oral gavage using the indicated doses and schedules. Tumor size was determined by magnetic-resonance imaging in the case of transgenic mice and by measuring diameters using a caliper in the case of xenografts. After treatment, mice were killed and tumors were explanted and, in some instances, subjected to immunohistochemical staining of markers of response. For more details, see *SI Methods*.

ACKNOWLEDGMENTS. This work was supported by Deutsche Krebshilfe Grant 107954, Fritz-Thyssen-Stiftung Grant 10.08.2.175, and German Ministry of Science and Education NGFNplus-program BMBF Grant 01GS08100 (to R.K.T.), by the Deutsche Forschungsgemeinschaft through SFB832 (to R.K.T. and L.C.H.), and National Cancer Institute Grant R01 CA121210 (to W.P.). S.F. holds a scholarship of the Cologne Fortune Program/Faculty of Medicine, University of Cologne.

- Sharma SV, Bell DW, Settleman J, Haber DA (2007) Epidermal growth factor receptor mutations in lung cancer. *Nat Rev Cancer* 7:169–181.
- Kantarjian H, et al. (2002) Hematologic and cytogenetic responses to imatinib mesylate in chronic myelogenous leukemia. *N Engl J Med* 346:645–652.
- Shah NP, et al. (2004) Overriding imatinib resistance with a novel ABL kinase inhibitor. *Science* 305:399–401.
- Wood LD, et al. (2007) The genomic landscapes of human breast and colorectal cancers. *Science* 318:1108–1113.
- Parsons DW, et al. (2008) An integrated genomic analysis of human glioblastoma multiforme. *Science* 321:1807–1812.
- Jones S, et al. (2008) Core signaling pathways in human pancreatic cancers revealed by global genomic analyses. *Science* 321:1801–1806.
- Ding L, et al. (2008) Somatic mutations affect key pathways in lung adenocarcinoma. *Nature* 455:1069–1075.
- McLendon R, et al. (2008) Comprehensive genomic characterization defines human glioblastoma genes and core pathways. *Nature* 455:1061–1068.
- Solit DB, et al. (2006) *BRAF* mutation predicts sensitivity to MEK inhibition. *Nature* 439:358–362.
- Engelman JA, et al. (2008) Effective use of PI3K and MEK inhibitors to treat mutant Kras G12D and PIK3CA H1047R murine lung cancers. *Nat Med* 14:1351–1356.
- Engelman JA, et al. (2005) ErbB-3 mediates phosphoinositide 3-kinase activity in gefitinib-sensitive non-small cell lung cancer cell lines. *Proc Natl Acad Sci USA* 102:3788–3793.
- Engelman JA, et al. (2007) *MET* amplification leads to gefitinib resistance in lung cancer by activating ERBB3 signaling. *Science* 316:1039–1043.
- Jaiswal BS, et al. (2009) Combined targeting of *BRAF* and *CRAF* or *BRAF* and PI3K effector pathways is required for efficacy in *NRAS* mutant tumors. *PLoS One* 4:e5717.
- Hoeflich KP, et al. (2009) In vivo antitumor activity of MEK and phosphatidylinositol 3-kinase inhibitors in basal-like breast cancer models. *Clin Cancer Res* 15:4649–4664.
- Pratilas CA, et al. (2009) (V600E)*BRAF* is associated with disabled feedback inhibition of *RAF*-*MEK* signaling and elevated transcriptional output of the pathway. *Proc Natl Acad Sci USA* 106:4519–4524.
- O'Reilly KE, et al. (2006) mTOR inhibition induces upstream receptor tyrosine kinase signaling and activates Akt. *Cancer Res* 66:1500–1508.
- Carracedo A, et al. (2008) Inhibition of mTORC1 leads to MAPK pathway activation through a PI3K-dependent feedback loop in human cancer. *J Clin Invest* 118:3065–3074.
- Alessi DR, Cuenda A, Cohen P, Dudley DT, Saltiel AR (1995) PD 098059 is a specific inhibitor of the activation of mitogen-activated protein kinase kinase in vitro and in vivo. *J Biol Chem* 270:27489–27494.
- Sos ML, et al. (2009) Predicting drug susceptibility of non-small cell lung cancers based on genetic lesions. *J Clin Invest* 119:1727–1740.
- Hara K, et al. (2002) Raptor, a binding partner of target of rapamycin (TOR), mediates TOR action. *Cell* 110:177–189.
- Kim DH, et al. (2002) mTOR interacts with raptor to form a nutrient-sensitive complex that signals to the cell growth machinery. *Cell* 110:163–175.
- Loewith R, et al. (2002) Two TOR complexes, only one of which is rapamycin sensitive, have distinct roles in cell growth control. *Mol Cell* 10:457–468.
- Zheng XF, Florentino D, Chen J, Crabtree GR, Schreiber SL (1995) TOR kinase domains are required for two distinct functions, only one of which is inhibited by rapamycin. *Cell* 82:121–130.
- Engelman JA, Luo J, Cantley LC (2006) The evolution of phosphatidylinositol 3-kinases as regulators of growth and metabolism. *Nat Rev Genet* 7:606–619.
- Zunder ER, Knight ZA, Houseman BT, Apsel B, Shokat KM (2008) Discovery of drug-resistant and drug-sensitizing mutations in the oncogenic PI3K isoform p110 α . *Cancer Cell* 14:180–192.
- Fan QW, et al. (2006) A dual PI3 kinase/mTOR inhibitor reveals emergent efficacy in glioma. *Cancer Cell* 9:341–349.
- Folkes AJ, et al. (2008) The identification of 2-(1H-indazol-4-yl)-6-(4-methanesulfonylpiperazin-1-ylmethyl)-4-morpholin-4-yl-thieno[3,2-d]pyrimidine (GDC-0941) as a potent, selective, orally bioavailable inhibitor of class I PI3 kinase for the treatment of cancer. *J Med Chem* 51:5522–5532.
- Perera SA, et al. (2009) HER2YVMA drives rapid development of adenocarcinoma lung tumors in mice that are sensitive to BIBW2992 and rapamycin combination therapy. *Proc Natl Acad Sci USA* 106:474–479.
- Regales L, et al. (2007) Development of new mouse lung tumor models expressing EGFR T790M mutants associated with clinical resistance to kinase inhibitors. *PLoS ONE* 2:e810.
- Friday BB, Adjei AA (2008) Advances in targeting the Ras/Raf/MEK/Erk mitogen-activated protein kinase cascade with MEK inhibitors for cancer therapy. *Clin Cancer Res* 14:342–346.
- Ji H, et al. (2007) Mutations in *BRAF* and *KRAS* converge on activation of the mitogen-activated protein kinase pathway in lung cancer mouse models. *Cancer Res* 67:4933–4939.
- Chou TC (2006) Theoretical basis, experimental design, and computerized simulation of synergism and antagonism in drug combination studies. *Pharmacol Rev* 58:621–681.
- Chou TC, Talalay P (1984) Quantitative analysis of dose-effect relationships: The combined effects of multiple drugs or enzyme inhibitors. *Adv Enzyme Regul* 22:27–55.
- Sharma SV, et al. (2006) A common signaling cascade may underlie "addiction" to the Src, BCR-ABL, and EGFR receptor oncogenes. *Cancer Cell* 10:425–435.
- Kobayashi S, et al. (2005) EGFR mutation and resistance of non-small-cell lung cancer to gefitinib. *N Engl J Med* 352:786–792.
- Pao W, et al. (2005) Acquired resistance of lung adenocarcinomas to gefitinib or erlotinib is associated with a second mutation in the EGFR kinase domain. *PLoS Med* 2:e73.
- Bean J, et al. (2007) *MET* amplification occurs with or without T790M mutations in EGFR mutant lung tumors with acquired resistance to gefitinib or erlotinib. *Proc Natl Acad Sci USA* 104:20932–20937.
- Sos ML, et al. (2009) PTEN loss contributes to erlotinib resistance in EGFR-mutant lung cancer by activation of Akt and EGFR. *Cancer Res* 69:3256–3261.
- Shah NP, et al. (2008) Transient potent BCR-ABL inhibition is sufficient to commit chronic myeloid leukemia cells irreversibly to apoptosis. *Cancer Cell* 14:485–493.

4.4 Chemogenomic Profiling Provides Insights into the Limited Activity of Irreversible EGFR Inhibitors in Tumor Cells Expressing the T790M EGFR Resistance Mutation

Martin L. Sos, Haridas B. Rode, Stefanie Heynck, Martin Peifer, Florian Fischer, Sabine Klüter, Vijaykumar G. Pawar, Cecile Reuter, Johannes M. Heuckmann, Jonathan Weiss, Lars Ruddigkeit, Matthias Rabiller, Mirjam Koker, Jeffrey R. Simard, Matthäus Getlik, Yuki Yuza, Tzu-Hsiu Chen, Heidi Greulich, Roman K. Thomas, and Daniel Rauh

Abstract of the publication

Reversible epidermal growth factor receptor (EGFR) inhibitors are the first class of small molecules to improve progression-free survival of patients with EGFR-mutated lung cancers. Second-generation EGFR inhibitors introduced to overcome acquired resistance by the T790M resistance mutation of EGFR have thus far shown limited clinical activity in patients with T790M-mutant tumors. In this study, we systematically analyzed the determinants of the activity and selectivity of the second-generation EGFR inhibitors. A focused library of irreversible as well as structurally corresponding reversible EGFR-inhibitors was synthesized for chemogenomic profiling involving over 79 genetically defined NSCLC and 19 EGFR-dependent cell lines. Overall, our results show that the growth-inhibitory potency of all irreversible inhibitors against the EGFR T790M resistance mutation was limited by reduced target inhibition, linked to decreased binding velocity to the mutant kinase. Combined treatment of T790M-mutant tumor cells with BIBW-2992 and the phosphoinositide-3-kinase/mammalian target of rapamycin inhibitor PI-103 led to synergistic induction of apoptosis. Our findings offer a mechanistic explanation for the limited efficacy of irreversible EGFR inhibitors in EGFR T790M gatekeeper-mutant tumors, and they prompt combination treatment strategies involving inhibitors that target signaling downstream of the EGFR.

Own contributions

For this study, I screened 15% of the cells showed in Figure 1C against the small molecule EGFR inhibitors BIBW2992, erlotinib, lapatinib and gefitinib and conducted the associated data analysis.

Concluding remarks

Most small molecules that are being used today to inhibit protein kinases, function as direct ATP competitor for binding into the ATP binding pocket of kinases. Here, we investigated the ability of irreversible EGFR inhibitors to abrogate EGFR signaling. These EGFR inhibitors show a higher potency to inhibit EGFR when compared to reversible inhibitors, but fail in the setting of EGFR inhibitor resistant versions of EGFR. However, potency could be restored by combination with PI3K pathway inhibitors. Together these results clearly show the need for structural novel molecules that are able to circumvent the steric clash with the gatekeeper methionine on position 790.

Chemogenomic Profiling Provides Insights into the Limited Activity of Irreversible EGFR Inhibitors in Tumor Cells Expressing the T790M EGFR Resistance Mutation

Martin L. Sos¹, Haridas B. Rode³, Stefanie Heynck¹, Martin Peifer¹, Florian Fischer¹, Sabine Klüter³, Vijaykumar G. Pawar³, Cecile Reuter¹, Johannes M. Heuckmann¹, Jonathan Weiss¹, Lars Ruddigkeit³, Matthias Rabiller³, Mirjam Koker¹, Jeffrey R. Simard³, Matthäus Getlik³, Yuki Yuza⁴, Tzu-Hsiu Chen^{5,7}, Heidi Greulich^{5,6,7}, Roman K. Thomas^{1,2,3}, and Daniel Rauh³

Abstract

Reversible epidermal growth factor receptor (EGFR) inhibitors are the first class of small molecules to improve progression-free survival of patients with *EGFR*-mutated lung cancers. Second-generation EGFR inhibitors introduced to overcome acquired resistance by the T790M resistance mutation of EGFR have thus far shown limited clinical activity in patients with T790M-mutant tumors. In this study, we systematically analyzed the determinants of the activity and selectivity of the second-generation EGFR inhibitors. A focused library of irreversible as well as structurally corresponding reversible EGFR-inhibitors was synthesized for chemogenomic profiling involving over 79 genetically defined NSCLC and 19 EGFR-dependent cell lines. Overall, our results show that the growth-inhibitory potency of all irreversible inhibitors against the *EGFR*^{T790M} resistance mutation was limited by reduced target inhibition, linked to decreased binding velocity to the mutant kinase. Combined treatment of T790M-mutant tumor cells with BIBW-2992 and the phosphoinositide-3-kinase/mammalian target of rapamycin inhibitor PI-103 led to synergistic induction of apoptosis. Our findings offer a mechanistic explanation for the limited efficacy of irreversible EGFR inhibitors in *EGFR*^{T790M} gatekeeper-mutant tumors, and they prompt combination treatment strategies involving inhibitors that target signaling downstream of the EGFR. *Cancer Res*; 70(3): 868–74. ©2010 AACR.

Introduction

Reversible epidermal growth factor receptor (EGFR) inhibitors were the first targeted therapeutics approved for the treatment of non-small cell lung cancer (NSCLC; refs. 1, 2). The 4-amino-quinazoline scaffold allows specific binding in the ATP-binding cleft of mutationally activated ERBB kinases (3).

Based on this scaffold, inhibitors such as gefitinib abrogate the oncogenic signaling of EGFR (4, 5), promote tumor shrinkage in *EGFR*-mutated patients, and thus, significantly extend progression-free survival of patients with late stage lung cancer (2, 6).

One of the greatest challenges for drug development is the emergence of *in cis* resistance mutations to tyrosine kinase inhibitors. For patients with *EGFR* mutant lung cancer with acquired drug resistance mutation of the gatekeeper (T790M; ref. 7), irreversible second-generation EGFR inhibitors (8) have been introduced but have thus far shown limited clinical efficacy (9, 10). We synthesized and studied the activity of a library of 19 structurally related ERBB inhibitors in genetically validated cellular models (11, 12).

Authors' Affiliations: ¹Max Planck Institute for Neurological Research with Klaus-Joachim Zülch Laboratories of the Max Planck Society and the Medical Faculty of the University of Köln, ²Center of Integrated Oncology and Department I of Internal Medicine, University of Köln, Cologne, Germany; ³Chemical Genomics Centre of the Max Planck Society, Dortmund, Germany; ⁴Department of Pediatrics, The Jikei University School of Medicine, Tokyo, Japan; ⁵Department of Medical Oncology, Dana-Farber Cancer Institute, Harvard Medical School, ⁶Department of Medicine, Brigham and Women's Hospital and Harvard Medical School, Boston, Massachusetts; and ⁷The Broad Institute of MIT and Harvard, Cambridge, Massachusetts

Note: Supplementary data for this article are available at Cancer Research Online (<http://cancerres.aacrjournals.org/>).

M.L. Sos, H.B. Rode, and S. Heynck contributed equally to this work.

R.K. Thomas and D. Rauh co-directed this project.

Corresponding Authors: Daniel Rauh, Chemical Genomics Centre, Otto-Hahn-Str. 15, D-44227 Dortmund, Germany. Phone: 49-231-9742-6480; Fax: 49-231-9742-6479; E-mail: daniel.rauh@cg.cgc.mpg.de and Roman Thomas, Max Planck Institute for Neurological Research, Gleueler Str. 50, D-50931 Cologne, Germany. E-mail: nini@nf.mpg.de.

doi: 10.1158/0008-5472.CAN-09-3106

©2010 American Association for Cancer Research.

Materials and Methods

A detailed description of the synthesis of all inhibitors and applied methods is given in the Supplementary Methods. All other compounds were purchased from commercial suppliers, dissolved in DMSO, and stored at -80°C. The collection of 84 NSCLC cells was established previously (11). Single nucleotide polymorphism arrays and mutational analyses were used for routine authentication of the cell lines (11). Ba/F3 cell lines were established and described previously (12) and tested for the expression of the mutant ERBB construct, using immunoblotting and Sanger sequencing. Viability

assays were performed measuring cellular ATP content (Cell-Titer-Glo; Promega). Immunoblotting was performed using standard procedures (13). For apoptosis assays, cells were treated with the respective compound for 24 to 96 h, stained with Annexin V-FITC/PI and analyzed by flow cytometry on a Canto instrument (BD Biosciences). The modeling of RL58 into EGFR-T790M was performed using PyMol (DeLano Scientific LLC). The structure was modeled by mapping the coordinates onto the erlotinib structure bound to EGFR (PDB code: 1m17). For covalent bond formation, velocity was measured determining fluorescence in black 384-well plates with a TECAN Safire² plate reader over time (excitation, 368 nm; emission, 420 nm).

Results

To identify the critical moieties of ERBB inhibitors determining potency and specificity, we synthesized (Supplementary Fig. S1) a library of irreversible 4-amino-quinazolines and quinolines together with their reversible counterparts and characterized their activity in biochemical assays (Fig. 1A). To obtain compounds with high structural similarity and to facilitate the interpretation of structure-activity relations of each modification, we varied the inhibitor structures (Fig. 1A).

To determine the activity of these compounds, we used a NSCLC cell line panel that consists of 18% EGFR- and ERBB2-mutated cells (Fig. 1B; ref. 11). We first genetically validated the dependency on EGFR signaling in *EGFR*-mutated cells using lentiviral-mediated gene silencing of EGFR (Supplementary Fig. S2A). We next confirmed the activity of our synthesized compounds and observed different levels of dephosphorylation of EGFR in the EGFR-dependent PC9 cells after 8 hours of treatment (Supplementary Fig. S2B).

We next characterized cellular compound activity (Supplementary Table S1) and performed hierarchical clustering for all screened cell lines ($n = 79/84$; Fig. 1C). This analysis revealed clustering of three subgroups of compounds as defined by their potency and specificity to target EGFR and ERBB2 (Fig. 1C). The first group exhibited low activity in ERBB-dependent cells and extended activity in non-ERBB-dependent cells (RL45, RL13, RL14, and RL7; Fig. 1C). A second group of inhibitors, showed high activity in *EGFR*-mutated cell lines and limited activity in *ERBB2*-mutated and ERBB-independent cells (RL20, RL2, RL11, RL6, erlotinib, RL10, RL23, RL58, RL50, gefitinib, PD168393, and RL3; Fig. 1C). In a third group, high activity in *EGFR*- and *ERBB2*-mutated cell lines was coupled to limited activity in ERBB-independent cells (lapatinib, BIBW-2992). Of note, none of the analyzed inhibitors showed high activity in T790M-EGFR gatekeeper mutant cell lines (H1975, H820). Thus, our analysis revealed the genotype-dependent activity of our ERBB inhibitor library and shows the limited effect of different electrophilic side chain substitutions on the potency of ERBB inhibitors against tumors expressing the T790M mutation.

We next screened a collection of Ba/F3 cells (12) expressing known EGFR and ERBB2 mutations with or without concomitant expression of the T790M mutation. We measured cellular viability (Supplementary Table S2) and per-

formed hierarchical clustering of the GI_{50} values. We observed high activity for all inhibitors in cells without a gatekeeper mutation with superior activity of irreversible inhibitors in the presence of insertion mutations and extracellular domain mutations of EGFR (Fig. 2A; Supplementary Fig. S3). Mirroring our results obtained in the panel of NSCLC cell lines, we observed a reduction of the activity of all inhibitors in the background of T790M mutations (Fig. 2A and B). Of note, the reduction of activity of irreversible inhibitors varied between the different concomitant mutations expressed with the EGFR gatekeeper T790M mutation in the Ba/F3 cell lines (Fig. 2A and B; Supplementary Table S2).

Dephosphorylation of the target tyrosine kinase was achieved at the nanomolar range in cells with single-activating EGFR mutations but not in cells coexpressing the T790M gatekeeper mutation (Fig. 2C). Thus, our results imply that although irreversible binding of EGFR inhibitors in gatekeeper-mutated EGFR is more potent than reversible inhibition, the potency of the inhibitors is dramatically reduced when compared with single activating EGFR mutations.

We next sought to determine the effect of the T790M mutation in EGFR on the velocity of covalent bond formation of an irreversible inhibitor in the ATP-binding pocket. For this purpose, we developed a fluorescent-based assay (Supplementary methods), which exploits the fact that covalent bond formation of the inhibitor with EGFR-Cys797 leads to a shift in fluorescence emission of the inhibitor (Fig. 3A). For PD168393 in EGFR^{L858R + T790M}, we observed a doubling of covalent bond-formation time (Fig. 3B), thus providing a mechanistic explanation for the limited ability of the irreversible inhibitors to inhibit the target.

We next validated the dependency on EGFR signaling in the *EGFR*^{L858R + T790M}-mutated H1975 cells through lentiviral-mediated gene silencing of EGFR (Supplementary Fig. S4). Based on our biochemical and cellular analyses, we speculated that the activity of irreversible inhibitors is primarily dictated by the initial reversible binding of the scaffold to the hinge region—a short flexible sequence of amino acids that connects the N-lobe and C-lobe of the kinase and forms key hydrogen bonding interactions with ATP-competitive inhibitors (Fig. 3A). These initial interactions may be critical for promoting the subsequent reaction of the electrophiles of such inhibitors with Cys797 of EGFR. Thus, we tested BIBW-2992, its reversible counterpart RL58, and erlotinib for their potency to dephosphorylate EGFR in H1975 cells (Fig. 3C). Confirming our hypothesis, RL58 dephosphorylated EGFR at concentrations 5-fold lower than erlotinib (Fig. 3C). Erlotinib and RL58 are similar in that they both contain a water-solubilizing moiety, although different, at the 7-position of a quinazoline core. Thus, the superior potency of RL58 might be explained by the 4-(dimethylamino)butanamide moiety found in the 6-position. The protonated tertiary amine of this moiety may form a charged interaction with the side chain of Asp800 located in a helix at the front lip of the ATP-binding pocket of EGFR (Fig. 3D), an additional interaction not observed for erlotinib.

Overall, our data derived from the covalent bond formation assays suggest that beyond the effect on the affinity

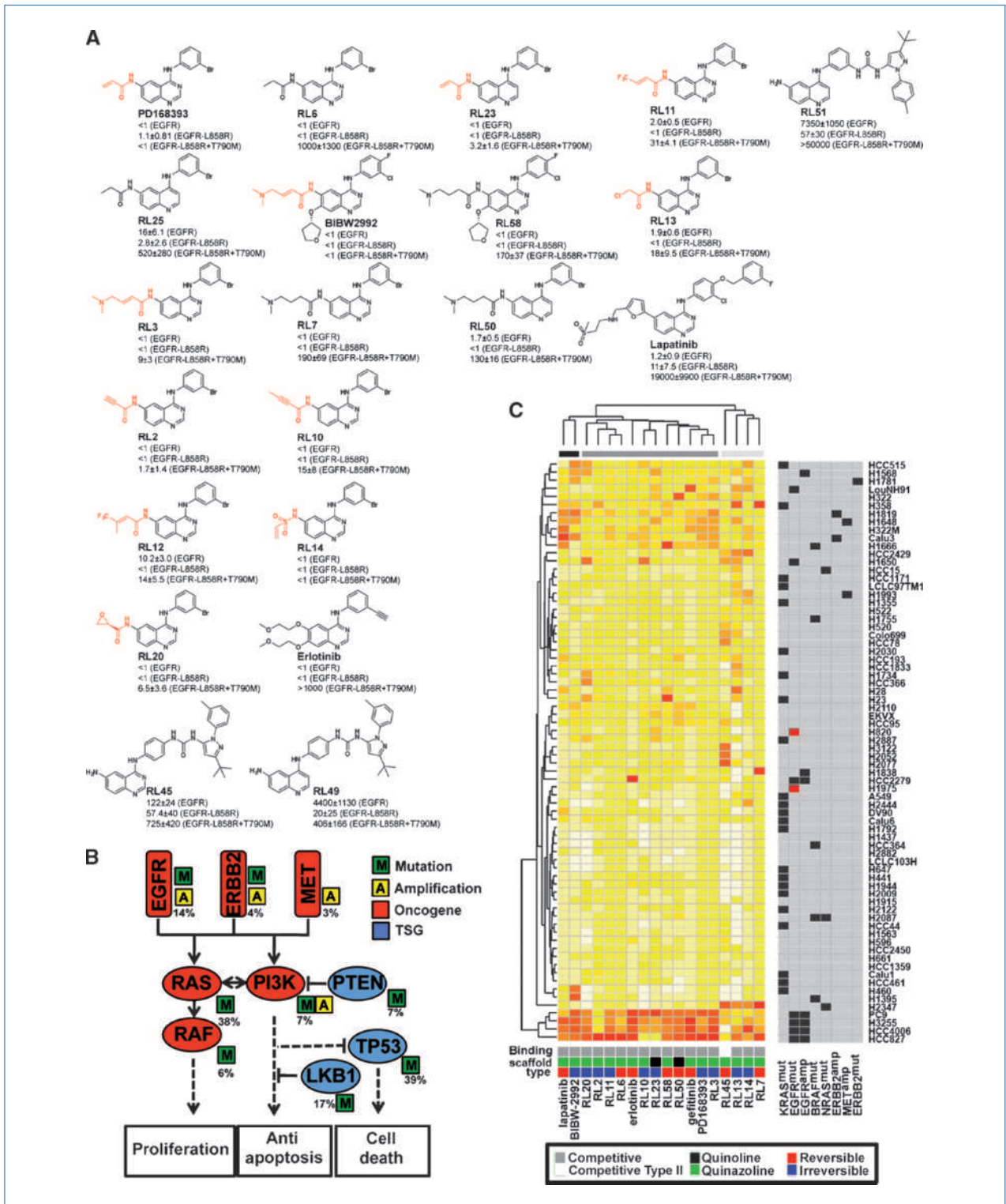


Figure 1. Profiling in NSCLC cell lines. A, the structures of ERBB inhibitors (red, reactive groups) and biochemical IC₅₀s (nmol/L). B, the prevalence of lesions involved in oncogenic signaling in lung cancer present in our cell line panel (20). C, a hierarchical cluster of cell lines and compounds, clustered according to GI₅₀ values. Three groups defined by their selectivity are marked in the upper part of the cluster (group 1, light gray squares; group 2, gray squares; group 3, black squares). The presence (black squares, mutation; red squares, T790M mutation) or absence (gray squares) of selected lesions is also depicted (right). Binding mode (gray, competitive; white, competitive type II), scaffold type (green, quinazoline; black, quinoline), and type of inhibitor (red, reversible; blue, irreversible) are displayed.

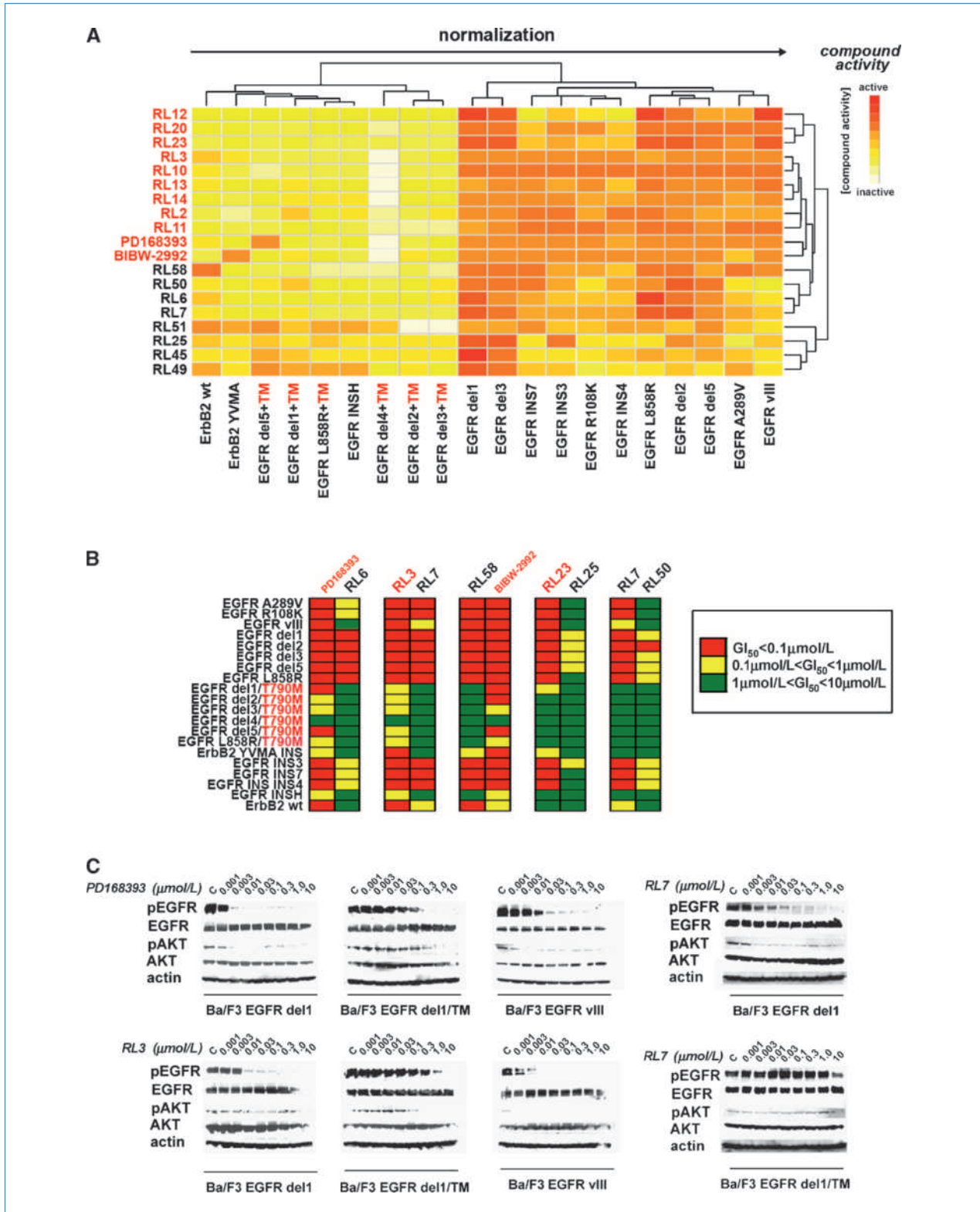


Figure 2. Profiling in ERBB-dependent Ba/F3 cell lines. A, a hierarchical cluster of Ba/F3 cell lines and screened compounds, clustered according to GI₅₀ values. B, GI₅₀ values across the screened Ba/F3 cell lines, for the ERBB-inhibitors. The respective range of compound activity is color-coded. C, activation status of EGFR and its signal transducer (AKT) were determined by immunoblotting after treatment of Ba/F3 cell lines (EGFR del1, EGFR del1/TM, EGFR vIII) with PD168393, RL3, or RL7.

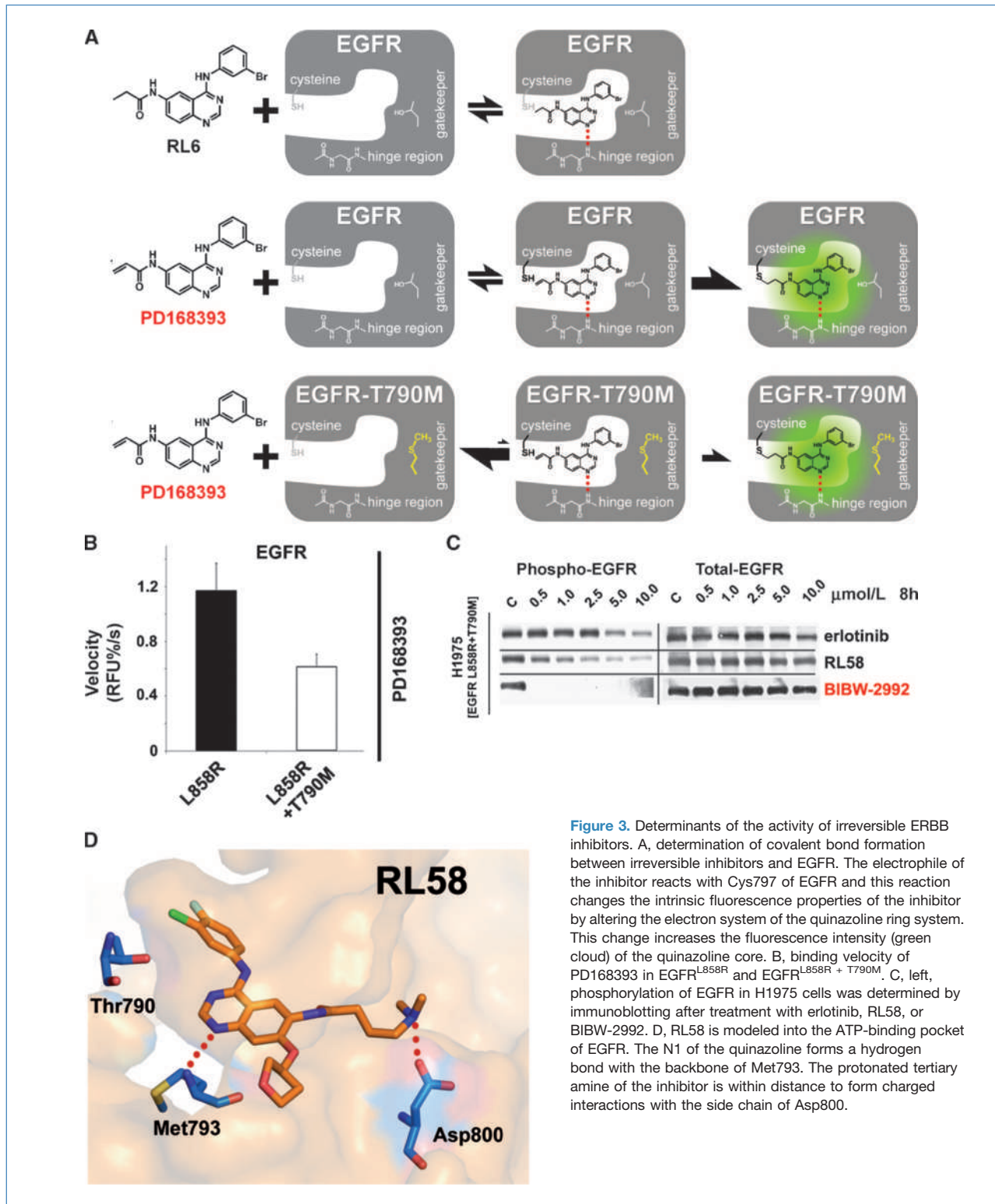


Figure 3. Determinants of the activity of irreversible ERBB inhibitors. **A**, determination of covalent bond formation between irreversible inhibitors and EGFR. The electrophile of the inhibitor reacts with Cys797 of EGFR and this reaction changes the intrinsic fluorescence properties of the inhibitor by altering the electron system of the quinazoline ring system. This change increases the fluorescence intensity (green cloud) of the quinazoline core. **B**, binding velocity of PD168393 in EGFR^{L858R} and EGFR^{L858R + T790M}. **C**, left, phosphorylation of EGFR in H1975 cells was determined by immunoblotting after treatment with erlotinib, RL58, or BIBW-2992. **D**, RL58 is modeled into the ATP-binding pocket of EGFR. The N1 of the quinazoline forms a hydrogen bond with the backbone of Met793. The protonated tertiary amine of the inhibitor is within distance to form charged interactions with the side chain of Asp800.

for ATP (14), the loss of activity of irreversible ERBB inhibitors within the context of the T790M mutation (8), may also be due to steric hindrance. This hindrance disrupts the initial reversible binding of these inhibitors in the ATP binding site

and delays covalent bond formation (Fig. 3B). However, this effect may be partially overcome by the introduction of additional protein-inhibitor interactions with amino acid side chains outside of the hinge region. This is highlighted

by the ability of RL58 to retain high potency against EGFR^{T790M} in both biochemical (Fig. 1A) and cellular (Fig. 3C) assays when compared with its irreversible counterpart BIBW-2992.

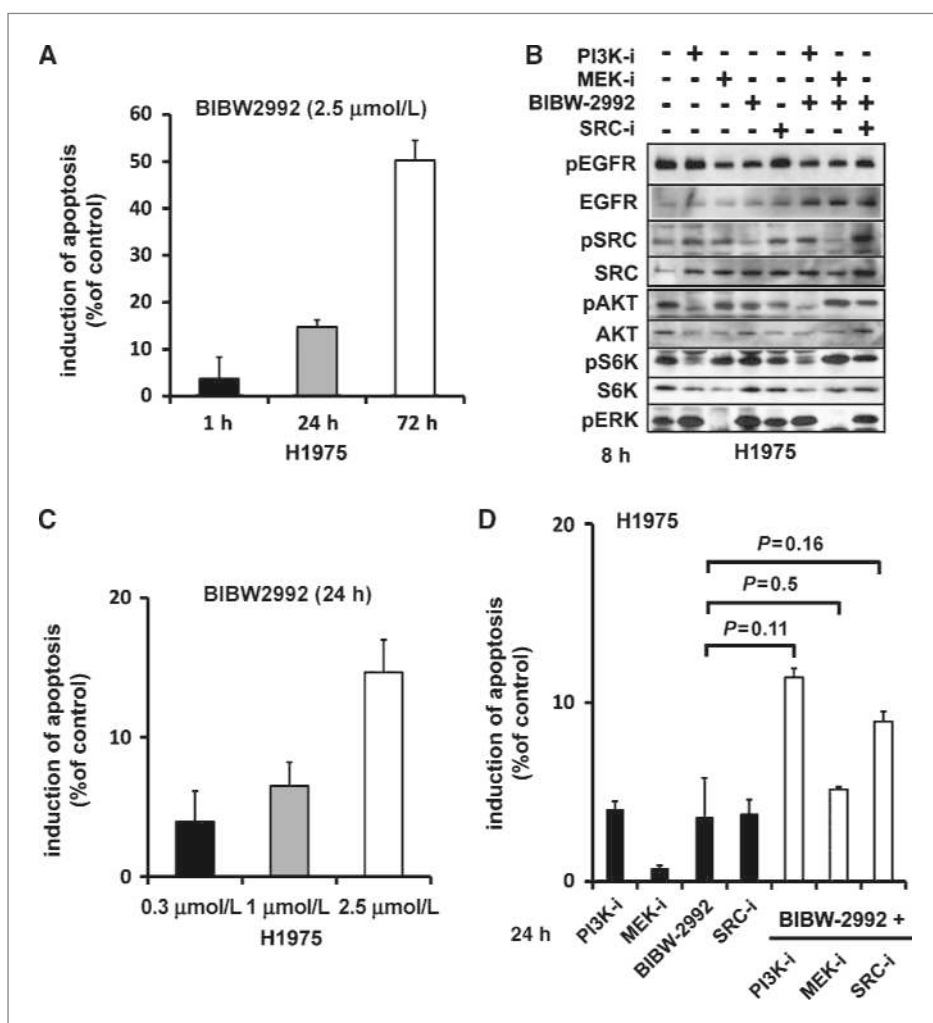
We speculated that inhibiting signaling downstream of EGFR might compensate for the limited activity of irreversible ERBB inhibitors (Fig. 4A) in T790M-mutated cells at clinically relevant concentrations. At clinically achievable doses (0.3 μmol/L), BIBW-2992 does not fully dephosphorylate either EGFR or the downstream signaling (Fig. 4B). Of note, inhibition of MEK (PD0325901) also leads to the dephosphorylation of EGFR, and dasatinib treatment does not lead to dephosphorylation of its primary target SRC in this setting (Fig. 4B). Induction of apoptosis achieved by BIBW-2992 alone (Fig. 4C) can be mimicked by dual inhibition with BIBW-2992 and the phosphoinositide-3-kinase (PI3K)/mammalian target of rapamycin inhibitor PI-103 (Fig. 4D), although PI-103 alone could induce apoptosis in these cells (ref. 15; Fig. 4D). Although statistically not significant, this combination is superior to BIBW-2992 single treatment as well as dual EGFR/MEK inhibition or dual EGFR/SRC inhibition

at clinically relevant concentrations (Fig. 4B and D). Thus, our data suggests that erlotinib-resistant lung cancer might be overcome by combined treatment with irreversible EGFR inhibitors and PI3K inhibitors.

Discussion

Here, we show that the gatekeeper mutation T790M in EGFR slows down the covalent bond formation of irreversible inhibitors, reduces target inhibition, and limits the cytotoxic activity of such inhibitors in cells expressing the resistance mutation. Furthermore, our structural analysis of the reversible counterpart of BIBW-2992 provides evidence that the first step of the non-covalent binding of irreversible inhibitors in the binding pocket might be responsible for the potency of such inhibitors. Initial preclinical studies had provided a rationale for irreversible EGFR inhibitors in the setting of T790M-related acquired erlotinib resistance (16, 17). However, in virtually all of these cases, cytotoxicity could only be achieved at clinically unachievable concentrations or combination therapy was required to augment this activity (18). Our systematic

Figure 4. Combined treatment of EGFR and PI3K signaling. A, induction of apoptosis after treatment with increasing concentrations of BIBW-2992 (H1975). B, phosphorylation of EGFR and its signal transducers were determined by immunoblotting after treatment with BIBW-2992 0.3 μmol/L, PI-103 0.5 μmol/L (PI3K-i), PD0325901 0.25 μmol/L (MEK-i) or dasatinib 0.25 μmol/L (SRC-i) in H1975 cells. C, the time-dependent induction of apoptosis after treatment with BIBW-2992 in H1975 cells. D, the induction of apoptosis after treatment with BIBW-2992 (0.3 μmol/L), PI-103 (0.5 μmol/L), PD0325901 at (0.25 μmol/L) dasatinib (0.25 μmol/L), and combinations (H1975). P, the comparison of the respective combination to single-treatment BIBW-2992.



approach is directed towards the T790M mutation in EGFR as a limiting factor in the efficacy of irreversible inhibitors being in line with previous reports (19).

In summary, we provide insights into the limited efficacy of second-generation ERBB inhibitors in erlotinib-resistant T790M gatekeeper-mutated cells, which might be overcome through combinatorial inhibition of EGFR and downstream PI3K signaling with a direct effect on the clinical evaluation of these drugs.

Disclosure of Potential Conflicts of Interest

R.K. Thomas: commercial research grant, AstraZeneca; commercial research support, Novartis; honoraria from speakers bureau, Roche and Infinity; consultant/advisory board, Sequenom. The other authors disclosed no potential conflicts of interest.

References

1. Paez JG, Janne PA, Lee JC, et al. EGFR mutations in lung cancer: correlation with clinical response to gefitinib therapy. *Science* 2004; 304:1497–500.
2. Lynch TJ, Bell DW, Sordella R, et al. Activating mutations in the epidermal growth factor receptor underlying responsiveness of non-small-cell lung cancer to gefitinib. *N Engl J Med* 2004;350: 2129–39.
3. Yun CH, Boggon TJ, Li Y, et al. Structures of lung cancer-derived EGFR mutants and inhibitor complexes: mechanism of activation and insights into differential inhibitor sensitivity. *Cancer Cell* 2007; 11:217–27.
4. Sharma SV, Bell DW, Settleman J, Haber DA. Epidermal growth factor receptor mutations in lung cancer. *Nat Rev Cancer* 2007;7:169–81.
5. Pao W, Miller V, Zakowski M, et al. EGF receptor gene mutations are common in lung cancers from “never smokers” and are associated with sensitivity of tumors to gefitinib and erlotinib. *Proc Natl Acad Sci U S A* 2004;101:13306–11.
6. Mok TS, Wu YL, Thongprasert S, et al. Gefitinib or carboplatin-paclitaxel in pulmonary adenocarcinoma. *N Engl J Med* 2009;361: 947–57.
7. Engelman JA, Janne PA. Mechanisms of acquired resistance to epidermal growth factor receptor tyrosine kinase inhibitors in non-small cell lung cancer. *Clin Cancer Res* 2008;14:2895–9.
8. Michalczyk A, Kluter S, Rode HB, et al. Structural insights into how irreversible inhibitors can overcome drug resistance in EGFR. *Bioorg Med Chem* 2008;16:3482–8.
9. Wong KK. HKI-272 in non small cell lung cancer. *Clin Cancer Res* 2007;13:s4593–6.
10. Eskens FA, Mom CH, Planting AS, et al. A phase I dose escalation study of BIBW 2992, an irreversible dual inhibitor of epidermal growth factor receptor 1 (EGFR) and 2 (HER2) tyrosine kinase in a

Acknowledgments

We thank Willem van Otterlo for helpful discussions and André Richters, Christian Grütter, and Armin Robubi for expert assistance during kinetic studies.

Grant Support

Deutsche Krebshilfe grant 107954, the Fritz-Thyssen-Stiftung grant 10.08.2.175, and the NGFNplus program of the German Ministry of Education and Research BMBF, grant 01GS08100 (R.K. Thomas); the Alexander von Humboldt Foundation (J.R. Simard); the German Ministry of Education and Research BMBF, grant 01GS08102 (D. Rauh); Schering Plough, Bayer-Schering Pharma, Merck-Serono, and Bayer CropScience.

The costs of publication of this article were defrayed in part by the payment of page charges. This article must therefore be hereby marked *advertisement* in accordance with 18 U.S.C. Section 1734 solely to indicate this fact.

Received 8/20/09; revised 11/7/09; accepted 12/3/09; published OnlineFirst 1/26/10.

2-week on, 2-week off schedule in patients with advanced solid tumours. *Br J Cancer* 2008;98:80–5.

11. Sos ML, Michel K, Zander T, et al. Predicting drug susceptibility of non-small cell lung cancers based on genetic lesions. *J Clin Invest* 2009;119:1727–40.
12. Yuza Y, Glatt KA, Jiang J, et al. Allele-dependent variation in the relative cellular potency of distinct EGFR inhibitors. *Cancer Biol Ther* 2007;6:661–7.
13. Sos ML, Koker M, Weir BA, et al. PTEN loss contributes to erlotinib resistance in EGFR-mutant lung cancer by activation of Akt and EGFR. *Cancer Res* 2009;69:3256–61.
14. Yun CH, Mengwasser KE, Toms AV, et al. The T790M mutation in EGFR kinase causes drug resistance by increasing the affinity for ATP. *Proc Natl Acad Sci U S A* 2008;105:2070–5.
15. Sos ML, Fischer S, Ullrich R, et al. Identifying genotype-dependent efficacy of single and combined PI3K- and MAPK-pathway inhibition in cancer. *Proc Natl Acad Sci U S A* 2009;106:18351–6.
16. Li D, Shimamura T, Ji H, et al. Bronchial and peripheral murine lung carcinomas induced by T790M-L858R mutant EGFR respond to HKI-272 and rapamycin combination therapy. *Cancer Cell* 2007;12:81–93.
17. Li D, Ambrogio L, Shimamura T, et al. BIBW2992, an irreversible EGFR/HER2 inhibitor highly effective in preclinical lung cancer models. *Oncogene* 2008;27:4702–11.
18. Regales L, Gong Y, Shen R, et al. Dual targeting of EGFR can overcome a major drug resistance mutation in mouse models of EGFR mutant lung cancer. *J Clin Invest* 2009;119:3000–10.
19. Godin-Heymann N, Ulkus L, Brannigan BW, et al. The T790M “gatekeeper” mutation in EGFR mediates resistance to low concentrations of an irreversible EGFR inhibitor. *Mol Cancer Ther* 2008;7:874–9.
20. Sos ML, Thomas RK. Systematically linking drug susceptibility to cancer genome aberrations. *Cell Cycle* 2009;8:3652–6.

4.5 Analysis of Compound Synergy in High-Throughput Cellular Screens by Population-Based Lifetime Modeling

Martin Peifer, Jonathan Weiss, Martin L. Sos, Mirjam Koker, Stefanie Heynck, Christian Netzer, Stefanie Fischer, Haridas Rode, Daniel Rauh, Jörg Rahnenführer, Roman K. Thomas

Abstract of the publication

Despite the successful introduction of potent anti-cancer therapeutics, most of these drugs lead to only modest tumorshrinkage or transient responses, followed by re-growth of tumors. Combining different compounds has resulted in enhanced tumor control and prolonged survival. However, methods querying the efficacy of such combinations have been hampered by limited scalability, analytical resolution, statistical feasibility, or a combination thereof. We have developed a theoretical framework modeling cellular viability as a stochastic lifetime process to determine synergistic compound combinations from high-throughput cellular screens. We apply our method to data derived from chemical perturbations of 65 cancer cell lines with two inhibitors. Our analysis revealed synergy for the combination of both compounds in subsets of cell lines. By contrast, in cell lines in which inhibition of one of both targets was sufficient to induce cell death, no synergy was detected, compatible with the topology of the oncogenically activated signaling network. In summary, we provide a tool for the measurement of synergy strength for combination perturbation experiments that might help define pathway topologies and direct clinical trials.

Own contributions

In this project, I contributed significantly to the compound synergy detection model proposed as well as to the experimental design of the screening pipeline that was involved in generating all of the data. The key step here was to develop a system that is both scalable in size and permits generation of accurate and reproducible data. Moreover, I have analyzed the single compound screening data (shown in figure 2) and applied the model described to screening data where both compounds from figure 2 were combined. Finally, I prepared Figure 3 as seen in the manuscript and was centrally involved in the process of manuscript preparation prior to submitting it to PLoSOne.

Unpublished data related to this manuscript

In parallel to the establishment of the model published in this manuscript, I also performed a large high-throughput cell-based inhibitor screen. The screen aims to answer four questions.

Firstly, how do cancer cells utilize the MAPK and PI3K pathways? Secondly, are there crossings at certain signaling nodes between these pathways? Thirdly, does combined inhibition of both pathways at various signaling nodes leads to a more severe phenotype than a single compound alone? Finally, can we link synergistic inhibitor combinations to genetic aberration leading to a predictor of sensitivity? To this end, I have screened 105 cancer cell lines originating from various tissues, against 17 inhibitors combined against each other resulting in 136 combinations. In addition each inhibitor was screened in single. All combinations were screened in six different concentrations and four replicates. To analyze the dataset, I applied the aforementioned synergy model to the screening data. Only positive synergy scores with a q-value <0.05 were taken into account and subjected to further analysis. This project is still ongoing.

Concluding remarks

In a previous study our group has already shown the benefit of combined PI3K and MAPK pathway inhibition. In this study, we developed a mathematical model that would allow us to utilize our already established cell based screening platform to systematically screen for small molecule inhibitor combinations. In addition we show that our model is in accordance to other mathematical models describing biological synergy, but also specialized to handle high-throughput screening data. We furthermore show that our synergy detection model can be used to identify cell lines where dual PI3K and EGFR inhibition has a synergistic effect.

Analysis of Compound Synergy in High-Throughput Cellular Screens by Population-Based Lifetime Modeling

Martin Peifer¹*, Jonathan Weiss¹, Martin L. Sos¹, Mirjam Koker¹, Stefanie Heynck¹, Christian Netzer², Stefanie Fischer¹, Haridas Rode⁴, Daniel Rauh⁴, Jörg Rahnenführer², Roman K. Thomas^{1,3,4}*

1 Max Planck Institute for Neurological Research with Klaus-Joachim-Zülch Laboratories of the Max Planck Society and the Medical Faculty of the University of Köln, Max-Planck Society, Köln, Germany, **2** Department of Statistics, Technical University of Dortmund, Dortmund, Germany, **3** Department I of Internal Medicine and Center of Integrated Oncology Köln – Bonn, University of Köln, Köln, Germany, **4** Chemical Genomics Center of the Max Planck Society, Max-Planck Society, Dortmund, Germany

Abstract

Despite the successful introduction of potent anti-cancer therapeutics, most of these drugs lead to only modest tumor-shrinkage or transient responses, followed by re-growth of tumors. Combining different compounds has resulted in enhanced tumor control and prolonged survival. However, methods querying the efficacy of such combinations have been hampered by limited scalability, analytical resolution, statistical feasibility, or a combination thereof. We have developed a theoretical framework modeling cellular viability as a stochastic lifetime process to determine synergistic compound combinations from high-throughput cellular screens. We apply our method to data derived from chemical perturbations of 65 cancer cell lines with two inhibitors. Our analysis revealed synergy for the combination of both compounds in subsets of cell lines. By contrast, in cell lines in which inhibition of one of both targets was sufficient to induce cell death, no synergy was detected, compatible with the topology of the oncogenically activated signaling network. In summary, we provide a tool for the measurement of synergy strength for combination perturbation experiments that might help define pathway topologies and direct clinical trials.

Citation: Peifer M, Weiss J, Sos ML, Koker M, Heynck S, et al. (2010) Analysis of Compound Synergy in High-Throughput Cellular Screens by Population-Based Lifetime Modeling. PLoS ONE 5(1): e8919. doi:10.1371/journal.pone.0008919

Editor: Ulrich Zanger, Dr. Margarete Fischer-Bosch Institute of Clinical Pharmacology, Germany

Received: November 2, 2009; **Accepted:** January 8, 2010; **Published:** January 27, 2010

Copyright: © 2010 Peifer et al. This is an open-access article distributed under the terms of the Creative Commons Attribution License, which permits unrestricted use, distribution, and reproduction in any medium, provided the original author and source are credited.

Funding: 1. Deutsche Krebshilfe (grant 107954) <http://www.krebshilfe.de/> 2. German Ministry of Science and Education (BMBF) as part of the German National Genome Research Network (NGFNplus) program (grant 01GS08100) <http://www.bmbf.de/en/> 3. Fritz-Thyssen Stiftung (grant 10.08.2.175) <http://www.fritz-thyssen-stiftung.de/> 4. Deutsche Forschungsgemeinschaft through SFB832 <http://www.dfg.de/en/index.html> The funders had no role in study design, data collection and analysis, decision to publish, or preparation of the manuscript.

Competing Interests: Roman K. Thomas has received research support from AstraZeneca and Novartis and honorarium from Böhringer-Ingelheim.

* E-mail: peifer@nf.mpg.de (MP); nini@nf.mpg.de (RT)

† These authors contributed equally to this work.

Introduction

The vision of personalized cancer medicine has recently become an achievable goal through the development of novel cancer therapeutics and the link of their efficacy to somatic genetic aberrations (or, “lesions”). Prominent examples are *ERBB2*-amplified breast cancers [1] that respond to *ERBB2* inhibition, BCR-ABL-translocated chronic myeloid leukemia patients that can be successfully treated with the ABL kinase inhibitor imatinib [2,3], or *EGFR*-mutant non-small cell lung cancers (NSCLC) that are sensitive to treatment with the EGFR inhibitors erlotinib and gefitinib [4]. However, the enthusiasm about this success has been dampened by limited tumor shrinkage in most patients and the occurrence of relapse after an initial response [5,6,7,8,9,10].

The concept of simultaneous targeting of more than one signaling pathway or pathway component has been pursued for many years as a promising strategy to increase treatment efficacy or prevent the emergence of drug resistance [11,12,13]. In the area of conventional cytotoxic chemotherapy, only the combination of multiple drugs has enabled actual cures for leukemia and lymphoma patients [14]. Additional examples include the successful combination of therapeutic antibodies and chemotherapy for treatment of lymphomas, as well as breast and colorectal cancer [15,16]. Finally, combining specific inhibitors of oncogenic signaling pathways has resulted in

highly synergistic treatment responses in clinically relevant tumor models [17,18,19]. Thus, systematic approaches to interrogate synergistic compound combinations and to link these to individual genetic lesions are required to move these combinations into clinical trials more rapidly. Another notion supporting the systematic study of such combination therapies comes from the careful biochemical dissection of oncogenic signaling pathways: it was shown that most of these pathways are interconnected by feedback loops [20,21,22]. Thus, simultaneously blocking two or more of such pathways might lead to activation of the alternate pathway by release of negative feedback loops. Accordingly, beyond the obvious benefit for drug discovery, such studies may help defining signaling pathway topology connected with individual genetic lesions.

Unfortunately, establishing synergistic compound combinations at greater scale is typically hampered by the necessity to screen multiple compound concentrations of one compound against different concentrations of another compound. Furthermore, many analytical approaches do not consider continued proliferation of viable cells and do not afford establishing statistically meaningful representations of screening data across a broad experimental range.

Several methods for the detection of compound synergy have been proposed [23,24,25,26]. In summary, the diverse definitions of synergy and methods for its detection are based on two

principles: Loewe additivity [27] and Bliss independence [28]. However, a precise methodological derivation of the analytical procedure and the close adaptation to an experimentally tractable setup amenable to high-throughput cellular screening have been lacking so far. We therefore set out to develop both a novel approach for high-throughput cell-based screening of multiple compound concentrations and a statistical framework to define synergy as a probabilistic lifetime process under single and combined chemical perturbations. We applied this model to screening data derived from a screen of a panel of genetically and phenotypically characterized NSCLC cell lines and determined global genetic settings in which synergy of the irreversible EGFR/ERBB2 inhibitor BIBW-2992 and a dual PI3K/mTOR inhibitor PI-103 is most pronounced.

Results

Population-Based Analysis of Cell Viability Measurements

We reasoned that cellular dose response that is commonly used for cell viability measurements is based on a change of the cellular growth rate when a given perturbation (in most cases, a chemical compound) is added in comparison to untreated cells. This description allows a probabilistic interpretation in terms of a stochastic waiting-time process. For a given compound concentration x , these ideas lead to the following relationship

$$v(x) = \exp\left(-\lambda t \left(1 - \frac{1}{1 + (x/K)^m}\right)\right) \quad (1)$$

where v is the modeled viability, t is the time at which the measurement has been carried out, and λ , K , m are the model parameters. Equivalently, the model can be interpreted such that each cell in the population has an exponentially distributed lifetime after the treatment. As rate of the exponential distribution we then obtain $\lambda \left(1 - (1 + (x/K)^m)^{-1}\right)$. In case of dual-specificity inhibitors (i.e., inhibitors inhibiting more than one target), sensitivity of both targets might be very distinct. It may happen that one target is already completely inhibited with the lowest concentration in the screen. To capture this effect, an offset λ_{off} , $\lambda_{off} \geq 0$ can be added to the model, leading to the rate $\lambda \left(1 - (1 + (x/K)^m)^{-1}\right) + \lambda_{off}$. Details of the mathematical model and its derivation are presented in the **Supplementary Note S1**.

Figure 1A shows the simulated individual lifetime of 1000 cells, which have been treated with two different compounds. Compound concentrations increase from the left to the right panels. Blue and red lines indicate the time of measurement and data points which are located at the yellow and white area represent cells which are still viable at the time of measurement when treated with compound one. Data points falling into the blue and white areas display viable cells after treatment with compound two. In case of a non-synergistic and non-antagonistic compound combinations the lifetime of the cells is given by the smallest lifetime when treated with either compound (white area). Translating the idea of “minimal lifetime” into a mathematical model leads to a product of the two single compound dose response curves modeled by **Eq. (1)** as non-synergistic combined effect (**Fig. 1b, blue curve**); this concept is compatible with Bliss independence. A simulation over a relatively small population on 1000 cells revealed that the simulated points closely correspond to the theoretical curves (**Fig. 1b**).

With this mathematical model we next sought to distinguish between synergy and antagonism of compound response curves

derived from high-throughput screening efforts (**Fig. 1C**). Starting from the high-throughput screening platform dose response curves from both single compounds as well as their combinations were determined for a large panel of genetically annotated non-small cell lung cancer cell lines. **Equation (1)** is then fitted to the dose response curve of each single compound screen. This yields the model parameters λ , K , m , from which the curve separating synergistic from antagonistic compound combinations can be computed according to **Eq. (S10)** of the **Supplementary Note S1**. For a given compound combination, the difference between the computed curve and the measurement is then a measure for synergy or antagonism, respectively. This measure is denoted by synergy strength. Due to the presence of noise, several different compound combinations are needed to filter out cell-lines, which show significant enrichment of synergy strength over different combinations. To this end, a rank sum approach is used. In order to account for multiple hypothesis testing the false-discovery rate (FDR) framework [29] was applied.

Applying the Model for Single Compound Screen of PI-103 and BIBW-2992

In order to validate the proposed model, **Eq. (1)**, we screened 65 of the 84 non-small cell lung cancer cell lines [9] against the irreversible EGFR/ERBB2 inhibitor BIBW2992 and the PI3K/mTOR inhibitor PI-103. We selected 4 out of the 65 cell lines and fitted the dose response curves to the corresponding data points (**Fig. 2A**). We next determined the difference between the viability predicted by the model and the experimentally determined values (model residuals). To assess the quality of the model we computed the median of the residuals over the concentrations for each compound and cell line (**Fig. 2B**). For both compounds, significant outliers are then identified under the assumption that the medians of the residuals are normally distributed around zero. Using a 5% level of significance and after correcting for multiple testing we identified only one outlier: Calu6 screened with PI-103 (FDR q-value = $7.6 \cdot 10^{-12}$). However, this outlier can safely be neglected since it did not distort the following analysis. In summary, the proposed model fits well to the measured data and is therefore a suitable basis for the identification of synergistic compound combinations.

Computing half-maximal-inhibitory concentrations (**Eq. (2)**, **Materials and Methods**) for PI-103 and BIBW-2992 (**Figure 2C**) shows no clear association between the genomic lesions and the single-agent activity of PI-103 with the used cell proliferation assay [19]. As expected, in the case of the irreversible EGFR/ERBB2 inhibitor BIBW-2992, cell lines dependent on EGFR and ERBB2 signaling (due to the presence of drug-sensitizing genetic alterations in these genes) are substantially enriched in the highly sensitive cell lines [30,31].

Application of the Model for Combinational Compound Screen of PI-103 with BIBW-2992

In order to test the accuracy of our model to detect synergy of compound combinations we next sought to systematically assess the viability of cells treated with a combination of the two compounds. With the EGFR/PI3K signaling cascade being one of the most frequently mutated pathways in lung cancer, we speculated that combined inhibition of EGFR- and PI3K/mTOR-signaling might be effective in our cell line panel of NSCLC cells. The presence of considerable experimental noise (**Fig. 2B**) makes it necessary to test different combinations for the determination of synergy. Therefore, seven compound dose combinations of PI-103 and BIBW-2992 were applied for the 65

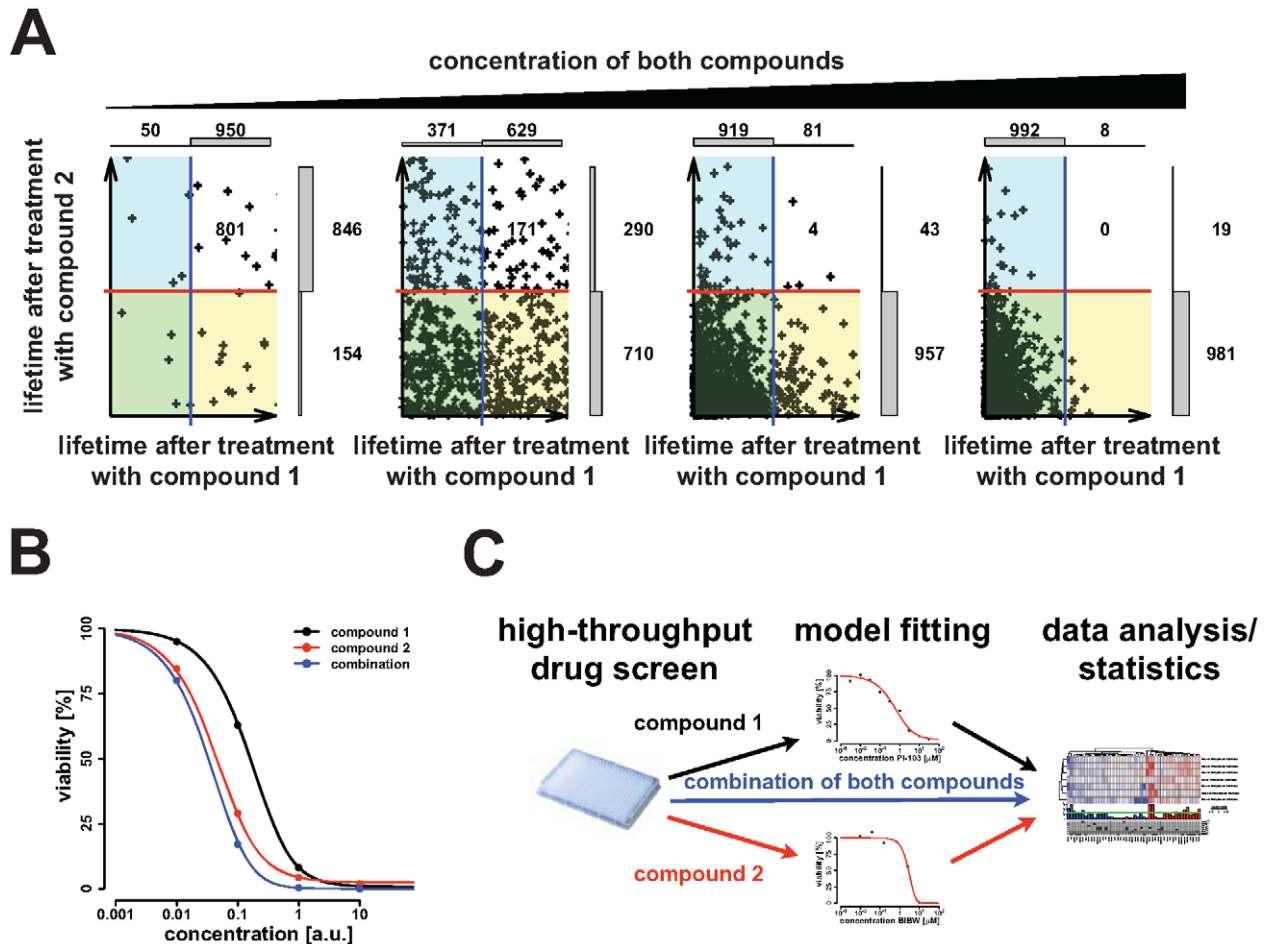


Figure 1. Overview of the model and method to detect synergistic compound combinations. (A) Model based simulation of the lifetime of 1000 cells after treatment. The x-axis corresponds to the lifetime after treating cells with compound 1 and the y-axis shows the lifetime after treatment with compound 2. Concentrations of both compounds are increased by a factor of 10 from left to right. Either the vertical blue line in case of compound 1 or the horizontal red line for compound 2 indicates time of measurement. Thus, the number of viable cells at measurement is given by the number of data points on the right side of the blue lines (after treatment with compound 1) or above the red line (in case of compound 2). Distributions of viable and dead cells are displayed by bars at the upper and right side of each panel. Combining both compounds and assuming that the combination of both compounds is neither synergistic nor antagonistic yields a certain number of viable cells that is represented by dots in the white area. This notion reflects the fact that the minimal lifetime between the two compounds (x and y-axis) has to be taken for the combination. (B) Theoretical dose response curves are shown for the previous example. Data points were computed from results of the simulation shown in (A). Even for the relatively small population of 1000 cells, the simulated data points and the theoretical curve match. (C) Scheme of the procedure to detect synergistic and antagonistic compound combinations. Starting from a high-throughput compound screen, the model is fitted to all single-agent measurements. From the fitted model parameters, curves are computed for each combination separating synergy from antagonism. Measured data of the combination screen are then compared to the computed curves and finally analyzed using a rank-based statistical test. doi:10.1371/journal.pone.0008919.g001

cell lines already used in the single screens. The curve, which separates synergistic from antagonistic combinations, is computed from the previously determined fits, which serves as basis for the synergy strength. We next computed this synergy score and applied hierarchical clustering to the data matrix of the synergy strength (Fig. 3A). This analysis revealed two distinct groups, separating cell lines according to synergistic and antagonistic behavior. To assess which cell lines in those clusters display a significantly synergistic or antagonistic response to combined EGFR-PI3K inhibition, we employed a rank sum-based statistical test (Fig. 3A). Ranks of synergy strength were computed over all cell lines but for each measured combination separately and summed over the seven combinations. Next, a statistical test was derived to test if high or low ranks were enriched. To correct for multiple testing all p-values were corrected using the false-discovery rate approach. Resulting q-values are shown in

Fig. 3A, where the horizontal green line indicates the chosen 5% false-discovery rate cutoff. We identified 11 cell lines, for which combined PI-103/BIBW-2992 treatment was significantly synergistic. Our analysis revealed that cell lines harboring either amplification or a mutation in either EGFR or ERBB2 were not enriched in the fraction of cell lines responding in synergistic fashion to the combination of both compounds. These results suggest that inhibition of ERBB-signaling in these cell lines is already sufficient to effectively shut down survival signaling. However, no other significant correlation between synergy strength and genotype could be observed (Fig. 3A).

To further validate our methodological framework, we compared our results with synergy predictions based on the combination index method [12,32,33]. While the combination index yielded a result in only 66% of the screening data analyzed, our approach yielded robust synergy scores across the entire data

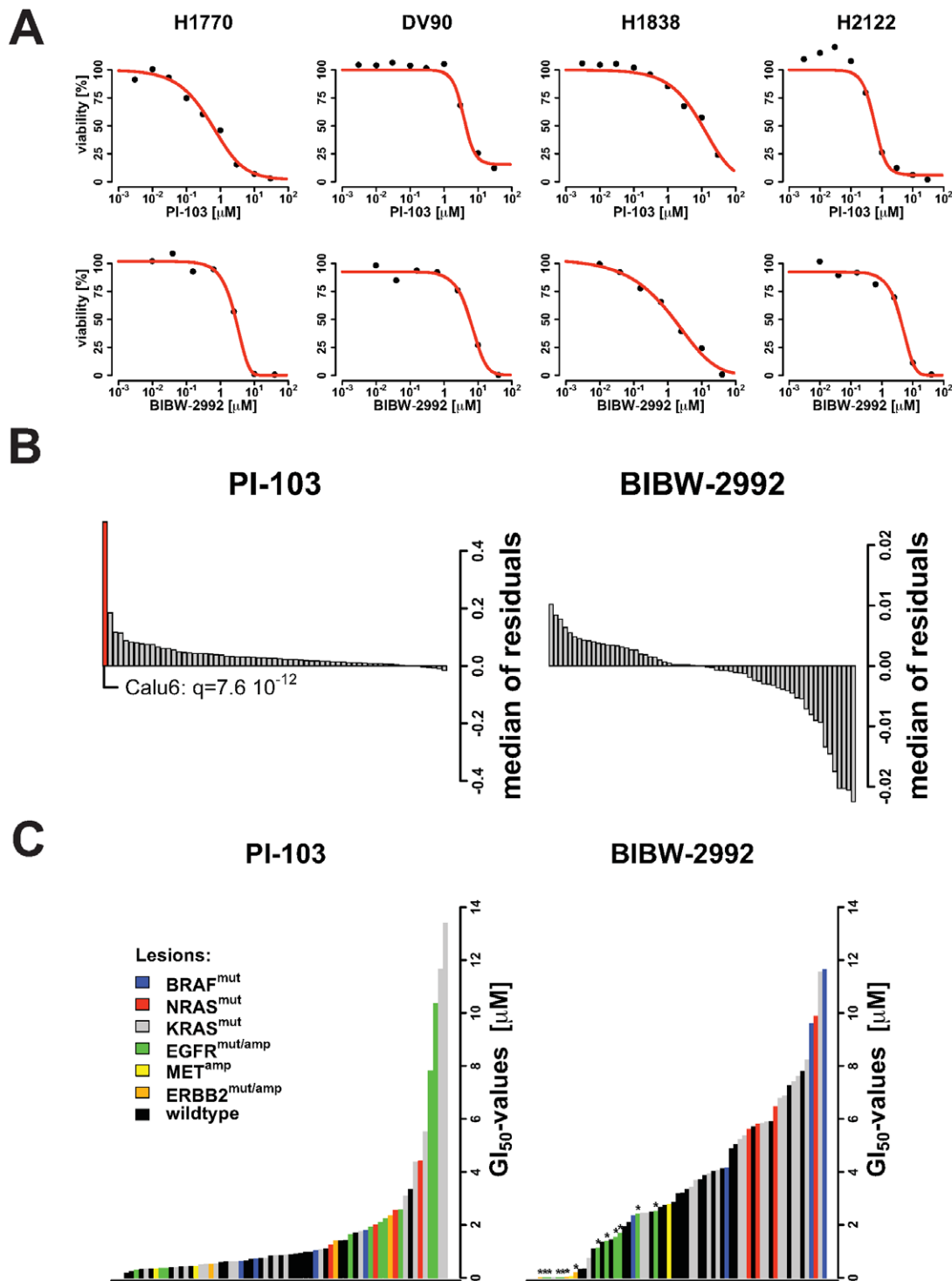


Figure 2. Results obtained from the single-compound screen of PI-103 and BIBW-2992. (A) Kill-curves are exemplarily shown for two compounds (PI-103 and BIBW-2992) and 4 cell lines. Solid red lines display the fitted model to the measured data shown by black points. (B) Analysis of the model residuals (i.e., difference between the measurements and the model prediction) for both compounds and each cell line. Shown are the distributions of the residuals' medians over the screened concentrations. A statistical test to detect significant outliers reveals that only the cell line Calu3 when screened against PI-103 is not compatible with the distribution of the median of residuals (FDR q-value = $7.6 \cdot 10^{-12}$); highlighted by a red bar. (C) Profiles of GI_{50} -values for PI-103 and BIBW-2992. GI_{50} -values were computed using the proposed model and sorted according to the sensitivity of the cell line to the inhibitions: most sensitive cell lines are on the left side and most resistant cell lines are shown on the right side. Colors symbolize most common genomic alterations in NSCLC. In case of EGFR^{mut/amp} and ERBB2^{mut/amp} a genomic alteration can either be a mutation or a gene copy number amplification (≥ 4 copies are considered as alteration), for MET^{amp} only amplifications are reported, the remaining alterations, BRAF^{mut}, NRAS^{mut}, KRAS^{mut} are mutations. For BIBW-2992, asterisks highlight those cell lines, which harbor lesions either in EGFR or ERBB2.
doi:10.1371/journal.pone.0008919.g002

set, thereby affording application to high-throughput screens. However, in the fraction of data that could be analyzed by both methods, synergistic cell lines determined with our method and the combination index method largely overlapped (**Fig. S1**). This is underscored by a regression analysis between the negative-log transformed combination index and the synergy strength score (**Fig. S2**), which showed a significant positive correlation ($r^2 = 0.45$; $p < 10^{-6}$). The enhanced robustness of our approach is largely due to the fact that it takes into account the entire dose response relationship and is not restricted to the behavior of a single point (**Supplementary Note S1**).

The observation that combination treatment is not beneficial in cell lines with oncogenic alterations in EGFR and ERBB2 indicates that there might be a relationship between activity of the individual compounds and synergy. In order to demonstrate such a relationship, we plotted the GI_{50} -values of PI-103 against those of BIBW-2992 and labeled all data points of cell lines with genetic aberrations in the EGFR/ERBB2 receptor tyrosine kinases (**Fig. 3B**). This analysis recapitulated the previous findings that cell lines, which are primarily dependent on EGFR/ERBB2 signaling ($GI_{50} < 0.1 \mu\text{M}$), do not benefit from the combination of ERBB/PI3K-pathway inhibition. Remarkably, our findings are in line with the general topology of the signaling pathways downstream of EGFR and ERBB2 (**Fig. 3C**). Since oncogenically activated EGFR and ERBB2 receptors preferentially signal through the PI3K pathway [19] combined blockade of those pathways is not expected to be synergistic for cells depending on EGFR or ERBB2. In other words, potent inhibition of strong oncogenic signals *upstream* is already sufficient to induce apoptosis, independent of the inhibition of further components *downstream* (**Fig. 3C**). The same seems to be valid for three cell lines with the lowest PI-103 GI_{50} -values. However, dependency on PI3K-mTOR signaling was generally less pronounced (expressed by higher GI_{50} -values) which might be a result of alternative pathways upstream PI3K such as the mitogen-activated protein kinase (MAPK) and feedback loops connecting the two pathways [19]. However, synergistic combinations clustered around a GI_{50} -value of $1 \mu\text{M}$ for PI-103. We therefore speculate that a supra-threshold activity of PI3K inhibition is needed to obtain synergy.

In order to provide a deeper characterization of the genotypes, we extended the previously used genetic annotation with significant copy number aberrations computed by GISTIC [34]. A complete list of all identified copy number aberrations and the mutation status of 7 genes is given for the cell lines showing synergistic behavior in **Table S1**. Similar to the analysis done in [9], we performed a k-nearest-neighbor prediction on this data set and found no significant predictor of synergy (**Table S2**). The inability to predict synergy from genetic lesions is probably hampered by the necessity to restrict the analysis to recurring and highly focal copy number lesions as identified by GISTIC and the focus on the most frequent gene mutations in NSCLC.

Discussion

Starting from general considerations about cell viability measurements, we derived a model for inferring cell survival curves from high-throughput cell-based screening data [35]. This model laid the basis for detection of synergy strength of compound combinations. Here, the central assumption is that the median-effect equation [12,32,33] is coupled linearly to a cell-killing rate under treatment. Validation of the model in a panel of 65 lung cancer cell lines perturbed using PI3K and EGFR/ERBB2 signaling pathway inhibitors revealed general rules of the signaling pathway topology downstream of genetically altered EGFR and

ERBB2 kinases. Thus, our approach affords analysis of synergy of compound combinations in high-throughput cell-based screens in scalable fashion.

Other approaches involving the network structure of complex biological systems have been proposed [24,35]. Our model has the advantage of permitting systematic statistical analyses of synergy employing generic laboratory cellular screening experiments involving a vast array of genetic cellular backgrounds. Another major advantage of our model is its stochastic nature describing the lifetime of cells under treatment. This allows a rigorous derivation of a synergy score when cells are treated with a combination of compounds. In fact, we confirmed Bliss independence [28] based on this computation but within a solid theoretical framework.

As application of the proposed analytical framework, we applied the method to single and combined screens of the PI3K inhibitor, PI-103 and the EGFR/ERBB2 inhibitor, BIBW-2992. Our model captured previous findings that genetic alterations in EGFR are predicting sensitivity of EGFR inhibitors [4,36,37]. Analysis of synergy between PI-103 and BIBW-2992 revealed that cell lines dependent on EGFR/ERBB2-signaling do not benefit from the combination (**Fig. 3A, B**), which is in line with the network topology suggesting a preferential linear downstream engagement of PI3K signaling downstream of oncogenically activated receptor tyrosine kinases [7,19]. Previous work carried out in transgenic EGFR and ERBB2-mutant mice showed substantial tumor regression when mice were treated with a combination of BIBW-2992 and rapamycin targeting mTOR (or more specifically TORC1) [30,31]. However, both transgenic alleles in these studies impair binding of quinazoline-based EGFR inhibitors, thus resulting in inefficient target inhibition [38]. Thus, adding downstream inhibition in the setting of incomplete upstream target inhibition can result in synergy, even though the pathway itself is linear (**Fig. 3C**). Here, crosstalk or an upstream branching into other signaling components can mediate such an effect. In our study, signaling through the MAPK pathway might substantially contribute to synergy since there are numerous interconnections between MAPK and PI3K signaling pathways.

In summary, we introduced a new methodological framework to detect synergy of compound combinations across a large panel of cancer cell lines. The analysis of a first combination screen supported a view of a mostly linear signaling pathway topology downstream of oncogenically activated EGFR/ERBB2 kinases [19]. Thus, beyond enabling high-throughput analyses of compound combinations, our approach affords general insights into pathway functionality and pathway interrelations.

Materials and Methods

Cells

The used cell line collection was previously described in [9]. Cells were routinely controlled for infection with mycoplasma by MycoAlert (www.cambrex.com) and were treated with antibiotics according to a previously published protocol [39] in case of infection.

Cell-Based Screening

All compounds were purchased from commercial suppliers or synthesized in house, dissolved in DMSO and stored at -80°C . Cells were plated into sterile microtiter plates using a Multidrop instrument (<http://www.thermo.com>) and cultured overnight. Compounds were then added in serial dilutions. Cellular viability was determined after 96h by measuring cellular ATP content using the CellTiter-Glo assay (www.promega.com). Plates were measured on a Mithras LB940 plate reader (www.bertholdtech.com).

Copy Number Analysis

Genomic DNA was extracted from cell lines using the PureGene kit (www.gentra.com) and hybridized to high-density oligonucleotide arrays (Affymetrix, Santa Clara, CA) interrogating 238,000 SNP loci on all chromosomes except Y, with a median intermarker distance of 5.2 kb (mean 12.2 kb; http://www.affymetrix.com). Array experiments were performed according to manufacturer's instructions. SNPs were genotyped by the Affymetrix Genotyping Tools Version 2.0 software. We applied GISTIC [34] to analyze the data set. The GISTIC algorithm was run using a copy number threshold of 4 in case of amplifications and 1 for deletions. To ensure compatibility of the copy number data with mutation data we dichotomized copy numbers with the following thresholds: 4 for amplifications and 1 for deletions.

Model Based Computation of GI₅₀-Values

Applying the half-maximal-inhibitory concentration concept ("GI₅₀-values") we set the viability to 50% in Eq. (1); followed by a few algebraic rearrangements yields the model-based computation of the GI₅₀-values:

$$GI_{50} = K \left(\frac{\log(2)}{\lambda t - \log(2)} \right)^{\frac{1}{m}} \text{ if } \lambda t > \log(3). \quad (2)$$

Positivity of the GI₅₀-values is guaranteed by the condition in Eq. (2). If this condition is not satisfied, no GI₅₀-value exists, i.e., the on-target inhibition is too weak to kill enough cells such that a viability of 50% can be reached.

Data Analysis and Statistics

The model of single-agent kill curves, Eq. (1), are fitted to data. To this end, a maximum likelihood approach is employed to estimate the model parameters λ , K , m . This requires non-linear optimization; we chose the Levenberg-Marquardt method for this optimization [40,41]. P-values were corrected for multiple testing using the false-discovery-rate approach [29]. The p-value adjustment as well as the cluster analysis was carried out in R version 2.7.1 (http://www.R-project.org).

Rank Sum Rest

We decided to employ a rank sum based approach to provide a statistical measure for synergy. This approach has the advantage that it also takes prevalence across different cell lines into account and does not purely rely on the synergy strength. This is an important and therapeutically relevant property of the statistical test.

Let us consider the synergy strength measure: $S_{ij} = V_{ij} - v_{0ij}$, where V_{ij} is the measured viability for the combination $i \in \{1, n_c\}$ and cell line $j \in \{1, m\}$. The computed curve separating synergy from antagonism, given by the product of both single compound dose response curves (**Eq. (S10), Supplementary Note S1**), is denoted by v_{0ij} . Ranks are computed over all cell lines j but for each combination i separately; resulting in the rank matrix R_{ij} . Utilizing that the ranks are uniformly distributed leads to the following variance of the ranks across the cell lines:

$$s_i^2 = \frac{n_i^2 - 1}{12}.$$

Moreover, under the null-hypothesis that there is no association between the ranks of each combination, the variance of the rank

sum $\sum_{i=1}^{n_c} R_{ij}$ is

$$s^2 = \sum_{i=1}^{n_c} s_i^2 = \frac{n_c(n_c^2 - 1)}{12}. \quad (3)$$

Relating the rank sum to the median is not useful in our case. If, e.g., S_{ij} is negative for all i and j (i.e., there is no sample showing synergistic behavior), a median centered rank sum test would assign a few samples as being synergistic. To derive the test statistics, which corrects for such an effect, we relate the rank sum to the rank where the synergy score S_{ij} changes its sign. To this end, we compute for each concentration i the rank that has the lowest absolute synergy score

$$m_i = R_{ik} \text{ where } k = \arg \min_{1 \leq j \leq n_i} |S_{ij}|.$$

Finally, the rank sum statistics we propose to test for synergy is given by

$$RS_j = s^{-1} \sum_{i=1}^{n_c} (R_{ij} - m_i) = \sqrt{\frac{12}{n_c(n_c^2 - 1)}} \sum_{i=1}^{n_c} (R_{ij} - m_i). \quad (4)$$

Under the null-hypothesis that there is no association between the ranks of different concentrations and that the synergy score fluctuates around zero, the distribution of RS_j can be approximated by a standard normal distribution. This approximation is asymptotically ($j \rightarrow \infty$) correct and used in our analysis.

Supporting Information

Supplementary Note S1 Analysis of compound synergy in high-throughput cellular screens by population-based lifetime modeling.

Found at: doi:10.1371/journal.pone.0008919.s001 (0.08 MB PDF)

Figure S1 Comparison between the combination index method and the method we propose. Shown is the clustered matrix of the synergy strength measure, as in Fig. 3A, together with the combination index. Significantly synergistic cell lines which were detected with our method are highlighted by red bars. Missing bars indicate that for those cell lines the computation of the combination index was not possible.

Found at: doi:10.1371/journal.pone.0008919.s002 (0.69 MB PDF)

Figure S2 Correlation analysis between both methods. To adapt the scale of both measures, we performed a transformation of the combination index using the negative logarithm. The regression line is displayed by the straight red line. Moreover, we found a significant positive correlation ($r^2 = 0.45$; $p < 10^{-6}$), which confirms that both methods follow the same trend.

Found at: doi:10.1371/journal.pone.0008919.s003 (0.12 MB PDF)

Table S1 Genomic annotation of all 11 cell lines showing synergistic behavior. Significant copy number regions were identified using GISTIC. To assure comparability with mutation data, copy numbers were dichotomized with the following thresholds: 4 in case of amplifications and 1 for deletions.

Found at: doi:10.1371/journal.pone.0008919.s004 (0.03 MB PDF)

Table S2 Multi-lesion predictor of synergy tested with the KNN method, Fishers exact test and t-test are displayed; here, only p-values smaller than 5% are shown. The Youden-Index (i.e., sensitivity+specificity-1) of zero indicates that the result has no predictive power. Found at: doi:10.1371/journal.pone.0008919.s005 (0.02 MB PDF)

References

- Slamon DJ, Leyland-Jones B, Shak S, Fuchs H, Paton V, et al. (2001) Use of chemotherapy plus a monoclonal antibody against HER2 for metastatic breast cancer that overexpresses HER2. *N Engl J Med* 344: 783–792.
- Druker BJ, Sawyers CL, Kantarjian H, Resta DJ, Reese SF, et al. (2001) Activity of a specific inhibitor of the BCR-ABL tyrosine kinase in the blast crisis of chronic myeloid leukemia and acute lymphoblastic leukemia with the Philadelphia chromosome. *N Engl J Med* 344: 1038–1042.
- Druker BJ, Talpaz M, Resta DJ, Peng B, Buchdunger E, et al. (2001) Efficacy and safety of a specific inhibitor of the BCR-ABL tyrosine kinase in chronic myeloid leukemia. *N Engl J Med* 344: 1031–1037.
- Pao W, Miller V, Zakowski M, Doherty J, Politi K, et al. (2004) EGF receptor gene mutations are common in lung cancers from “never smokers” and are associated with sensitivity of tumors to gefitinib and erlotinib. *Proc Natl Acad Sci U S A* 101: 13306–13311.
- Engelman JA, Zejnullahu K, Mitsudomi T, Song Y, Hyland C, et al. (2007) MET amplification leads to gefitinib resistance in lung cancer by activating ERBB3 signaling. *Science* 316: 1039–1043.
- Kobayashi S, Boggon TJ, Dayaram T, Janne PA, Kocher O, et al. (2005) EGFR mutation and resistance of non-small-cell lung cancer to gefitinib. *N Engl J Med* 352: 786–792.
- Pao W, Miller VA, Politi KA, Riely GJ, Somwar R, et al. (2005) Acquired resistance of lung adenocarcinomas to gefitinib or erlotinib is associated with a second mutation in the EGFR kinase domain. *PLoS Med* 2: e73.
- Sos ML, Koker M, Weir BA, Heynck S, Rabinovsky R, et al. (2009) PTEN loss contributes to erlotinib resistance in EGFR-mutant lung cancer by activation of Akt and EGFR. *Cancer Res* 69: 3256–3261.
- Sos ML, Michel K, Zander T, Weiss J, Frommolt P, et al. (2009) Predicting drug susceptibility of non-small cell lung cancers based on genetic lesions. *J Clin Invest* 119: 1727–1740.
- Bean J, Brennan C, Shih JY, Riely G, Viale A, et al. (2007) MET amplification occurs with or without T790M mutations in EGFR mutant lung tumors with acquired resistance to gefitinib or erlotinib. *Proc Natl Acad Sci U S A* 104: 20932–20937.
- Borisy AA, Elliott PJ, Hurst NW, Lee MS, Lehar J, et al. (2003) Systematic discovery of multicomponent therapeutics. *Proc Natl Acad Sci U S A* 100: 7977–7982.
- Chou TC (2006) Theoretical basis, experimental design, and computerized simulation of synergism and antagonism in drug combination studies. *Pharmacol Rev* 58: 621–681.
- Komarova NL, Wodarz D (2005) Drug resistance in cancer: principles of emergence and prevention. *Proc Natl Acad Sci U S A* 102: 9714–9719.
- Diehl V, Thomas RK, Re D (2004) Part II: Hodgkin’s lymphoma—diagnosis and treatment. *Lancet Oncol* 5: 19–26.
- Hurwitz H, Fehrenbacher L, Novotny W, Cartwright T, Hainsworth J, et al. (2004) Bevacizumab plus irinotecan, fluorouracil, and leucovorin for metastatic colorectal cancer. *N Engl J Med* 350: 2335–2342.
- Junttila TT, Akita RW, Parsons K, Fields C, Lewis Phillips GD, et al. (2009) Ligand-independent HER2/HER3/PI3K complex is disrupted by trastuzumab and is effectively inhibited by the PI3K inhibitor GDC-0941. *Cancer Cell* 15: 429–440.
- Engelman JA, Chen L, Tan X, Crosby K, Guimaraes AR, et al. (2008) Effective use of PI3K and MEK inhibitors to treat mutant Kras G12D and PIK3CA H1047R murine lung cancers. *Nat Med* 14: 1351–1356.
- Regales L, Gong Y, Shen R, de Stanchina E, Vivanco I, et al. (2009) Dual targeting of EGFR can overcome a major drug resistance mutation in mouse models of EGFR mutant lung cancer. *J Clin Invest* (in press).
- Sos ML, Fischer S, Ullrich R, Peifer M, Heuckmann JM, et al. (2009) Identifying genotype-dependent efficacy of single and combined PI3K- and MAPK-pathway inhibition in cancer. *Proc Natl Acad Sci U S A* (in press).
- Carracedo A, Ma L, Teruya-Feldstein J, Rojo F, Salmena L, et al. (2008) Inhibition of mTORC1 leads to MAPK pathway activation through a PI3K-dependent feedback loop in human cancer. *J Clin Invest* 118: 3065–3074.
- O’Reilly KE, Rojo F, She QB, Solit D, Mills GB, et al. (2006) mTOR inhibition induces upstream receptor tyrosine kinase signaling and activates Akt. *Cancer Res* 66: 1500–1508.
- Pratilas CA, Taylor BS, Ye Q, Viale A, Sander C, et al. (2009) (V600E)BRAF is associated with disabled feedback inhibition of RAF-MEK signaling and elevated transcriptional output of the pathway. *Proc Natl Acad Sci U S A* 106: 4519–4524.
- Berenbaum MC (1989) What is synergy? *Pharmacol Rev* 41: 93–141.
- Fitzgerald JB, Schoeberl B, Nielsen UB, Sorger PK (2006) Systems biology and combination therapy in the quest for clinical efficacy. *Nat Chem Biol* 2: 458–466.
- Greco WR, Bravo G, Parsons JC (1995) The search for synergy: a critical review from a response surface perspective. *Pharmacol Rev* 47: 331–385.
- Lehar J, Krueger A, Zimmermann G, Borisy A (2008) High-order combination effects and biological robustness. *Mol Syst Biol* 4: 215.
- Loewe S (1953) The problem of synergism and antagonism of combined drugs. *Arzneim Forsch* 3: 285–290.
- Bliss CI (1956) The calculation of microbial assays. *Bacteriol Rev* 20: 243–258.
- Benjamini Y, Hochberg Y (1995) Controlling the False Discovery Rate: A Practical and Powerful Approach to Multiple Testing. *J R Stat Soc B* 57: 289–300.
- Li D, Ambrogio L, Shimamura T, Kubo S, Takahashi M, et al. (2008) BIBW2992, an irreversible EGFR/HER2 inhibitor highly effective in preclinical lung cancer models. *Oncogene* 27: 4702–4711.
- Perera SA, Li D, Shimamura T, Raso MG, Ji H, et al. (2009) HER2YVMA drives rapid development of adenocarcinoma lung tumors in mice that are sensitive to BIBW2992 and rapamycin combination therapy. *Proc Natl Acad Sci U S A* 106: 474–479.
- Chou TC (1976) Derivation and properties of Michaelis-Menten type and Hill type equations for reference ligands. *J Theor Biol* 59: 253–276.
- Chou TC, Talalay P (1984) Quantitative analysis of dose-effect relationships: the combined effects of multiple drugs or enzyme inhibitors. *Adv Enzyme Regul* 22: 27–55.
- Beroukhim R, Getz G, Nghiemphu L, Barretina J, Hsueh T, et al. (2007) Assessing the significance of chromosomal aberrations in cancer: methodology and application to glioma. *Proc Natl Acad Sci U S A* 104: 20007–20012.
- Calzolari D, Bruschi S, Coquin L, Schofield J, Feala JD, et al. (2008) Search algorithms as a framework for the optimization of drug combinations. *PLoS Comput Biol* 4: e1000249.
- Lynch TJ, Bell DW, Sordella R, Gurubhagavatula S, Okimoto RA, et al. (2004) Activating mutations in the epidermal growth factor receptor underlying responsiveness of non-small-cell lung cancer to gefitinib. *N Engl J Med* 350: 2129–2139.
- Paez JG, Janne PA, Lee JC, Tracy S, Greulich H, et al. (2004) EGFR mutations in lung cancer: correlation with clinical response to gefitinib therapy. *Science* 304: 1497–1500.
- Sos ML, Rode H, Heynck S, Peifer M, Fischer F, et al. (2009) Insights into the limited activity of irreversible EGFR inhibitors in tumor cells expressing the T790M EGFR resistance mutation from chemo-genomics profiling. (submitted).
- Uphoff CC, Drexler HG (2005) Eradication of mycoplasma contaminations. *Methods Mol Biol* 290: 25–34.
- Marquardt DW (1963) An Algorithm for Least-Squares Estimation of Nonlinear Parameters. *Journal of the Society for Industrial and Applied Mathematics* 11: 431–441.
- Press WH, Teukolsky SA, Vetterling WT, Flannery BP (1992) *Numerical Recipes in C*. Cambridge: Cambridge University Press.

Author Contributions

Conceived and designed the experiments: MP JW MLS RKT. Performed the experiments: JW MLS MK SH SF. Analyzed the data: MP CN JR RKT. Contributed reagents/materials/analysis tools: CN HR DR JR. Wrote the paper: MP JW MLS RKT.

4.6 Frequent and Focal FGFR1 Amplification Associates with Therapeutically Tractable FGFR1 Dependency in Squamous Cell Lung Cancer

Jonathan Weiss, Martin L. Sos, Danila Seidel, Martin Peifer, Thomas Zander, Johannes M. Heuckmann, Roland T. Ullrich, Roopika Menon, Sebastian Maier, Alex Soltermann, Holger Moch, Patrick Wagener, Florian Fischer, Stefanie Heynck, Mirjam Koker, Jakob Schöttle, Frauke Leenders, Franziska Gabler, Ines Dabow, Silvia Querings, Lukas C. Heukamp, Hyatt Balke-Want, Sascha Ansén, Daniel Rauh, Ingelore Baessmann, Janine Altmüller, Zoe Wainer, Matthew Conron, Gavin Wright, Prudence Russell, Ben Solomon, Elisabeth Brambilla, Christian Brambilla, Philippe Lorimier, Steinar Sollberg, Odd Terje Brustugun, Walburga Engel-Riedel, Corinna Ludwig, Iver Petersen, Jörg Sängler, JoachimClement, Harry Groen, WimTimens, Hannie Sietsma, Erik Thunnissen, Egbert Smit, Daniëlle Heideman, Federico Cappuzzo, Claudia Ligorio, Stefania Damiani, Michael Hallek, Rameen Beroukhim, William Pao, Bert Klebl, Matthias Baumann, Reinhard Buettner, Karen Ernestus, Erich Stoelben, Jürgen Wolf, Peter Nürnberg, Sven Perner, Roman K. Thomas

Abstract of the publication

Lung cancer remains one of the leading causes of cancer-related death in developed countries. Although lung adenocarcinomas with EGFR mutations or EML4-ALK fusions respond to treatment by epidermal growth factor receptor (EGFR) and anaplastic lymphoma kinase (ALK) inhibition, respectively, squamous cell lung cancer currently lacks therapeutically exploitable genetic alterations. We conducted a systematic search in a set of 232 lung cancer specimens for genetic alterations that were therapeutically amenable and then performed high-resolution gene copy number analyses. We identified frequent and focal fibroblast growth factor receptor 1 (FGFR1) amplification in squamous cell lung cancer (n = 155), but not in other lung cancer subtypes, and, by fluorescence in situ hybridization, confirmed the presence of FGFR1 amplifications in an independent cohort of squamous cell lung cancer samples (22% of cases). Using cellbased screening with the FGFR inhibitor PD173074 in a large (n = 83) panel of lung cancer cell lines, we demonstrated that this compound inhibited growth and induced apoptosis specifically in those lung cancer cells carrying amplified FGFR1. We validated the FGFR1 dependence of FGFR1-amplified cell lines by FGFR1 knockdown and by ectopic expression of an FGFR1-resistant allele (FGFR1V561M), which rescued FGFR1-amplified cells from PD173074-mediated cytotoxicity. Finally, we showed that inhibition of FGFR1 with a small molecule led to significant tumor shrinkage in vivo. Thus, focal FGFR1 amplification is common in squamous cell lung cancer and associated with tumor growth and survival, suggesting that FGFR inhibitors may be a viable therapeutic option in this cohort of patients.

Own contributions

I led the functional cell biology part of this discovery, while the genetic discovery part was led by other scientists in the laboratory. My scientific responsibilities included the screening of the cell lines, the analysis of compound effects on cells bearing the amplification, the signaling associated with the amplification and the validation of the relevant target of the compound using chemical genetics and RNA interference. Specifically, I screened half of the cell lines shown in figure 2A against PD173074, an inhibitor of the Fibroblast Growth Factor Receptor Family (FGFRs). I further analyzed the screening data and found, by integrating chromosomal gene copy number data of the cell lines, that FGFR1 amplification was the only predictor for sensitivity towards PD173074. Furthermore, I screened a subpanel of cell lines for induction of apoptosis in the presence of PD173074. I could show that the same cell lines, that were sensitive in the initial screen, also exhibited a significantly higher rate of apoptosis. This data directly led to figure 2C. I also performed western blot analysis of signaling events after treatment with different dosages of PD173074 in the *FGFR1* amplified cell lines H520 and H1581 and the *EGFR* mutated cell line HCC827. Phosphorylation of FGFR1, FRS2a, Akt, ERK and S6K protein was assessed and revealed that FGFR1 signals via the MAPK but not the PI3K pathway. This data directly led to figure 2E. In addition, I confirmed that FGFR1 is the critical target of PD173074 in *FGFR1* amplified cells. Therefore I mutated the cDNA sequence of *FGFR1* by SDM,

leading to a change in the amino acid sequence from a valine into a methionine on position 561. Analog to the T341M mutation in *cSRC*, this mutation abrogates the binding of PD173074 into the ATP binding pocket of FGFR1. I expressed both, wildtype and mutated FGFR1 in the *FGFR1*-amplified cell line H1581, treated both with PD173074 and monitored the resulting phenotype. Expression of mutated FGFR1, but not wildtype FGFR1 was able to rescue the PD173074 induced phenotype. This experiment directly led to figure 3A. Finally, I packaged lentiviral particles containing either no insert or a shRNA targeting the mRNA of FGFR1. I transduced H1581 cell with both particles and could show that knockdown of FGFR1 reproduced the phenotype induced by PD173074. These observations lead to figure 3B.

I was centrally involved in writing of the manuscript. I prepared all figures that I had produced data for and I was centrally involved in the editing process until final acceptance of the paper.

For the supplement, I produced the data for supplementary Figure 3, where I could show that *FGFR1* amplification also leads to a higher amount of FGFR1 protein as assessed by western blotting. For supplementary figure 4A, I determined the amount of Fibroblast Growth Factor 2 (FGF2) in cell cultures starved for 24 hours. No significant amount of FGF2 could be observed in the supernatant of *FGFR1* amplified cells, indicating that FGFR1 signaling is not dependent on external FGFs. For supplementary figure 4B, I analyzed the level of phosphorylation of FGFR1 in cells that had been cultured in medium that contained either no serum, 10% FCS, 50ng/ml FGF2 or FGF9 and 50ng/ml FGF2+ PD173074 (1 μ M). In H1581 cells, FGFR1 was phosphorylated even in the absence of serum but could be boosted by addition of FGF2 or 9. For supplementary figure 5, I performed co-immunoprecipitation to determine the specificity of phospho FGFR antibody used in the study. For supplementary figure 7, I packaged 5 different shRNA constructs targeting the mRNA encoded by either *WHSC1L1* or *FLJ4358* (two genes in close proximity to FGFR1) in lentiviral particles and transduced H1581 cells. Following Puromycin selection, I assessed cell number and could show that knockdown of either gene had no severe effect on the cells. Together, these results confirmed the results from the chemical-genetic experiments that, namely, FGFR1 is the relevant gene residing in the 8p amplification.

Unpublished data

In addition to the data published, I screened breast cancer cell lines harboring *FGFR1* amplifications as well as cancer cell lines that harbor *FGF3*, *4* and *19* amplifications for sensitivity against PD173074. However, none of the *FGF3*, *4*, *19* amplified cells and only one of the *FGFR1*-amplified breast cancer cell line (HCC1599) was sensitive towards PD173074. I also determined the transformation ability of wildtype and mutated FGFR1 in NIH3T3 and Ba/F3 cell line systems. While V561M mutated FGFR1 could transform both cell types, over-expression of FGFR1 wildtype did not. Together, these results suggest that the genomic structure of the amplification differs between breast and squamous-cell lung cancer. These findings are in line with the data obtained by two pharmaceutical companies that work with us in the area of FGFR inhibition. They also found a mixed sensitivity of *FGFR1*-amplified breast cancers to FGFR inhibition. Furthermore, our preliminary transformation experiments show that *FGFR1* amplifications are necessary but not sufficient for transformation in the tumor cells bearing the amplification.

Concluding remarks

In this study, we identify *FGFR1* amplification as being predictive for FGFR1 inhibitor sensitivity in *FGFR1* amplified tumor cells. Furthermore, we investigated primary lung tumor samples and identified *FGFR1* amplifications in up to 20% of primary samples only in squamous cell lung carcinomas. Of note, we could not find any significant amplification in one of the other histological subtypes of primary lung tumor samples. Moreover, we confirmed FGFR1 as being the target of FGFR inhibitors in *FGFR1* amplified tumor cells. These results clearly demonstrate the need to screen patients suffering from squamous cell carcinomas for *FGFR1* amplification and treat these subsequently with FGFR inhibitors. In fact, based on our results, several studies have been initiated worldwide that assess the efficacy of FGFR inhibitors specifically in *FGFR1*-amplified lung cancer. One of the trials is a first-in-man trial conducted at the University of Cologne.

LUNG CANCER

Frequent and Focal *FGFR1* Amplification Associates with Therapeutically Tractable FGFR1 Dependency in Squamous Cell Lung Cancer

Jonathan Weiss,^{1*} Martin L. Sos,^{1*†} Danila Seidel,^{1,2*} Martin Peifer,¹ Thomas Zander,³ Johannes M. Heuckmann,¹ Roland T. Ullrich,¹ Roopika Menon,⁴ Sebastian Maier,⁴ Alex Soltermann,⁵ Holger Moch,⁵ Patrick Wagener,⁶ Florian Fischer,¹ Stefanie Heynck,¹ Mirjam Koker,¹ Jakob Schöttle,¹ Frauke Leenders,^{1,2} Franziska Gabler,^{1,2} Ines Dabow,^{1,2} Silvia Querings,¹ Lukas C. Heukamp,⁷ Hyatt Balke-Want,¹ Sascha Ansén,³ Daniel Rauh,⁸ Ingelore Baessmann,⁹ Janine Altmüller,⁹ Zoe Wainer,¹⁰ Matthew Conron,¹⁰ Gavin Wright,¹⁰ Prudence Russell,¹¹ Ben Solomon,¹² Elisabeth Brambilla,^{13,14} Christian Brambilla,^{13,14} Philippe Lorimier,¹³ Steinar Sollberg,¹⁵ Odd Terje Brustugun,^{16,17} Walburga Engel-Riedel,¹⁸ Corinna Ludwig,¹⁸ Iver Petersen,¹⁹ Jörg Sänger,²⁰ Joachim Clement,²¹ Harry Groen,²² Wim Timens,²³ Hannie Sietsma,²³ Erik Thunnissen,²⁴ Egbert Smit,²⁵ Daniëlle Heideman,²⁴ Federico Cappuzzo,²⁶ Claudia Ligorio,²⁷ Stefania Damiani,²⁷ Michael Hallek,^{3,28} Rameen Beroukhi,^{29,30,31,32} William Pao,³³ Bert Klebl,³⁴ Matthias Baumann,³⁴ Reinhard Buettner,⁷ Karen Ernestus,³⁵ Erich Stoelben,¹⁸ Jürgen Wolf,^{2,3} Peter Nürnberg,^{8,28} Sven Perner,⁴ Roman K. Thomas^{1,2,3,8†}

(Published 15 December 2010; Volume 2 Issue 62 62ra93; revised 19 January 2011)

Lung cancer remains one of the leading causes of cancer-related death in developed countries. Although lung adenocarcinomas with *EGFR* mutations or *EML4-ALK* fusions respond to treatment by epidermal growth factor receptor (EGFR) and anaplastic lymphoma kinase (ALK) inhibition, respectively, squamous cell lung cancer currently lacks therapeutically exploitable genetic alterations. We conducted a systematic search in a set of 232 lung cancer specimens for genetic alterations that were therapeutically amenable and then performed high-resolution gene copy number analyses. We identified frequent and focal fibroblast growth factor receptor 1 (*FGFR1*) amplification in squamous cell lung cancer ($n = 155$), but not in other lung cancer subtypes, and, by fluorescence in situ hybridization, confirmed the presence of *FGFR1* amplifications in an independent cohort of squamous cell lung cancer samples (22% of cases). Using cell-based screening with the FGFR inhibitor PD173074 in a large ($n = 83$) panel of lung cancer cell lines, we demonstrated that this compound inhibited growth and induced apoptosis specifically in those lung cancer cells carrying amplified *FGFR1*. We validated the FGFR1 dependence of *FGFR1*-amplified cell lines by FGFR1 knockdown and by ectopic expression of an *FGFR1*-resistant allele (*FGFR1*^{V561M}), which rescued *FGFR1*-amplified cells from PD173074-mediated cytotoxicity. Finally, we showed that inhibition of FGFR1 with a small molecule led to significant tumor shrinkage in vivo. Thus, focal *FGFR1* amplification is common in squamous cell lung cancer and associated with tumor growth and survival, suggesting that FGFR inhibitors may be a viable therapeutic option in this cohort of patients.

INTRODUCTION

Oncogenic protein kinases are frequently implicated as potential targets for cancer treatment. For examples, the *ERBB2* amplification in breast cancer is associated with clinical response to antibodies targeting ERBB2 (1), and *KIT* or *PDGFRA* (platelet-derived growth factor receptor A) mutations in gastrointestinal stromal tumors lead to sensitivity to the *KIT/ABL/PDGFR* inhibitor imatinib (2). In lung adenocarcinoma, patients with *EGFR*-mutant tumors (3–5) experience tumor shrinkage and prolonged progression-free survival when treated with epidermal growth factor receptor (EGFR) inhibitors (6). Furthermore, *EML4-ALK* gene fusion-positive lung cancers can be effectively treated with anaplastic lymphoma kinase (ALK) inhibitors (7, 8).

However, these alterations almost exclusively occur in the rare adenocarcinomas of patients who never smoked, but are uncommon in squamous cell lung cancer, which is almost invariably associated with smoking (9). Although previous studies have reported recurrent genetic alterations in squamous cell lung cancer (10), no therapeutically tract-

able targets have so far been identified. Thus, therapeutic options for squamous cell lung cancer patients remain scarce, because molecularly targeted drugs such as erlotinib, gefitinib, pemetrexed, and cetuximab are either poorly active (6, 11) or contraindicated (for example, bevacizumab) (12). These observations emphasize the need for new “druggable” targets in squamous cell lung cancer patients.

RESULTS

To identify therapeutically relevant genome alterations in squamous cell lung cancer, we analyzed 155 primary squamous cell lung cancer specimens using Affymetrix 6.0 SNP (single-nucleotide polymorphism) arrays, which yielded high-resolution genomic profiles (median inter-marker distance <1 kb). To separate driver lesions from random noise, we applied the GISTIC algorithm (13, 14). We identified 25 significant amplification peaks, including the previously described amplification of

SOX2 on chromosome 3q26.33 (Fig. 1A and table S1) (10) and 26 significant deletions (fig. S1 and table S1). The second most significant amplification ($q = 8.82 \times 10^{-28}$) peak was identified on 8p12 and included *FGFR1* (fibroblast growth factor receptor 1) as well as *FLJ43582* in each amplified sample (Fig. 1A). This region spanned 133 kb (table S1) and was amplified at high amplitude (four or more copies) in 15 of 155 (9.7%) squamous cell lung cancer specimens (Fig. 1A). Notably, 11 of the tumors with *FGFR1* amplification were from smokers, whereas none of these were from patients who had never smoked (table S2). Ten of the 15 tumors with amplified amounts of *FGFR1* also harbored a mutation in *TP53* (table S2). Moreover, patients who had tumors with *FGFR1* amplification [copy number > 9 in fluorescence in situ hybridization (FISH) analysis] had a nonsignificant trend toward inferior survival compared to patients whose tumors lacked *FGFR1* amplifications (copy number = 2 in FISH analysis) (fig. S2). We next analyzed copy number alterations in lung adenocarcinoma specimens ($n = 77$) and found no significant ($q > 0.25$) amplification (four or more copies; 1.3%) at 8p12 (Fig. 1B).

Finally, we analyzed a publicly available lung cancer SNP array data set (14) for the presence of *FGFR1* amplifications (four or more copies); *FGFR1* was amplified in 6 of 581 (1%) nonsquamous cell lung cancers (Fig. 1C). Thus, *FGFR1* amplification is significantly enriched in squamous cell lung cancer when compared to our own adenocarcinoma data set ($P = 0.03$) (table S3) and when compared to a published data set of nonsquamous cell lung cancer ($P < 0.0001$) (Fig. 1C). FISH using an 8p12-specific probe on an independent set of 153 squamous cell lung cancers confirmed the presence of frequent high-level amplification of *FGFR1* in 34 of 153 (22%) patients (Fig. 1D and table S4), 27 of whom were current smokers and none of whom were nonsmokers. We note that FISH is not sensitive to the admixture of nontumoral cells; thus, focal amplification of *FGFR1* is likely to be more frequent in squamous cell lung cancer than as estimated by SNP arrays (table S4) (15). We also sequenced the *FGFR1* gene in 94 squamous cell lung cancers and 94 adenocarcinomas and found one mutation (*FGFR1*^{P578H}) in the adenocarcinoma cohort, indicating that *FGFR1* mutations might play only a minor role and might not drive alterations in the pathogenesis of lung cancer (16).

Next, we performed high-throughput cell line screening (17, 18) to determine the activity of the non-isoform-specific FGFR inhibitor PD173074 (19) in a collection of 83 lung cancer cell lines (table S5) (17, 20). Of all cell lines tested, four had a half-maximal growth-inhibitory

concentration (GI₅₀ values) below 1.0 μ M (Fig. 2A); remarkably, three of the four sensitive lung cancer cell lines exhibited focal amplification at 8p12 by 6.0 SNP array analysis (Fig. 2B), suggesting that *FGFR1* amplifications are significantly ($P = 0.0002$) associated with FGFR inhibitor activity (Fig. 2A). As expected, *FGFR1*-amplified cells expressed higher amounts of total FGFR1 protein (fig. S3). One (H520) of the three *FGFR1*-amplified cell lines that were sensitive to PD173074 was derived from a squamous cell lung cancer patient (table S5). We next tested whether amplification of *FGFR1* could be linked with sensitivity to FGFR inhibition in an unbiased fashion. Application of a *K*-nearest neighbor-based analysis, followed by leave-one-out cross-validation (17), revealed *FGFR1* amplification to be the only genetic predictor of PD173074 sensitivity that retained significance following Bonferroni-based multiple testing correction ($P < 0.05$; table S6). Previous studies indicated that expression of FGFR ligands might contribute to the sensitivity to FGFR inhibitors in lung cancer (21). We did not observe elevated amounts of FGF2 in the *FGFR1*-amplified cell lines (fig. S4A), nor did we observe a difference in the expression of FGFR ligands between patients harboring *FGFR1* amplification and those without *FGFR1* amplification (fig. S4B). However, *FGFR1*-amplified cells showed robust phosphorylation of FGFR, suggesting ligand-independent activation, which was further enhanced upon addition of exogenous FGF2 or FGF9 (fig. S4C), compatible with paracrine activation of FGFR1 in *FGFR1*-amplified cells. We next measured induction of apoptosis in *FGFR1*-amplified cells after treatment with PD173074 and found a significant ($P = 0.008$) enrichment of *FGFR1*-amplified lung cancer cells in the group of sensitive cells (Fig. 2C and table S7). Furthermore, FGFR inhibition led to decreased colony formation of *FGFR1*-amplified but not of *EGFR*-mutant cells in soft agar (Fig. 2D), further enforcing the notion that amplification of *FGFR1* drives proliferation of these lung cancer cell lines. Treatment with PD173074 reduced the amounts of phosphorylated FGFR1 (fig. S5) and of the adaptor molecule FRS2 in a dose-dependent manner only in *FGFR1*-amplified cells, but not in the *EGFR*-mutant cell line HCC827 (Fig. 2E). We also observed inhibition of phosphorylation of extracellular signal-regulated kinase (ERK) but not of AKT and S6, indicating that the mitogen-activated protein kinase (MAPK) pathway, and not the phosphatidylinositol 3-kinase (PI3K) pathway, is the major signaling pathway engaged by amplified *FGFR1* (Fig. 2E).

To validate FGFR1 as the critical target of PD173074 in *FGFR1*-amplified lung cancer cells, we ectopically expressed the V561M mutation (22) at the gatekeeper position of FGFR1 (*FGFR1*^{V561M}),

¹Max Planck Institute for Neurological Research, Klaus-Joachim-Zülch Laboratories of the Max Planck Society and the Medical Faculty of the University of Cologne, 50931 Cologne, Germany. ²Laboratory of Translational Cancer Genomics, Center of Integrated Oncology Köln-Bonn, University of Cologne, 50924 Cologne, Germany. ³Department I of Internal Medicine and Center of Integrated Oncology Köln-Bonn, University of Cologne, 50924 Cologne, Germany. ⁴Institute of Pathology, Comprehensive Cancer Center, University Hospital Tübingen, 72076 Tübingen, Germany. ⁵Institute for Surgical Pathology, University Hospital Zurich, 8091 Zurich, Switzerland. ⁶Department of Surgery, Weill Medical College, Cornell University, New York, NY 10065, USA. ⁷Institute of Pathology, University of Bonn, 53123 Bonn, Germany. ⁸Chemical Genomics Center, Max Planck Society, 44227 Dortmund, Germany. ⁹Cologne Center for Genomics and Institute for Genetics, University of Cologne, 50931 Cologne, Germany. ¹⁰Department of Surgical Oncology, Peter MacCallum Cancer Centre, Melbourne, 3002 Victoria, Australia. ¹¹Department of Pathology, St. Vincent's Hospital, Melbourne, 3065 Victoria, Australia. ¹²Department of Haematology and Medical Oncology, Peter MacCallum Cancer Centre, Melbourne, 3002 Victoria, Australia. ¹³Department of Pathology, Université Joseph Fourier, 38041 Grenoble, France. ¹⁴Institut Albert Bonniot INSERM U823, Université Joseph Fourier, 38042 Grenoble, France. ¹⁵Department of Thoracic Surgery, Rikshospitalet, Oslo University Hospital, 0027 Oslo, Norway. ¹⁶Department of Radiation Biology, Norwegian Radium Hospital, N-0310 Oslo, Norway. ¹⁷Department of Oncology, Radiumhospitalet, Oslo University Hospital, N-0310 Oslo, Norway. ¹⁸Thoracic Surgery, Lungenklinik Merheim, Kliniken der Stadt Köln gGmbH, 51109 Cologne, Germany. ¹⁹Institute of

Pathology, Jena University Hospital, Friedrich-Schiller-University, 07743 Jena, Germany. ²⁰Institute for Pathology Bad Berka, 99438 Bad Berka, Germany. ²¹Department for Internal Medicine II, University Clinic Jena, Friedrich-Schiller University, 07740 Jena, Germany. ²²Department of Pulmonary Diseases, University Medical Centre Groningen, 9713 GZ Groningen, Netherlands. ²³Department of Pathology, University Medical Centre Groningen, 9713 GZ Groningen, Netherlands. ²⁴Department of Pathology, VU University Medical Center Amsterdam, 1007 MB Amsterdam, Netherlands. ²⁵Department of Pulmonary Diseases, VU University Medical Center Amsterdam, 1007 MB Amsterdam, Netherlands. ²⁶Department of Medical Oncology, Ospedale Civile, 57100 Livorno, Italy. ²⁷Department of Haematology and Oncologic Science, University Hospital Bologna, 40138 Bologna, Italy. ²⁸Cologne Excellence Cluster on Cellular Stress Responses in Aging-Associated Diseases, University of Cologne, 50931 Cologne, Germany. ²⁹Department of Cancer Biology, Dana-Farber Cancer Institute, Boston, MA 02115, USA. ³⁰Department of Medicine, Brigham and Women's Hospital, Boston, MA 02115, USA. ³¹Department of Medicine, Harvard Medical School, Boston, MA 02115, USA. ³²Cancer Program, Broad Institute, Cambridge, MA 02115, USA. ³³Vanderbilt-Ingram Cancer Center, Nashville, TN 37212, USA. ³⁴Lead Discovery Center GmbH, 44227 Dortmund, Germany. ³⁵Department of Pathology, Hospital Merheim, Kliniken der Stadt Köln gGmbH, 51109 Cologne, Germany.

*These authors contributed equally to this work.

†To whom correspondence should be addressed. E-mail: martin.sos@nf.mpg.de (M.L.S.); nini@nf.mpg.de (R.K.T.)

preventing access of the compound to the hinge region of the kinase (23) (fig. S6). Expression of *FGFR1*^{V561M} in *FGFR1*-amplified lung cancer cells abolished PD173074-mediated cytotoxicity and dephosphorylation of FGFR (Fig. 3A), consistent with the notion that FGFR1 is the critical target of PD173074 in *FGFR1*-amplified lung cancer cells. Furthermore, in a panel of 105 biochemically screened kinases, FGFR1 was one of only two kinases strongly inhibited by PD173074 (table S8), recapitulating previous studies (22).

The high analytical resolution of the 6.0 SNP arrays, together with the large size of our data set, limited the number of candidate genes in the 8p12 amplicon to only two genes, *FGFR1* and *FLJ43582*. A previous study analyzing the 8p12 locus in lung cancer applying lower-resolution techniques suggested *WHSC1L1* to be the relevant oncogene in the 8p12 amplicon (24). To test whether genes other than *FGFR1* drive tumorigenesis in the 8p12-amplified tumors, we silenced the genes *WHSC1L1* (24) and *FLJ43582* using five different short hairpin RNA (shRNA) constructs in the 8p12-amplified lung cancer cell line H1581. Although silencing of either one of these genes did not inhibit cellular viability (fig. S7), silencing of *FGFR1* strongly reduced the viability of the *FGFR1*-amplified lung cancer cells (Fig. 3B). In light of the focality of the 8p12 amplicon (including *FGFR1* and *FLJ43582*) and the lack of effect of shRNA-mediated knockdown of either *FLJ43582* or *WHSC1L1* in *FGFR1*-amplified cells, our data suggest that *FGFR1* is the relevant target in these cells. Notably, the cell line H1703, which bears a copy number gain at 8p12 and that had been reported to depend on *WHSC1L1* (24), was not sensitive to FGFR inhibition (fig. S8). By contrast, H1703 cells depend on PDGFRA for their survival (25) because of amplification (copy number >2.8) of the gene encoding this kinase (26, 27). Thus, our data suggest that the gene targeted by the 8p12 amplicon is primarily *FGFR1* and its amplification induces FGFR1 dependency.

Finally, treatment with PD173074 (100 mg/kg, twice a day) resulted in tumor shrinkage in mice engrafted with *FGFR1*-amplified cells (Fig. 3C). This reduction in tumor size was paralleled by reduction in the amounts of phospho-ERK but not of phospho-AKT in immu-

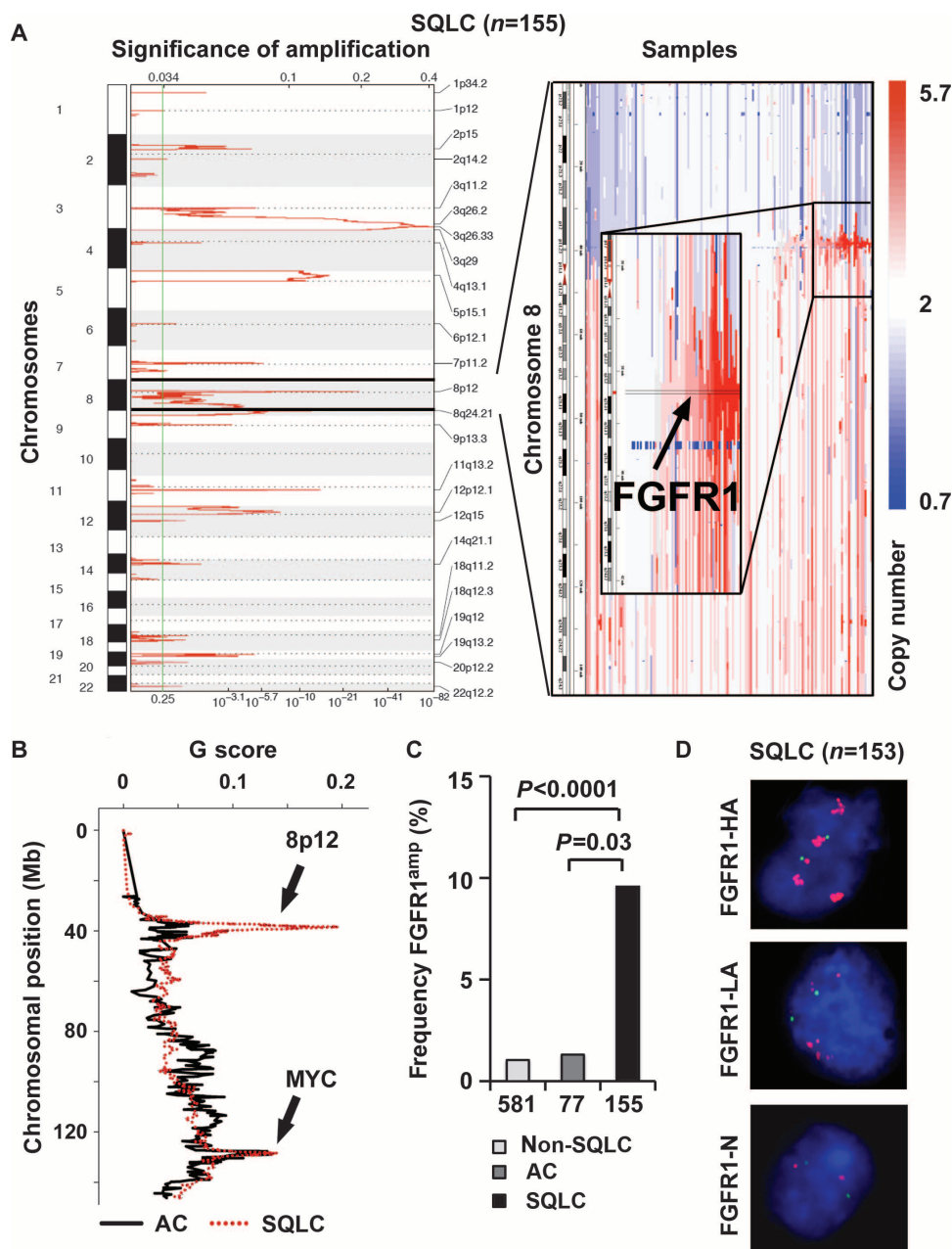


Fig. 1. *FGFR1* is amplified in squamous cell lung cancer (SQLC). **(A)** Left panel: Significant (14) [FDR (false discovery rate) value; x axis] amplifications across all chromosomes (y axis) in SQLC (n = 155) as assessed by GISTIC. Right panel: Copy number alterations (blue, deletion; white, copy number-neutral; red, amplification) at chromosome 8 (y axis) across all SQLC samples (x axis). Samples are ordered according to focal amplification of *FGFR1*. **(B)** Significant (G score; y axis) copy number changes in adenocarcinoma (AC; n = 77) (black line) and SQLC (red dotted line) at chromosome 8. The q value for the presence of 8p12 amplification is 8.82×10^{-28} for SQLC and greater than 0.25 for adenocarcinoma. The chromosomal positions of *FGFR1* (8p12) and *MYC* are highlighted (black arrows). **(C)** Frequency of *FGFR1* amplification (% of samples \geq copy number 4; y axis) in non-SQLC from a published data set (14), adenocarcinoma, and SQLC. P values indicate statistical significance. **(D)** FISH analysis (green, control; red, *FGFR1*) of 153 SQLC samples (FGFR1-HA: copy number >9; FGFR1-LA: copy number >2 and <9; FGFR1-N: copy number 2). Presented are example images from the three different *FGFR1* amplification groups.

nohistochemical analyses of explanted tumors, validating our in vitro findings that MAPK signaling is the key pathway engaged by amplified *FGFR1* (fig. S9A). Treatment at 50 mg/kg twice a day resulted in only a minimal exposure when compared to the gavage of 100 mg/kg twice a day because of the short half-life of the compound in vivo (fig. S9B). Thus, although we cannot formally exclude inhibitory effects on VEGFR2 (vascular endothelial growth factor receptor 2), the observed tumor regression is likely to be mediated by inhibition of FGFR1. In contrast, xenografted *EGFR*-mutant H1975 cells did not show signs of regression upon PD173074 treatment (fig. S9C). Thus, *FGFR1* amplification leads to FGFR1 dependency in vivo.

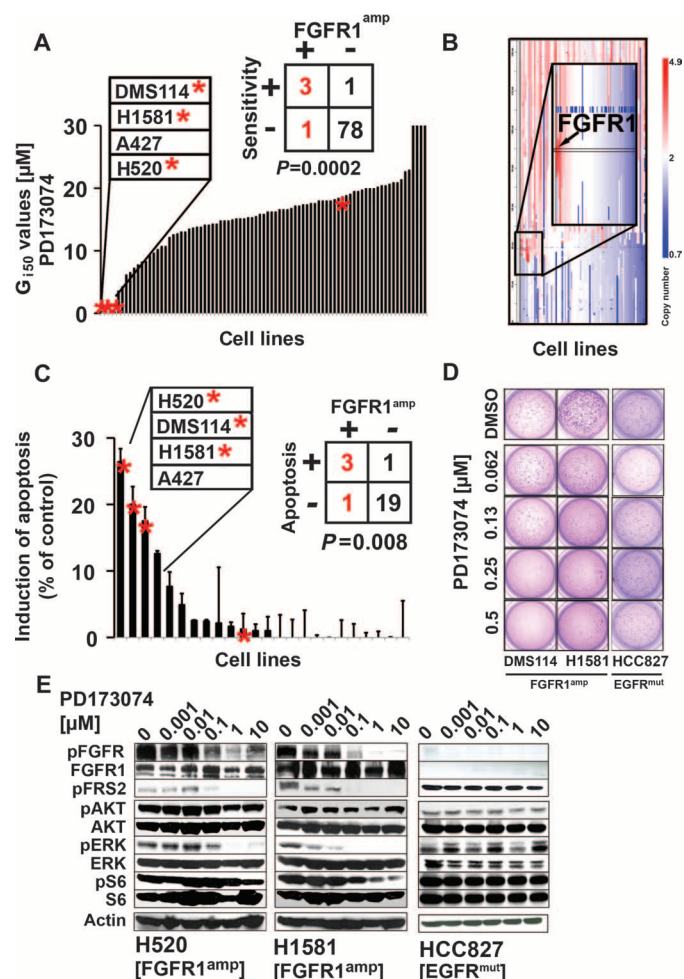


Fig. 2. *FGFR1* amplifications are associated with FGFR inhibitor activity. (A) GI_{50} values (y axis) of PD173074 across 83 lung cancer cell lines (x axis). *FGFR1*-amplified (copy number ≥ 4) cell lines are marked with asterisks. (B) Copy number alterations (x axis; blue, deletion; white, copy number 2; red, amplification) on chromosome 8 with a zoom in on 8p12 (*FGFR1* locus is highlighted) across all cell lines (y axis). (C) Induction of apoptosis (difference between PD173074 at 1 μ M and DMSO control after 72 hours; y axis) across 24 cell lines (x axis; asterisks denote *FGFR1* amplification copy number ≥ 4) as measured by flow cytometry (after annexin V/PI staining). (D) *FGFR1*-amplified cell lines were plated in soft agar and treated with either DMSO (control) or decreasing concentrations of PD173074. (E) Phosphorylation of FGFR and of downstream molecules in *FGFR1*-amplified (H1581 and H520) and in *FGFR1* wild-type (*EGFR*-mutant) cells (HCC827) after treatment with PD173074 as assessed by immunoblotting.

DISCUSSION

Here, we have identified frequent high-level amplification of *FGFR1* in squamous cell lung cancer of smokers; this amplification sensitizes the tumors to FGFR1 inhibition. Previous studies in lung cancer cohorts of mixed subtypes and low technological resolution (24, 28) or small size (10) have reported occasional amplification of the 8p locus in lung cancer. However, the large size of our sample set was necessary to reveal the high prevalence of this amplicon in squamous cell lung cancer (~10%) in comparison to other lung cancer subtypes (1%). Given the insensitivity of FISH analyses to admixture of nontumoral cells, the true prevalence of this amplification is likely to still be substantially underestimated by SNP arrays and to be up to 20%. We conclude that *FGFR1* amplification is one of the hallmark alterations in squamous cell lung cancer, similar to amplification of *SOX2*. These two alterations were almost completely mutually exclusive (table S9), suggesting an epistatic

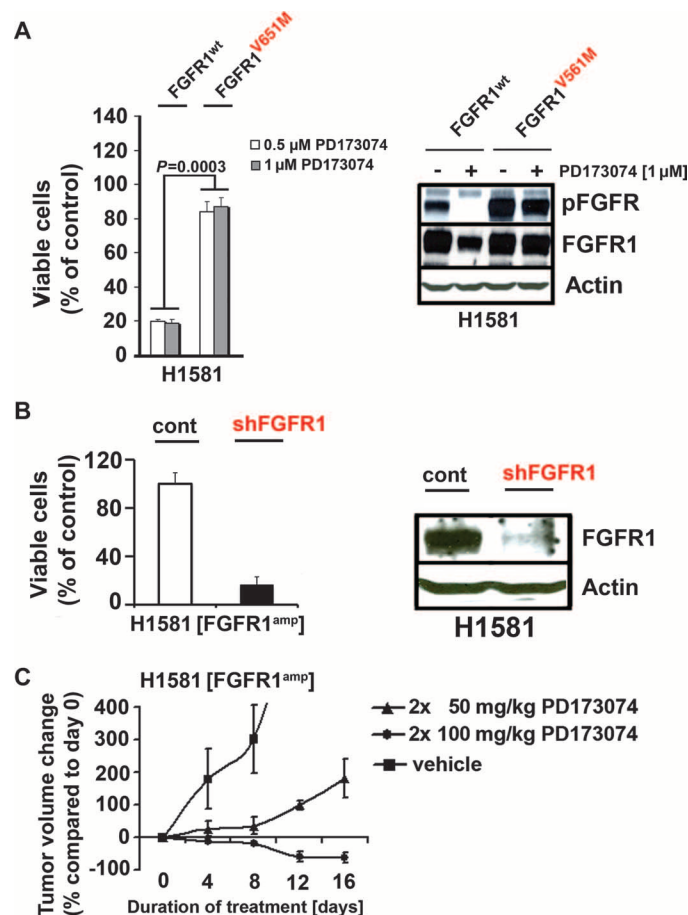


Fig. 3. *FGFR1*-amplified cells are dependent on FGFR1 in vitro and in vivo. (A) Left panel: Viability (PD173074 treatment as compared to DMSO control) of *FGFR1*-amplified cells expressing wild-type (wt) or mutant (V561M) *FGFR1* treated with PD173074 [0.5 μ M (white bars) and 1.0 μ M (gray bars)]. Right panel: Phosphorylation of FGFR in the *FGFR1*^{V561M} and *FGFR1*^{wt} cells detected by immunoblotting. (B) Left panel: Viability (PD173074 treatment as compared to DMSO control; y axis) of H1581 cells after transduction with control shRNA or shRNA targeting *FGFR1*. Right panel: Silencing of *FGFR1* in H1581 cells was confirmed by immunoblotting. (C) In mice engrafted with H1581 cells treated with either vehicle or PD173074 (dosage as indicated; y axis), tumor volume was measured over time (x axis).

Downloaded from stm.sciencemag.org on January 26, 2011

relationship. Furthermore, *FGFR1* amplification induced a strong *FGFR1* dependency that could be exploited therapeutically, resulting in induction of apoptosis. Thus, *FGFR1* amplification represents an opportunity for targeted therapy in squamous cell lung cancer. We therefore suggest that *FGFR1* inhibitors, which are currently in clinical testing in tumor types bearing genetic alterations in *FGFR* genes (29–31), should be evaluated in patients with *FGFR1*-amplified squamous cell lung cancer.

MATERIALS AND METHODS

Genomic analyses

The tumor specimens analyzed in this study have been collected under local Institutional Review Board approval. All patients gave written informed consent. Genomic DNA was hybridized to Affymetrix 6.0 SNP arrays following the manufacturer's instructions. Raw signal intensities were normalized and modeled with a Gaussian mixture model. Background-corrected intensities were normalized across all arrays of one batch by quantile normalization. Raw copy numbers were calculated by dividing the normalized tumor-derived signal intensities by the mean signal intensities derived from the normal samples hybridized in the same batch. Raw copy number data were segmented by circular binary segmentation and visualized in the integrated genome viewer (IGV) (32). GISTIC was performed as described previously (13, 14). The human genome build hg18 was used. Dideoxy sequencing was performed on whole-genome amplified DNA of primary tumors. Cell lines were sequenced with complementary DNA (cDNA). All raw data are publicly available [Gene Expression Omnibus (GEO); GSE25016].

Tissue microarray construction

Tissue microarray slides were obtained from formalin-fixed, paraffin-embedded lung squamous cell carcinoma samples. The tissue microarrays contained samples of a total of 172 patients from the University Hospital Zurich; each of these samples was present in duplicate cores, each core 0.6 mm in diameter (33). A second tissue microarray of 22 patients from Weill Cornell Medical Center was obtained, with each sample present in triplicate cores, each core 0.6 mm in diameter. Subsequently, 153 samples were used for FISH analysis.

Gene expression

After RNA isolation, biotin-labeled complementary RNA (cRNA) preparation was performed with Epicentre TargetAmp Kit (Epicentre Biotechnologies) and Biotin-16-UTP (10 mM; Roche Molecular Biochemicals) or Illumina TotalPrep RNA Amplification Kit (Ambion). Biotin-labeled cRNA (1.5 µg) was hybridized to Sentrix whole-genome bead chips WG6 version 2 (Illumina) and scanned on the Illumina BeadStation 500X. For data collection, we used Illumina BeadStudio 3.1.1.0 software. Gene pattern analysis platform (34) was used to visualize the normalized data.

FGFR1 amplification FISH assay

A FISH assay was used to detect the *FGFR1* amplification at the chromosomal level on the tissue microarrays. We performed fluorescence signal detection with two probes on chromosome 8. The reference probe is located on a stable region of chromosome 8p23.2 and selected on the basis of SNP array analysis. Only samples where the control bacterial artificial chromosome (BAC) was detectable were used for the determination of the copy number of *FGFR1*. The target probe is located on the

FGFR1 locus spanning 8p11.23 to 8p11.22. We used the digoxigenin-labeled BAC clones CTD 2523O9, which produces a green signal, as reference probe. The target probe was labeled with biotin to produce a red signal with RP11-148D21 BAC clones (Invitrogen). Deparaffinized sections were pretreated with a 100 mM tris and 50 mM EDTA solution at 92.8°C for 15 min and digested with Digest-All III (dilution, 1:2) at 37°C for 14 min; *FGFR1* FISH probes were denatured at 73°C for 5 min and immediately placed on ice. Subsequently, the tissue sections and *FGFR1* FISH probes were co-denatured at 94°C for 3 min and hybridized overnight at 37°C. After hybridization, washing was done with 2× SSC at 75°C for 5 min, and the fluorescence detection was performed with streptavidin–Alexa 594 conjugates (dilution 1:200) and antibodies to digoxigenin–fluorescein isothiocyanate (FITC) (dilution, 1:200). Slides were then counterstained with 4',6-diamidino-2-phenylindole (DAPI) and mounted. The samples were analyzed under a 63× oil immersion objective with a fluorescence microscope (Zeiss) equipped with appropriate filters, a charge-coupled device camera, and the FISH imaging and capturing software Metafer 4 (Metasystems). The evaluation of the tests was done independently by three experienced evaluators (R.M., S.M., and S.P.). At least 100 nuclei per case were evaluated. The thresholds for assigning a sample to the *FGFR1* “high-amplification” group were a copy number of nine. All samples that had a copy number below nine and above two were assigned to the group of “low-amplification” cohort. All the remaining samples were assigned “normal.”

Cell lines and reagents

Cell lines were obtained from the American Type Culture Collection (ATCC), the German Resource Centre for Biological Material (DSMZ), or from our own and other cell culture collections and were maintained as described previously. PD173074 was purchased from commercial suppliers, dissolved in dimethyl sulfoxide (DMSO) or vehicle solution, and stored at –20°C.

Cell line screening

Cell line screening was performed as previously described (17) with various concentrations of PD173074. Viability was determined after 96 hours by measuring cellular adenosine triphosphate (ATP) content (CellTiter-Glo, Promega). Half-maximal inhibitory concentrations (GI₅₀) were determined with the statistical data analysis software “R” with the package “ic50.”

Apoptosis

For determination of apoptosis, cells were seeded in six-well plates, incubated for 24 hours, treated with either DMSO (control) or 1.0 µM PD173074 for 72 hours, and stained with annexin V and propidium iodide (PI). Finally, the cells were analyzed on a FACSCanto flow cytometer (BD Biosciences). The difference between the relative percentage of annexin V/PI–positive cells treated with DMSO and cells treated with PD173074 was determined (induction of apoptosis rate).

Lentiviral RNA interference and retroviral expression

The V561M mutation was introduced into *FGFR1* cloned in pBABE-Puro by site-directed mutagenesis. Replication-incompetent retroviruses were produced by cotransfection with the pCL-ampho plasmid in human embryonic kidney (HEK) 293T cells. Hairpin shRNA targeting the different genes was ordered from Sigma. All sequences are given in table S10. Replication-incompetent lentiviruses were produced from pLKO.1-Puro–based vectors by cotransfection with Δ8.9 and pMGD2 in 293T cells as described previously (35). After transduction, cells were

selected with puromycin (1.5 µg/ml), and 5 days after selection, cells were counted with trypan blue.

Western blotting

The following antibodies were used for immunoblotting: β-actin (MP Bioscience); phospho-FGFR (Tyr⁶⁵³, Tyr⁶⁵⁴), phospho-FRS2 (Tyr¹⁹⁶), phospho-AKT (Ser⁴⁷³), phospho-S6, S6, AKT, phospho-ERK, and ERK (Cell Signaling Technology); total FGFR1 (Santa Cruz Biotechnology); and horseradish peroxidase (HRP)-conjugated antibodies to rabbit and mouse (Millipore).

Soft agar assay

Cells were suspended in growth media containing 10% fetal calf serum (FCS) and 0.6% agar and plated in triplicate on 50 µl of solidified growth medium (10% FCS; 1.0% agar). Growth medium containing indicated compound concentrations was added on top. Colonies were analyzed with the Scanalyzer imaging system (LemnaTec).

Xenograft mouse models

All animal procedures were approved by the local animal protection committee and the local authorities. Tumor cells (5×10^6) were injected subcutaneously into male nude mice. After the tumors reached a size of at least 50 mm³, the animals were treated twice daily by oral gavage with PD173074 (15 mg/ml for 50 mg/kg or 30 mg/ml for 100 mg/kg schedule) dissolved in vehicle (sodium lactate) or vehicle detergent alone. Tumor size was monitored by measuring perpendicular diameters as described previously (17). For the determination of tumor growth under treatment with PD173074, each experiment presented in the figures compromises the measurement of five different tumors.

Statistical analyses

Tests for statistical significance were either two-tailed *t* tests or Fisher's exact tests. Prediction of compound activity was performed with the KNN algorithm as described previously (17). Multiple hypothesis testing was performed with the statistical data analysis software R using *P* value adjustment.

SUPPLEMENTARY MATERIAL

www.sciencetranslationalmedicine.org/cgi/content/full/2/62/62ra93/DC1

Methods

- Fig. S1. Significant deletions are observed in squamous cell lung cancer.
- Fig. S2. *FGFR1* amplification has no significant impact on overall survival of SCLC patients.
- Fig. S3. *FGFR1* amplification correlates with *FGFR1* protein expression.
- Fig. S4. Expression of FGFR ligands does not correlate with *FGFR1* amplification status.
- Fig. S5. Treatment of *FGFR1*-amplified cell line H520 with PD173074 leads to dephosphorylation of *FGFR1* as measured by immunoprecipitation.
- Fig. S6. PD173074 binds inside the ATP-binding pocket of *FGFR1*.
- Fig. S7. Knockdown of genes adjacent to *FGFR1* on 8p12 does not affect cell viability.
- Fig. S8. PD173074 is not active in the *PDGFRA*- and *FGFR1*-amplified cell line H1703.
- Fig. S9. PD173074 shows antitumor activity in vivo.
- Table S1. Significant amplifications and deletions are noted in a subset of 155 SCLC samples.
- Table S2. Clinical features and co-occurrent mutations of *FGFR1*-amplified SCLC samples.
- Table S3. Significant amplifications and deletions are noted in a subset of 77 adenocarcinoma samples.
- Table S4. *FGFR1* amplification is detected using FISH on tumor microarrays.
- Table S5. *G150* values are not associated with mutation status across the lung cancer cell line panel.
- Table S6. KNN algorithm-based scoring predicts PD173074 sensitivity.
- Table S7. PD173074 induces apoptosis in *FGFR1*-amplified cell lines.
- Table S8. PD173074 has specific activity against two kinases.
- Table S9. *FGFR1* and *SOX2* amplification in squamous cell lung carcinoma.
- Table S10. Sequences of all shRNA constructs that were used in the study.

References

REFERENCES AND NOTES

1. D. J. Slamon, B. Leyland-Jones, S. Shak, H. Fuchs, V. Paton, A. Bajamonde, T. Fleming, W. Eiermann, J. Wolter, M. Pegram, J. Baselga, L. Norton, Use of chemotherapy plus a monoclonal antibody against HER2 for metastatic breast cancer that overexpresses HER2. *N. Engl. J. Med.* **344**, 783–792 (2001).
2. M. C. Heinrich, C. L. Corless, G. D. Demetri, C. D. Blanke, M. von Mehren, H. Joensuu, L. S. McGreevey, C. J. Chen, A. D. Van den Abbeele, B. J. Druker, B. Kiese, B. Eisenberg, P. J. Roberts, S. Singer, C. D. Fletcher, S. Silberman, S. Dimitrijevic, J. A. Fletcher, Kinase mutations and imatinib response in patients with metastatic gastrointestinal stromal tumor. *J. Clin. Oncol.* **21**, 4342–4349 (2003).
3. W. Pao, V. Miller, M. Zakowski, J. Doherty, K. Politi, I. Sarkaria, B. Singh, R. Heelan, V. Rusch, L. Fulton, E. Mardis, D. Kupfer, R. Wilson, M. Kris, H. Varmus, EGF receptor gene mutations are common in lung cancers from "never smokers" and are associated with sensitivity of tumors to gefitinib and erlotinib. *Proc. Natl. Acad. Sci. U.S.A.* **101**, 13306–13311 (2004).
4. J. G. Paez, P. A. Jänne, J. C. Lee, S. Tracy, H. Greulich, S. Gabriel, P. Herman, F. J. Kaye, N. Lindeman, T. J. Boggon, K. Naoki, H. Sasaki, Y. Fujii, M. J. Eck, W. R. Sellers, B. E. Johnson, M. Meyerson, *EGFR* mutations in lung cancer: Correlation with clinical response to gefitinib therapy. *Science* **304**, 1497–1500 (2004).
5. T. J. Lynch, D. W. Bell, R. Sordella, S. Gurubhagavatula, R. A. Okimoto, B. W. Brannigan, P. L. Harris, S. M. Hasserlat, J. G. Supko, F. G. Haluska, D. N. Louis, D. C. Christiani, J. Settleman, D. A. Haber, Activating mutations in the epidermal growth factor receptor underlying responsiveness of non-small-cell lung cancer to gefitinib. *N. Engl. J. Med.* **350**, 2129–2139 (2004).
6. T. S. Mok, Y. L. Wu, S. Thongprasert, C. H. Yang, D. T. Chu, N. Saijo, P. Sunpaweravong, B. Han, B. Margono, Y. Ichinose, Y. Nishiwaki, Y. Ohe, J. J. Yang, B. Chewaskulyong, H. Jiang, E. L. Duffield, C. L. Watkins, A. A. Armour, M. Fukuoka, Gefitinib or carboplatin–paclitaxel in pulmonary adenocarcinoma. *N. Engl. J. Med.* **361**, 947–957 (2009).
7. M. Soda, Y. L. Choi, M. Enomoto, S. Takada, Y. Yamashita, S. Ishikawa, S. Fujiwara, H. Watanabe, K. Kurashina, H. Hatanaka, M. Bando, S. Ohno, Y. Ishikawa, H. Aburatani, T. Niki, Y. Sohara, Y. Sugiyama, H. Mano, Identification of the transforming *EML4-ALK* fusion gene in non-small-cell lung cancer. *Nature* **448**, 561–566 (2007).
8. E. L. Kwak, Y. J. Bang, D. R. Camidge, A. T. Shaw, B. Solomon, R. G. Maki, S. H. Ou, B. J. Dezube, P. A. Jänne, D. B. Costa, M. Varella-Garcia, W. H. Kim, T. J. Lynch, P. Fidias, H. Stubbs, J. A. Engelman, L. V. Sequist, W. Tan, L. Gandhi, M. Mino-Kenudson, G. C. Wei, S. M. Shreeve, M. J. Ratain, J. Settleman, J. G. Christensen, D. A. Haber, K. Wilner, R. Salgia, G. I. Shapiro, J. W. Clark, A. J. Iafrate, Anaplastic lymphoma kinase inhibition in non-small-cell lung cancer. *N. Engl. J. Med.* **363**, 1693–1703 (2010).
9. S. A. Khuder, Effect of cigarette smoking on major histological types of lung cancer: A meta-analysis. *Lung Cancer* **31**, 139–148 (2001).
10. A. J. Bass, H. Watanabe, C. H. Mermel, S. Yu, S. Perner, R. G. Verhaak, S. Y. Kim, L. Wardwell, P. Tamayo, I. Gat-Viks, A. H. Ramos, M. S. Woo, B. A. Weir, G. Getz, R. Beroukhi, M. O'Kelly, A. Dutt, O. Rozenblatt-Rosen, P. Dziunycz, J. Komisarof, L. R. Chirieac, C. J. Lafargue, V. Scheble, T. Willbertz, C. Ma, S. Rao, H. Nakagawa, D. B. Stairs, L. Lin, T. J. Giordano, P. Wagner, J. D. Minna, A. F. Gazdar, C. Q. Zhu, M. S. Brose, I. Ceccanello, U. Ribeiro Jr., S. K. Marie, O. Dahl, R. A. Shivdasani, M. S. Tsao, M. A. Rubin, K. K. Wong, A. Regev, W. C. Hahn, D. G. Beer, A. K. Rustgi, M. Meyerson, *SOX2* is an amplified lineage-survival oncogene in lung and esophageal squamous cell carcinomas. *Nat. Genet.* **41**, 1238–1242 (2009).
11. R. Pirkker, J. R. Pereira, A. Szczesna, J. von Pawel, M. Krzakowski, R. Ramlau, I. Vynnychenko, K. Park, C. T. Yu, V. Ganul, J. K. Roh, E. Bajetta, K. O'Byrne, F. de Marinis, W. Eberhardt, T. Goddemeier, M. Emig, U. Gatzemeier; FLEX Study Team, Cetuximab plus chemotherapy in patients with advanced non-small-cell lung cancer (FLEX): An open-label randomised phase III trial. *Lancet* **373**, 1525–1531 (2009).
12. A. Sandler, R. Gray, M. C. Perry, J. Brahmer, J. H. Schiller, A. Dowlati, R. Lilienbaum, D. H. Johnson, Paclitaxel–carboplatin alone or with bevacizumab for non-small-cell lung cancer. *N. Engl. J. Med.* **355**, 2542–2550 (2006).
13. R. Beroukhi, G. Getz, L. Nghiemphu, J. Barretina, T. Hsueh, D. Linhart, I. Vivanco, J. C. Lee, J. H. Huang, S. Alexander, J. Du, T. Kau, R. K. Thomas, K. Shah, H. Soto, S. Perner, J. Prensner, R. M. DeBiasi, F. Demicheli, C. Hattori, M. A. Rubin, L. A. Garraway, S. F. Nelson, L. Liao, P. S. Mischel, T. F. Cloughesy, M. Meyerson, T. A. Golub, E. S. Lander, I. K. Mellingshoff, W. R. Sellers, Assessing the significance of chromosomal aberrations in cancer: Methodology and application to glioma. *Proc. Natl. Acad. Sci. U.S.A.* **104**, 20007–20012 (2007).
14. R. Beroukhi, C. H. Mermel, D. Porter, G. Wei, S. Raychaudhuri, J. Donovan, J. Barretina, J. S. Boehm, J. Dobson, M. Urashima, K. T. McHenry, R. M. Pinchback, A. H. Ligon, Y. J. Cho, L. Haery, H. Greulich, M. Reich, W. Winckler, M. S. Lawrence, B. A. Weir, K. E. Tanaka, D. Y. Chiang, A. J. Bass, A. Loo, C. Hoffman, J. Prensner, T. Liefeld, Q. Gao, D. Yecies, S. Signoretti, E. Maher, F. J. Kaye, H. Sasaki, J. E. Tepper, J. A. Fletcher, J. Taberner, J. Baselga, M. S. Tsao, F. Demicheli, M. A. Rubin, P. A. Janne, M. J. Daly, C. Nucera, R. L. Levine, B. L. Ebert, S. Gabriel, A. K. Rustgi, C. R. Antonescu, M. Ladanyi, A. Letai, L. A. Garraway, M. Loda, D. G. Beer, L. D. True, A. Okamoto, S. L. Pomeroy, S. Singer, T. R. Golub, E. S. Lander, G. Getz, W. R. Sellers, M. Meyerson, The landscape of somatic copy-number alteration across human cancers. *Nature* **463**, 899–905 (2010).

15. B. A. Weir, M. S. Woo, G. Getz, S. Perner, L. Ding, R. Beroukchim, W. M. Lin, M. A. Province, A. Kraja, L. A. Johnson, K. Shah, M. Sato, R. K. Thomas, J. A. Barletta, I. B. Borecki, S. Broderick, A. C. Chang, D. Y. Chiang, L. R. Chirieac, J. Cho, Y. Fujii, A. F. Gazdar, T. Giordano, H. Greulich, M. Hanna, B. E. Johnson, M. G. Kris, A. Lash, L. Lin, N. Lindeman, E. R. Mardis, J. D. McPherson, J. D. Minna, M. B. Morgan, M. Nadel, M. B. Orringer, J. R. Osborne, B. Ozenberger, A. H. Ramos, J. Robinson, J. A. Roth, V. Rusch, H. Sasaki, F. Shepherd, C. Sougnez, M. R. Spitz, M. S. Tsao, D. Twomey, R. G. Verhaak, G. M. Weinstock, D. A. Wheeler, W. Winckler, A. Yoshizawa, S. Yu, M. F. Zakowski, Q. Zhang, D. G. Beer, I. I. Wistuba, M. A. Watson, L. A. Garraway, M. Ladanyi, W. D. Travis, W. Pao, M. A. Rubin, S. B. Gabriel, R. A. Gibbs, H. E. Varmus, R. K. Wilson, E. S. Lander, M. Meyerson, Characterizing the cancer genome in lung adenocarcinoma. *Nature* **450**, 893–898 (2007).
16. C. Greenman, P. Stephens, R. Smith, G. L. Dalgleish, C. Hunter, G. Bignell, H. Davies, J. Teague, A. Butler, C. Stevens, S. Edkins, S. O'Meara, I. Vastrik, E. E. Schmidt, T. Avis, S. Barthorpe, G. Bhamra, G. Buck, B. Choudhury, J. Clements, J. Cole, E. Dicks, S. Forbes, K. Gray, K. Halliday, R. Harrison, K. Hills, J. Hinton, A. Jenkinson, D. Jones, A. Menzies, T. Mironenko, J. Perry, K. Raine, D. Richardson, R. Shepherd, A. Small, C. Tofts, J. Varian, T. Webb, S. West, S. Widaa, A. Yates, D. P. Cahill, D. N. Louis, P. Goldstraw, A. G. Nicholson, F. Brasseur, L. Looijenga, B. L. Weber, Y. E. Chiew, W. Fazio, M. F. Greaves, A. R. Green, P. Campbell, E. Birney, D. F. Easton, G. Chenevix-Trench, M. H. Tan, S. K. Khoo, B. T. Teh, S. T. Yuen, S. Y. Leung, R. Wooster, P. A. Futreal, M. R. Stratton, Patterns of somatic mutation in human cancer genomes. *Nature* **446**, 153–158 (2007).
17. M. L. Sos, K. Michel, T. Zander, J. Weiss, P. Frommolt, M. Peifer, D. Li, R. Ullrich, M. Koker, F. Fischer, T. Shimamura, D. Rauh, C. Mermel, S. Fischer, I. Stückrath, S. Heynck, R. Beroukchim, W. Lin, W. Winckler, K. Shah, T. LaFramboise, W. F. Moriarty, M. Hanna, L. Tolosi, J. Rahnenführer, R. Verhaak, D. Chiang, G. Getz, M. Hellmich, J. Wolf, L. Girard, M. Peyton, B. A. Weir, T. H. Chen, H. Greulich, J. Barretina, G. I. Shapiro, L. A. Garraway, A. F. Gazdar, J. D. Minna, M. Meyerson, K. K. Wong, R. K. Thomas, Predicting drug susceptibility of non-small cell lung cancers based on genetic lesions. *J. Clin. Invest.* **119**, 1727–1740 (2009).
18. U. McDermott, S. V. Sharma, L. Dowell, P. Greninger, C. Montagut, J. Lamb, H. Archibald, R. Raudales, A. Tam, D. Lee, S. M. Rothenberg, J. G. Supko, R. Sordella, L. E. Ullkus, A. J. Iafrate, S. Maheswaran, C. N. Njauw, H. Tsao, L. Drew, J. H. Hanke, X. J. Ma, M. G. Erlander, N. S. Gray, D. A. Haber, J. Settleman, Identification of genotype-correlated sensitivity to selective kinase inhibitors by using high-throughput tumor cell line profiling. *Proc. Natl. Acad. Sci. U.S.A.* **104**, 19936–19941 (2007).
19. M. Mohammadi, S. Froum, J. M. Hamby, M. C. Schroeder, R. L. Panek, G. H. Lu, A. V. Eliseenkova, D. Green, J. Schlessinger, S. R. Hubbard, Crystal structure of an angiogenesis inhibitor bound to the FGF receptor tyrosine kinase domain. *EMBO J.* **17**, 5896–5904 (1998).
20. M. L. Sos, S. Fischer, R. Ullrich, M. Peifer, J. M. Heuckmann, M. Koker, S. Heynck, I. Stückrath, J. Weiss, F. Fischer, K. Michel, A. Goel, L. Regales, K. A. Politi, S. Perera, M. Getlik, L. C. Heukamp, S. Ansén, T. Zander, R. Beroukchim, H. Kashkar, K. M. Shokat, W. R. Sellers, D. Rauh, C. Orr, K. P. Hoeflich, L. Friedman, K. K. Wong, W. Pao, R. K. Thomas, Identifying genotype-dependent efficacy of single and combined PI3K- and MAPK-pathway inhibition in cancer. *Proc. Natl. Acad. Sci. U.S.A.* **106**, 18351–18356 (2009).
21. L. Marek, K. E. Ware, A. Fritzsche, P. Hercule, W. R. Helton, J. E. Smith, L. A. McDermott, C. D. Coldren, R. A. Nemenoff, D. T. Merrick, B. A. Helfrich, P. A. Bunn Jr., L. E. Heasley, Fibroblast growth factor (FGF) and FGF receptor-mediated autocrine signaling in non-small-cell lung cancer cells. *Mol. Pharmacol.* **75**, 196–207 (2009).
22. W. Zhou, W. Hur, U. McDermott, A. Dutt, W. Xian, S. B. Ficarro, J. Zhang, S. V. Sharma, J. Brugge, M. Meyerson, J. Settleman, N. S. Gray, A structure-guided approach to creating covalent FGFR inhibitors. *Chem. Biol.* **17**, 285–295 (2010).
23. S. Blencke, B. Zech, O. Engkvist, Z. Greff, L. Orfi, Z. Horváth, G. Kéri, A. Ullrich, H. Daub, Characterization of a conserved structural determinant controlling protein kinase sensitivity to selective inhibitors. *Chem. Biol.* **11**, 691–701 (2004).
24. G. Tonon, K. K. Wong, G. Maulik, C. Brennan, B. Feng, Y. Zhang, D. B. Khatry, A. Protopopov, M. J. You, A. J. Aguirre, E. S. Martin, Z. Yang, H. Ji, L. Chin, R. A. Depinho, High-resolution genomic profiles of human lung cancer. *Proc. Natl. Acad. Sci. U.S.A.* **102**, 9625–9630 (2005).
25. K. Rikova, A. Guo, Q. Zeng, A. Possemato, J. Yu, H. Haack, J. Nardone, K. Lee, C. Reeves, Y. Li, Y. Hu, Z. Tan, M. Stokes, L. Sullivan, J. Mitchell, R. Wetzel, J. Macneill, J. M. Ren, J. Yuan, C. E. Bakalarski, J. Villen, J. M. Kornhauser, B. Smith, D. Li, X. Zhou, S. P. Gygi, T. L. Gu, R. D. Polakiewicz, J. Rush, M. J. Comb, Global survey of phosphotyrosine signaling identifies oncogenic kinases in lung cancer. *Cell* **131**, 1190–1203 (2007).
26. U. McDermott, R. Y. Ames, A. J. Iafrate, S. Maheswaran, H. Stubbs, P. Greninger, K. McCutcheon, R. Milano, A. Tam, D. Y. Lee, L. Lucien, B. W. Brannigan, L. E. Ullkus, X. J. Ma, M. G. Erlander, D. A. Haber, S. V. Sharma, J. Settleman, Ligand-dependent platelet-derived growth factor receptor (PDGFR)- α activation sensitizes rare lung cancer and sarcoma cells to PDGFR kinase inhibitors. *Cancer Res.* **69**, 3937–3946 (2009).
27. A. H. Ramos, A. Dutt, C. Mermel, S. Perner, J. Cho, C. J. Lafargue, L. A. Johnson, A. C. Stiedl, K. E. Tanaka, A. J. Bass, J. Barretina, B. A. Weir, R. Beroukchim, R. K. Thomas, J. D. Minna, L. R. Chirieac, N. I. Lindeman, T. Giordano, D. G. Beer, P. Wagner, I. I. Wistuba, M. A. Rubin, M. Meyerson, Amplification of chromosomal segment 4q12 in non-small cell lung cancer. *Cancer Biol. Ther.* **8**, 2042–2050 (2009).
28. X. Zhao, B. A. Weir, T. LaFramboise, M. Lin, R. Beroukchim, L. Garraway, J. Beheshti, J. C. Lee, K. Naoki, W. G. Richards, D. Sugarbaker, F. Chen, M. A. Rubin, P. A. Jänne, L. Girard, J. Minna, D. Christiani, C. Li, W. R. Sellers, M. Meyerson, Homozygous deletions and chromosome amplifications in human lung carcinomas revealed by single nucleotide polymorphism array analysis. *Cancer Res.* **65**, 5561–5570 (2005).
29. J. S. Reis-Filho, P. T. Simpson, N. C. Turner, M. B. Lambros, C. Jones, A. Mackay, A. Grigoriadis, D. Sarrico, K. Savage, T. Dexter, M. Iravani, K. Fenwick, B. Weber, D. Hardisson, F. C. Schmitt, J. Palacios, S. R. Lakhani, A. Ashworth, *FGFR1* emerges as a potential therapeutic target for lobular breast carcinomas. *Clin. Cancer Res.* **12**, 6652–6662 (2006).
30. N. Turner, R. Grose, Fibroblast growth factor signalling: From development to cancer. *Nat. Rev. Cancer* **10**, 116–129 (2010).
31. N. Turner, A. Pearson, R. Sharpe, M. Lambros, F. Geyer, M. A. Lopez-Garcia, R. Natrajan, C. Marchio, E. Iorns, A. Mackay, C. Gillett, A. Grigoriadis, A. Tutt, J. S. Reis-Filho, A. Ashworth, *FGFR1* amplification drives endocrine therapy resistance and is a therapeutic target in breast cancer. *Cancer Res.* **70**, 2085–2094 (2010).
32. <http://www.broadinstitute.org/igv/>.
33. S. Perner, P. L. Wagner, A. Soltermann, C. LaFargue, V. Tischler, B. A. Weir, W. Weder, M. Meyerson, T. J. Giordano, H. Moch, M. A. Rubin, TTF1 expression in non-small cell lung carcinoma: Association with *TTF1* gene amplification and improved survival. *J. Pathol.* **217**, 65–72 (2009).
34. <http://www.broadinstitute.org/cancer/software/genepattern/>.
35. M. L. Sos, H. B. Rode, S. Heynck, M. Peifer, F. Fischer, S. Klüter, V. G. Pawar, C. Reuter, J. M. Heuckmann, J. Weiss, L. Ruddigkeit, M. Rabiller, M. Koker, J. R. Simard, M. Getlik, Y. Yuza, T. H. Chen, H. Greulich, R. K. Thomas, D. Rauh, Chemogenomic profiling provides insights into the limited activity of irreversible EGFR inhibitors in tumor cells expressing the T790M EGFR resistance mutation. *Cancer Res.* **70**, 868–874 (2010).
36. **Acknowledgments:** We thank M. Meyerson and A. Bass for sharing unpublished data and C. Reinhardt and A. Ullrich for discussion. **Funding:** This work was supported by the Deutsche Krebshilfe (grant 107954 to R.K.T.); the German Ministry of Science and Education (BMBF) as part of the NGFNplus program (grants 01GS08100 to R.K.T. and 01GS08101 to J. Wolf and P.N.); the Max Planck Society (M.J.F.A.NEUR8061 to R.K.T.); the Deutsche Forschungsgemeinschaft (DFG) through SFB (TP6 to R.K.T. and R.T.U.); TP5 to L.C.H. and R. Buettner); the Ministry for Innovation, Science, Research and Technology of the State of Nordrhein-Westfalen (MIWT, 4000-12 09 to R.K.T. and B.K.); and an anonymous foundation to R.K.T. E.B. and C.B. were supported by the PNES INCA grant 2008. B.S. was supported by the International Association for the Study of Lung Cancer Young Investigator Award. W.P. was supported by a grant from the NIH National Cancer Institute. Z.W. was supported by the Royal Australasian College of Surgeons and a Raelene Boyle Scholarship. G.W. was supported by the Australasian Society of Cardiac and Thoracic Surgeons Foundation Grant, Peter MacCallum Foundation Grant, and a private research donation from family and friends of former patients. **Author contributions:** J. Weiss and M.L.S. designed and performed the experiments, analyzed the data, and wrote the manuscript. D.S. designed the experiments and analyzed the data. M.P., T.Z., F.L., and D.R. analyzed the data. J.M.H., R.T.U., R.M., S.M., F.F., S.H., M.K., J. Schöttle, F.G., I.D., S.Q., L.C.H., H.B.-W., I.B., and J.A. performed the experiments and discussed the data. A.S., H.M., P.W., S.A., Z.W., M.C., G.W., P.R., B.S., E.B., C.B., P.L., S.S., O.T.B., W.E.-R., C.L., I.P., J. Sängler, J.C., H.G., W.T., H.S., E.T., E. Smit, D.H., F.C., C.L., S.D., M.H., R. Beroukchim, W.P., B.K., M.B., R. Buettner, K.E., E. Stoelben, J. Wolf, and P.N. contributed critical tumor specimens and contributed to the discussion of the data. S.P. reviewed tumor histology, analyzed the FISH data, and wrote the manuscript. R.K.T. conceived the project, designed the experiments, analyzed the data, and wrote the manuscript. **Competing interests:** R.K.T. receives consulting and lecture fees from Sequenom, Sanofi-Aventis, Merck, Roche, Infinity, Boehringer, AstraZeneca, and ATLAS Biolabs, as well as research support from Novartis and AstraZeneca. J. Wolf is a member of advisory boards of Roche, AstraZeneca, Novartis, Amgen, Bayer, and Merck and has received lecture fees from Roche, AstraZeneca, and Merck. R. Beroukchim receives consulting fees from Novartis Institutes for BioMedical Research. W.P. receives consulting fees from Molecular MD, AstraZeneca, BMS, and Symphony Evolution. H.G. received research support from Eli Lilly, Roche, and Boehringer Ingelheim through the University Medical Center Groningen. The other authors declare that they have no competing interests. **Accession numbers:** All raw data are publicly available (GEO; GSE25016).

Submitted 6 July 2010

Accepted 24 November 2010

Published 15 December 2010

10.1126/scitranslmed.3001451

Citation: J. Weiss, M. L. Sos, D. Seidel, M. Peifer, T. Zander, J. M. Heuckmann, R. T. Ullrich, R. Menon, S. Maier, A. Soltermann, H. Moch, P. Wagener, F. Fischer, S. Heynck, M. Koker, J. Schöttle, F. Leenders, F. Gabler, I. Dabow, S. Quering, L. C. Heukamp, H. Balke-Want, S. Ansén, D. Rauh, I. Baessmann, J. Altmüller, Z. Wainer, M. Conron, G. Wright, P. Russell, B. Solomon, E. Brambilla, C. Brambilla, P. Lorimier, S. Sollberg, O. T. Brustugun, W. Engel-Riedel, C. Ludwig, I. Petersen, J. Sängler, J. Clement, H. Groen, W. Timens, H. Sietsma, E. Thunnissen, E. Smit, D. Heidemann, F. Cappuzzo, C. Ligorio, S. Damiani, M. Hallek, R. Beroukchim, W. Pao, B. Klebl, M. Baumann, R. Buettner, K. Ernestus, E. Stoelben, J. Wolf, P. Nürnberg, S. Perner, R. K. Thomas, Frequent and focal *FGFR1* amplification associates with therapeutically tractable *FGFR1* dependency in squamous cell lung cancer. *Sci. Transl. Med.* **2**, 62ra93 (2010).

5.0 Discussion

High-throughput compound screens of large panels of genomically annotated lung cancer cell lines not only allow the identification of predictive markers for sensitivity towards a certain compound, but also shed light onto the underlying molecular mechanisms tumor cells employ to become oncogenic. The Ph.D. thesis presented here aims for the identification of genes, previously unrecognized as driving genes in lung cancer, as well as to understand how these genes elicit signal transduction pathways to support tumor development. In the course of this thesis, two novel therapeutically trackable genes were identified as being genomically altered in lung cancer and functionally validated as being targets of the respective inhibitor. As proof of principle, *EGFR* mutations in conjunction with absent *KRAS* mutations were identified as the most significant predictor for *EGFR* inhibitor sensitivity across the screened cell line panel (54). These results are in perfect accordance with previous reports (9,26,55,56). In another proof of principle experiment, we identified amplified *SRC* as a driver of the malignant phenotype of H322M cells by screening our published cell line collection against the small molecule inhibitor dasatinib (54), clearly demonstrating that our approach is able to identify novel and also scarce targets. Since *SRC* amplifications remains scarce in lung cancer cell lines investigated so far, we developed a novel algorithm that allowed the identification of *SRC* as a possible target of Dasatinib in the H322M cell line (54). Although v-*SRC* was the first gene discovered to be transforming healthy cells (57), the human version of *SRC* (*cSRC*), harboring a regulatory subunit at the C terminus, so far failed to be transforming (58). Surprisingly, genetic alterations in this well characterized human proto-oncogene have never been discovered, although one controversial (and unvalidated) report had claimed somatic mutations in *SRC* in colorectal cancer (59). Thus, our finding of rare but significant amplification of the *SRC* gene in lung cancer is the first demonstration of its role as a bona-fide oncogene in humans. Despite the fact that the potent effect of dasatinib treatment on H322M cells could be abolished by ectopically expressing a mutated version of *cSRC* (54), it remains unlikely that *cSRC* is the sole transforming factor in these cells, since *cSRC* expression alone is not sufficient to transform primary cells (58). A possible explanation for the observed sensitivity towards inhibition of *cSRC* would be that it acts directly downstream of Receptor Tyrosine Kinases (RTKs) (60) and its primary function in these cells is not a direct signal producer, but to elicit a direct amplification of RTK signals into more downstream signaling pathways. Alternatively, *cSRC* amplifications might function in conjunction with other genetic alterations to drive tumorigenesis. In this regard, *SRC* amplifications are similar to *FGFR1* amplifications, also discovered by our lab, that are necessary but not sufficient to transform human cells. Our *cSRC*-related findings formally proved the relevance of our approach to identify possible targets in lung cancer.

The next step in the course of the thesis was the development of a novel biologic/mathematical model that allows the detection of compound combinations being synergistic in high throughput compound screens (HTS) (61). General approaches to identify synergistic behavior in a variety of biological scenarios (62), where not suitable for analyzing high-throughput screening data or do not properly discriminate between simple additional effect and real synergy. Whereas our model specifically allows the analysis of HTS screening data in regards to synergistic effects. A mandatory feature of RTK functioning as oncogenes is the ability to utilize cell internal signaling pathways for transfer of the oncogenic signal. Inhibition of a single pathway, by e.g., small molecule inhibitors, can lead to the same phenotype as seen after direct RTK inhibition, indicating that the kinases inhibited rely on only one pathway to transfer a signal into the cell. By contrast, an only partial cellular response indicates that the kinase inhibited rely on more than one signaling pathway. An initial study performed in the group demonstrated the more potent, synergistic effect of the combined PI3K and MAPK pathway inhibition in RTK driven cell lines (25), using the synergy detection model mentioned above. This raises the question if the existing screening platform can be extended to systematically screen for pathway usage in tumor cells. With this screen, not only we aimed to systematically answer the question of how tumor cells use the MAPK and PI3K pathways to transfer signals from the membrane through the cell into the nucleus, but also if both pathways are internally connected and show cross signaling. To further investigate this question, a HT compound screen

where 17 compounds were systematically combined with each other on 105 genetically annotated cell lines, was performed in the course of the thesis. Clinically, together with the genomic information about the cell lines used, this screen has the potential to give new insights about new therapeutic treatment options in patients. Experimentally, these efforts were essential in establishing novel screening methods in the lab allowing to screen up to more than 1500 compounds against more than a hundred cell lines.

As one of the first results of the before-mentioned cell line screen, we identified FGFR1 as a new, clinically relevant, target in squamous cell carcinomas of the lung (35). By screening the small molecule inhibitor PD173074 (63) against our panel of genomically annotated cell lines followed by analysis with K-NN based prediction model (64), we were able to show that *FGFR1* amplification as being the best scoring predictor for PD173074 sensitivity. *In-vivo* treatment of nude mice, harboring *FGFR1* amplified tumors, with PD173074 leads to tumor shrinkage similar to the treatment *in-vitro* (35). To formally prove, that FGFR1 is the relevant target of PD173074 in *FGFR1* amplified cell lines, a mutant version of FGFR1 (FGFR1_V561M) was expressed and showed to be rescuing the PD173074 induced phenotype. Furthermore, shRNA mediated knockdown of FGFR1 in a *FGFR1*-amplified cell line showed to have the same effect that treatment with PD173074 (35). Both approaches proved that FGFR1 is the relevant target in these cell lines. Similar findings by Ashworth and colleagues suggest that *FGFR1* is also a clinical relevant target in breast cancer cell lines (34). However, preliminary unpublished computational analyses from our lab and my own cellular data support a different genomic architecture of the 8p amplification in breast as compared to squamous-cell lung cancer, possibly involving other genes. Other studies, investigating the 8p12 locus in primary tumor specimens suggested *WHSC1L1* (65) or *BRF2* (66) to be the relevant target of the 8p12 amplification. However, both studies were either limited by the available experimental resolution at the time of study (65) or by the small size of the sample cohort used (66), probably leading to an inaccurate amplification characterization. The study performed in the course of the thesis circumvented both limitations by using high resolution Affymetrix 6.0 SNP arrays and by using a total of 155 primary squamous cell carcinoma samples. Most importantly, studies of primary lung adenocarcinoma samples revealed 8p12 amplifications at only a very low frequency (35), as was also shown by others (66). In addition, the results regarding signaling events clearly show that upon treatment with PD173074, phosphorylation of ERK but not of Akt is lost. These results are in accordance with other studies, showing that FGFRs primarily signals via the MAPK but not the PI3K pathway (32). And finally, we showed that *FGFR1* amplification leads to higher amount of FGFR1 protein and that FGFR1 is primarily activated by itself, rather than by autocrine FGF secretion. The results presented in this thesis, strongly suggest usage of FGFR1 inhibitors to treat patients harboring FGFR1 amplified squamous cell carcinomas, a lung carcinoma subtype being strongly connected to smoking and to this point no indication for targeted therapies. A clinical phase I trial is about to begin early 2011, Cologne being one of two centers worldwide to treat patients harboring *FGFR1* amplified squamous cell carcinomas with FGFR inhibitors.

Taken together, the data presented here clearly demonstrate that screening of a large panel of genomically characterized cell lines led to the identification of two genes, previously unproven to be involved in the onset of lung cancer. In a proof of concept screen, the *cSRC* gene, encoding for an intracellular tyrosine kinase acting downstream of Receptor Tyrosine Kinases (RTKs), was identified as being relevant in lung tumor derived cell lines and (rarely) in primary lung cancers. Due to the observation that dual PI3K and MAPK pathway inhibition leads to a stronger induction of apoptosis in our lung cancer cell line panel, 107 cell lines were screened towards a total of 136 compound combinations to identify synergistic acting inhibitor pairs and also to shed light into pathway interaction downstream of RTKs. Since most patients that are treated with small molecule kinase inhibitors will eventually suffer a relapse due to secondary mutations in the kinase inhibited by treatment, this screen will most likely lead to novel treatment options downstream of mutated RTKs. And finally, the identification of FGFR1 as novel and possible clinical relevant target exquisitely in squamous cell lung cancer, a subtype closely related to smoking and until today no indication for targeted therapies further underscores the power of our integrated cancer genomics approach. Amplification of this gene is predictive for sensitivity towards FGFR inhibitors *in-vitro* and *in-vivo* and

clinical trials starting this year will address this prediction in patients suffering from *FGFR1* amplified squamous cell lung cancers.

6.0 References

1. Raven, RW. *The Theory and Practice of Oncology*, (Parthenon, 1990).
2. Weinberg, RA. *The biology of cancer*, (Garland Science, 2007).
3. Hecht, S. S., Upadhyaya, P. & Wang, M. Reactions of alpha-acetoxy-N-nitrosopyrrolidine and crotonaldehyde with DNA. *IARC Sci Publ*, 147-154 (1999).
4. Zhong, Y., Carmella, S. G., Upadhyaya, P., Hochalter, J. B. *et al.* Immediate Consequences of Cigarette Smoking: Rapid Formation of Polycyclic Aromatic Hydrocarbon Diol Epoxides. *Chem Res Toxicol* (2011).
5. Kadouri, L., Bercovich, D., Elimelech, A., Lerer, I. *et al.* A novel BRCA-1 mutation in Arab kindred from east Jerusalem with breast and ovarian cancer. *BMC Cancer* **7**, 14 (2007).
6. Hanahan, D. & Weinberg, R. A. The hallmarks of cancer. *Cell* **100**, 57-70 (2000).
7. Datta, S. R., Brunet, A. & Greenberg, M. E. Cellular survival: a play in three Akts. *Genes Dev* **13**, 2905-2927 (1999).
8. Greulich, H., Chen, T. H., Feng, W., Janne, P. A. *et al.* Oncogenic transformation by inhibitor-sensitive and -resistant EGFR mutants. *PLoS Med* **2**, e313 (2005).
9. Paez, J. G., Janne, P. A., Lee, J. C., Tracy, S. *et al.* EGFR mutations in lung cancer: correlation with clinical response to gefitinib therapy. *Science* **304**, 1497-1500 (2004).
10. Dawson, T. & Wynford-Thomas, D. Does autocrine growth factor secretion form part of a mechanism which paradoxically protects against tumour development? *Br J Cancer* **71**, 1136-1141 (1995).
11. Dawson, T. P., Radulescu, A. & Wynford-Thomas, D. Expression of mutant p21ras induces insulin-like growth factor 1 secretion in thyroid epithelial cells. *Cancer Res* **55**, 915-920 (1995).
12. Nevins, J. R. The Rb/E2F pathway and cancer. *Hum Mol Genet* **10**, 699-703 (2001).
13. Watson, J. D. Origin of concatemeric T7 DNA. *Nat New Biol* **239**, 197-201 (1972).
14. Counter, C. M., Avilion, A. A., LeFeuvre, C. E., Stewart, N. G. *et al.* Telomere shortening associated with chromosome instability is arrested in immortal cells which express telomerase activity. *EMBO J* **11**, 1921-1929 (1992).
15. Greider, C. W. & Blackburn, E. H. Identification of a specific telomere terminal transferase activity in Tetrahymena extracts. *Cell* **43**, 405-413 (1985).
16. Fidler, I. J. The pathogenesis of cancer metastasis: the 'seed and soil' hypothesis revisited. *Nat Rev Cancer* **3**, 453-458 (2003).
17. Pleasance, E. D., Cheetham, R. K., Stephens, P. J., McBride, D. J. *et al.* A comprehensive catalogue of somatic mutations from a human cancer genome. *Nature* **463**, 191-196 (2010).
18. Dalgliesh, G. L., Furge, K., Greenman, C., Chen, L. *et al.* Systematic sequencing of renal carcinoma reveals inactivation of histone modifying genes. *Nature* **463**, 360-363 (2010).
19. Campbell, P. J., Yachida, S., Mudie, L. J., Stephens, P. J. *et al.* The patterns and dynamics of genomic instability in metastatic pancreatic cancer. *Nature* **467**, 1109-1113 (2010).
20. TheTCGA, consortium Comprehensive genomic characterization defines human glioblastoma genes and core pathways. *Nature* **455**, 1061-1068 (2008).
21. Ding, L., Getz, G., Wheeler, D. A., Mardis, E. R. *et al.* Somatic mutations affect key pathways in lung adenocarcinoma. *Nature* **455**, 1069-1075 (2008).
22. Vanhaesebroeck, B., Guillermet-Guibert, J., Graupera, M. & Bilanges, B. The emerging mechanisms of isoform-specific PI3K signalling. *Nat Rev Mol Cell Biol* **11**, 329-341 (2010).
23. Sos, M. L., Koker, M., Weir, B. A., Heynck, S. *et al.* PTEN loss contributes to erlotinib resistance in EGFR-mutant lung cancer by activation of Akt and EGFR. *Cancer Res* **69**, 3256-3261 (2009).
24. Wu, C. L., Zukerberg, L. R., Ngwu, C., Harlow, E. *et al.* In vivo association of E2F and DP family proteins. *Mol Cell Biol* **15**, 2536-2546 (1995).

25. Sos, M. L., Fischer, S., Ullrich, R., Peifer, M. *et al.* Identifying genotype-dependent efficacy of single and combined PI3K- and MAPK-pathway inhibition in cancer. *Proc Natl Acad Sci U S A* **106**, 18351-18356 (2009).
26. Lynch, T. J., Bell, D. W., Sordella, R., Gurubhagavatula, S. *et al.* Activating mutations in the epidermal growth factor receptor underlying responsiveness of non-small-cell lung cancer to gefitinib. *N Engl J Med* **350**, 2129-2139 (2004).
27. Heinrich, M. C., Corless, C. L., Demetri, G. D., Blanke, C. D. *et al.* Kinase mutations and imatinib response in patients with metastatic gastrointestinal stromal tumor. *J Clin Oncol* **21**, 4342-4349 (2003).
28. Di Fiore, P. P., Pierce, J. H., Kraus, M. H., Segatto, O. *et al.* erbB-2 is a potent oncogene when overexpressed in NIH/3T3 cells. *Science* **237**, 178-182 (1987).
29. Engelman, J. A., Zejnullahu, K., Mitsudomi, T., Song, Y. *et al.* MET amplification leads to gefitinib resistance in lung cancer by activating ERBB3 signaling. *Science* **316**, 1039-1043 (2007).
30. Herbst, H., Anagnostopoulos, J., Heinze, B., Durkop, H. *et al.* ALK gene products in anaplastic large cell lymphomas and Hodgkin's disease. *Blood* **86**, 1694-1700 (1995).
31. Soda, M., Choi, Y. L., Enomoto, M., Takada, S. *et al.* Identification of the transforming EML4-ALK fusion gene in non-small-cell lung cancer. *Nature* **448**, 561-566 (2007).
32. Turner, N. & Grose, R. Fibroblast growth factor signalling: from development to cancer. *Nat Rev Cancer* **10**, 116-129 (2010).
33. Salvesen, H. B., Carter, S. L., Mannelqvist, M., Dutt, A. *et al.* Integrated genomic profiling of endometrial carcinoma associates aggressive tumors with indicators of PI3 kinase activation. *Proc Natl Acad Sci U S A* **106**, 4834-4839 (2009).
34. Turner, N., Pearson, A., Sharpe, R., Lambros, M. *et al.* FGFR1 amplification drives endocrine therapy resistance and is a therapeutic target in breast cancer. *Cancer Res* **70**, 2085-2094 (2010).
35. Weiss, J., Sos, M. L., Seidel, D., Peifer, M. *et al.* Frequent and focal FGFR1 amplification associates with therapeutically tractable FGFR1 dependency in squamous cell lung cancer. *Sci Transl Med* **2**, 62ra93 (2010).
36. Weinstein, I. B. Cancer. Addiction to oncogenes--the Achilles heel of cancer. *Science* **297**, 63-64 (2002).
37. Druker, B. J., Talpaz, M., Resta, D. J., Peng, B. *et al.* Efficacy and safety of a specific inhibitor of the BCR-ABL tyrosine kinase in chronic myeloid leukemia. *N Engl J Med* **344**, 1031-1037 (2001).
38. Kwak, E. L., Bang, Y. J., Camidge, D. R., Shaw, A. T. *et al.* Anaplastic lymphoma kinase inhibition in non-small-cell lung cancer. *N Engl J Med* **363**, 1693-1703 (2010).
39. Mok, T. S., Wu, Y. L., Thongprasert, S., Yang, C. H. *et al.* Gefitinib or carboplatin-paclitaxel in pulmonary adenocarcinoma. *N Engl J Med* **361**, 947-957 (2009).
40. Bringham, B. A., Bunn, P. A., Jr., Minna, J. D., Cohen, M. H. *et al.* Growth rates of small cell bronchogenic carcinomas. *Cancer* **42**, 2880-2886 (1978).
41. Wilke, H., Achterrath, W., Schmoll, H. J., Gunzer, U. *et al.* Etoposide and split-dose cisplatin in small-cell lung cancer. *Am J Clin Oncol* **11**, 572-578 (1988).
42. Schmoll, HJ, Höffken, K & Possinger, K. *Kompendium Internistische Onkologie Standards in Diagnostik und Therapie*, (Springer, 2005).
43. Collins, L. G., Haines, C., Perkel, R. & Enck, R. E. Lung cancer: diagnosis and management. *Am Fam Physician* **75**, 56-63 (2007).
44. Khuder, S. A. Effect of cigarette smoking on major histological types of lung cancer: a meta-analysis. *Lung Cancer* **31**, 139-148 (2001).
45. Scott, W. J., Howington, J., Feigenberg, S., Movsas, B. *et al.* Treatment of non-small cell lung cancer stage I and stage II: ACCP evidence-based clinical practice guidelines (2nd edition). *Chest* **132**, 234S-242S (2007).

46. Fukuoka, M., Yano, S., Giaccone, G., Tamura, T. *et al.* Multi-institutional randomized phase II trial of gefitinib for previously treated patients with advanced non-small-cell lung cancer (The IDEAL 1 Trial) [corrected]. *J Clin Oncol* **21**, 2237-2246 (2003).
47. Miller, V. A., Kris, M. G., Shah, N., Patel, J. *et al.* Bronchioloalveolar pathologic subtype and smoking history predict sensitivity to gefitinib in advanced non-small-cell lung cancer. *J Clin Oncol* **22**, 1103-1109 (2004).
48. Maemondo, M., Inoue, A., Kobayashi, K., Sugawara, S. *et al.* Gefitinib or chemotherapy for non-small-cell lung cancer with mutated EGFR. *N Engl J Med* **362**, 2380-2388 (2010).
49. Rosell, R., Moran, T., Queralt, C., Porta, R. *et al.* Screening for epidermal growth factor receptor mutations in lung cancer. *N Engl J Med* **361**, 958-967 (2009).
50. Soda, M., Takada, S., Takeuchi, K., Choi, Y. L. *et al.* A mouse model for EML4-ALK-positive lung cancer. *Proc Natl Acad Sci U S A* **105**, 19893-19897 (2008).
51. Pao, W., Miller, V. A., Politi, K. A., Riely, G. J. *et al.* Acquired resistance of lung adenocarcinomas to gefitinib or erlotinib is associated with a second mutation in the EGFR kinase domain. *PLoS Med* **2**, e73 (2005).
52. Kobayashi, S., Boggon, T. J., Dayaram, T., Janne, P. A. *et al.* EGFR mutation and resistance of non-small-cell lung cancer to gefitinib. *N Engl J Med* **352**, 786-792 (2005).
53. Bass, A. J., Watanabe, H., Mermel, C. H., Yu, S. *et al.* SOX2 is an amplified lineage-survival oncogene in lung and esophageal squamous cell carcinomas. *Nat Genet* **41**, 1238-1242 (2009).
54. Sos, M. L., Michel, K., Zander, T., Weiss, J. *et al.* Predicting drug susceptibility of non-small cell lung cancers based on genetic lesions. *J Clin Invest* **119**, 1727-1740 (2009).
55. Pao, W., Miller, V., Zakowski, M., Doherty, J. *et al.* EGF receptor gene mutations are common in lung cancers from "never smokers" and are associated with sensitivity of tumors to gefitinib and erlotinib. *Proc Natl Acad Sci U S A* **101**, 13306-13311 (2004).
56. Sequist, L. V., Bell, D. W., Lynch, T. J. & Haber, D. A. Molecular predictors of response to epidermal growth factor receptor antagonists in non-small-cell lung cancer. *J Clin Oncol* **25**, 587-595 (2007).
57. Brugge, J. S. & Erikson, R. L. Identification of a transformation-specific antigen induced by an avian sarcoma virus. *Nature* **269**, 346-348 (1977).
58. Iba, H., Takeya, T., Cross, F. R., Hanafusa, T. *et al.* Rous sarcoma virus variants that carry the cellular src gene instead of the viral src gene cannot transform chicken embryo fibroblasts. *Proc Natl Acad Sci U S A* **81**, 4424-4428 (1984).
59. Irby, R. B., Mao, W., Coppola, D., Kang, J. *et al.* Activating SRC mutation in a subset of advanced human colon cancers. *Nat Genet* **21**, 187-190 (1999).
60. Kim, L. C., Song, L. & Haura, E. B. Src kinases as therapeutic targets for cancer. *Nat Rev Clin Oncol* **6**, 587-595 (2009).
61. Peifer, M., Weiss, J., Sos, M. L., Koker, M. *et al.* Analysis of compound synergy in high-throughput cellular screens by population-based lifetime modeling. *PLoS ONE* **5**, e8919 (2010).
62. Chou, T. C. Theoretical basis, experimental design, and computerized simulation of synergism and antagonism in drug combination studies. *Pharmacol Rev* **58**, 621-681 (2006).
63. Mohammadi, M., Froum, S., Hamby, J. M., Schroeder, M. C. *et al.* Crystal structure of an angiogenesis inhibitor bound to the FGF receptor tyrosine kinase domain. *EMBO J* **17**, 5896-5904 (1998).
64. Golub, T. R., Slonim, D. K., Tamayo, P., Huard, C. *et al.* Molecular classification of cancer: class discovery and class prediction by gene expression monitoring. *Science* **286**, 531-537 (1999).
65. Tonon, G., Wong, K. K., Maulik, G., Brennan, C. *et al.* High-resolution genomic profiles of human lung cancer. *Proc Natl Acad Sci U S A* **102**, 9625-9630 (2005).
66. Lockwood, W. W., Chari, R., Coe, B. P., Thu, K. L. *et al.* Integrative genomic analyses identify BRF2 as a novel lineage-specific oncogene in lung squamous cell carcinoma. *PLoS Med* **7**, e1000315 (2010).

7.0 Appendix

7.1 Acknowledgments

As in many situations in live, this piece of work would have never been possible with the support, encouragement and cheer up from a lot of people. I am deeply indebted to each one each one, but unfortunately I can only mention a few.

First, I would like to thank my supervisor PD. Dr. Roman Thomas for the opportunity to conduct my thesis in his group. Roman has always been a constant source of inspiration, support and encouraging ideas. He always gave me the confidence and freedom to pursue my own ideas and always pushed me a little bit further than I believed possible.

I would like to thank Prof. Hinrich Abken and Prof. Matthias Hammerschmidt for supervising my thesis and also for the possibility to graduate so uncomplicated and fast.

Thanks to all the members of the “Thomas” and “Ullrich” labs, where every one contributes something unique, resulting in a great mixture of characters and makes it great place to work.

Thanks to Mirjam Koker and Stefanie Heynck for all the tips and tricks, fun and jokes during the every-day lab sessions.

To my fellow graduate students, Danila Seidel, Johannes Heuckmann and Florian Fischer for a great time in and out of the lab and the helping hands in times of trouble.

A special thanks to the Drs.:

Martin Sos who showed me how to take each small step in a big project.

Martin Peifer, for everything I know about statistics, his enthusiasm for my ideas and the endless discussions about science and life.

Thomas Zander, who taught me about the clinical aspects of cancer and has always been a constant source of encouragement and great ideas.

And finally to Anne Raspel, who keeps everything together.

Also thanks to my whole family and especially to my parents, grandparents and siblings: Vincent, Damian, Magnus, Josefine and Kathrin for their cheers and support that made this work possible.

To my stepfather, Daniel Mahr, for continues encouragement and help over all these years.

To my girlfriend Eva, who has always been at my side.

And finally thanks to all my friends, unfortunately far too many to thank each one alone.

7.2 Academic Curriculum Vitae

Personal Data

Born	February 19th 1981
In	Cologne
Citizenship	German

Studies

2008 – Today	PhD. Thesis under supervision of PD. Dr. Roman Thomas
2007	Diploma in biology (“Top Mark”) From the University of Cologne Under supervision of Prof. Dr. Markus Müschen Diploma thesis „ <i>The tumor antigen TACSTD1 is required to maintain pluripotency and selfrenewal in human embryonic stem cells</i> “
2004	Pre-diploma in biology from the University of Cologne
2002 – 2007	Studies in biology at the University of Cologne

Internships

2006 – 2007	Diplomathesis under supervision of Prof. Dr. Markus Müschen at the Children’s Hospital Los Angeles
2005	Internship at the Forschungszentrum Jülich in the group of PD. Dr. Arnd Baumann
2005	Internship at the institute for pharmacology in the group of Prof. Dr. Stefan Herzig

Publications

Frequent and focal FGFR1 amplification associates with therapeutically tractable FGFR1 dependency in squamous cell lung cancer.

Weiss J, Sos ML*, Seidel D*, Peifer M, Zander T et. al.
Sci Transl Med. 2010 Dec 15;2(62):62ra93.

Analysis of compound synergy in high-throughput cellular screens by population-based lifetime modeling.

Martin Peifer*, Jonathan Weiss*, Martin L. Sos*, Mirjam Koker, Stefanie Heynck et. al.
PLoS One. 2010 Jan 27;5(1):e8919.

*Contributed equally

Insights into the limited activity of irreversible EGFR inhibitors in tumor cells expressing the T790M EGFR resistance mutation from chemo-genomics profiling

Martin Sos, Haridas Rode, Stefanie Heynck, Martin Peifer, Florian Fischer et. al.
Cancer Res. 2010 Feb 1;70(3):868-74.

Sos ML, Fischer S, Ullrich R, Peifer M, Heuckmann JM

Identifying genotype-dependent efficacy of single and combined PI3K- and MAPK-pathway inhibition in cancer.

Proc Natl Acad Sci U S A. 2009 Oct 27;106(43):18351-6.

Predicting drug susceptibility of non-small cell lung cancers based on genetic lesions.

Sos ML*, Michel K*, Zander T*, Weiss J*, Frommolt P* et. al.
J Clin Invest. 2009 Jun;119(6):1727-40. doi: 10.1172/JCI37127.

*Contributed equally

PTEN loss contributes to erlotinib resistance in EGFR-mutant lung cancer by activation of Akt and EGFR.

Sos ML, Koker M, Weir BA, Heynck S, Rabinovsky R et. al.
Cancer Res. 2009 Apr 15;69(8):3256-61.

The WNT receptor FZD7 contributes to self-renewal signaling of human embryonic stem cells.

Melchior K, Weiss J, Zaehres H, Kim YM, Lutzko C, Roosta N, Hescheler J, Müschen M.
Biol Chem. 2008 Jul;389(7):897-903.

Conferences attended

December 2010	Multidisciplinary Symposium of thoracic oncology, Chicago, Illinois
April 2009	AACR Annual Meeting, Denver, Colorado
Dezember 2008	NGFN Kickoff Meeting, Munich

Technical skills

Cell based techniques:

Cell culture techniques (adhered and suspensions cells)

Colony formation assays based on soft agar

Flow cytometry (FACS)

Handling of Lenti and Retroviral supernatants

Design, performance and analysis of high throughput cell based small molecule inhibitor screens

Molecular techniques:

Molecular DNA cloning techniques

DNA and RNA extraction

cDNA synthesis

Quantitative real-time PCR

Protein techniques:

Protein extraction

Western blot, Immunoprecipitation

Language skills

German (Native Speaker)

English (Business Fluent)

Workshops and Trainings

July 2010 Training Statistic software R

July 2010 Training in the structural biology software

November 2010 Scientific writing course by BioScript

Getting funded writing course by BioScript

Software skills

MS Office (advanced)

Adobe Photoshop (advanced)

Statistic software R (basic)

7.3 Erklärung

Ich versichere, dass ich die von mir vorgelegte Dissertation selbständig angefertigt, die benutzten Quellen und Hilfsmittel vollständig angegeben und die Stellen der Arbeit - einschließlich Tabellen, Karten, und Abbildungen - , die anderen Werken im Wortlaut oder dem Sinn nach entnommen sind, in jedem Einzelfall als Entlehnung kenntlich gemacht habe; dass diese Dissertation noch keiner anderen Fakultät oder Universität zur Prüfung vorgelegen hat; dass sie – abgesehen von unten angegebenen Teilpublikationen – noch nicht veröffentlicht worden ist sowie, dass ich eine solche Veröffentlichung vor Abschluss des Promotionsverfahrens nicht vornehmen werde. Die Bestimmungen dieser Promotionsordnung sind mir bekannt. Die von mir vorgelegte Dissertation ist von PD. Dr.med. Roman Thomas betreut worden.

Teilpublikationen:

Ich versichere, dass ich alle Angaben wahrheitsgemäß nach bestem Wissen und Gewissen gemacht habe und verpflichte mich, jedmögliche, die obigen Angaben betreffenden Veränderungen, dem Promotionsausschuss unverzüglich mitzuteilen.

Köln, den 26.01.2011

Ort, Datum

.....
Unterschrift